



Review

Coordination chemistry of 1,3,5-triaza-7-phosphaadamantane (PTA) and derivatives. Part II. The quest for tailored ligands, complexes and related applications

Jorge Bravo^{a,*}, Sandra Bolaño^a, Luca Gonsalvi^b, Maurizio Peruzzini^{b,*}

^a Departamento de Química Inorgánica, Universidade de Vigo, Campus Universitario, E-36310 Vigo, Spain

^b Consiglio Nazionale delle Ricerche, Istituto di Chimica dei Composti Organometallici (ICCOM-CNR), Via Madonna del Piano 10, 50019 Sesto Fiorentino (Firenze), Italy

Contents

1. Introduction.....	556
2. Ligand structural modifications.....	556
3. Transition-metal complexes of PTA and derivatives.....	560
3.1. Chromium, molybdenum and tungsten complexes.....	560
3.2. Manganese and rhenium complexes.....	561
3.3. Iron, ruthenium and osmium complexes.....	563
3.4. Cobalt, rhodium and iridium complexes.....	579
3.5. Nickel, palladium and platinum complexes.....	585
3.6. Copper, silver and gold complexes.....	590
3.7. Zinc complexes.....	595
4. Catalytic applications of transition-metal complexes of PTA and its derivatives.....	596
5. Medicinal chemistry of PTA complexes and structural derivatives.....	602
Acknowledgements.....	606
References.....	606

ARTICLE INFO

Article history:

Received 29 May 2009

Accepted 7 August 2009

Available online 15 August 2009

Dedicated to Prof Fausto Calderazzo, a pioneer of organometallic chemistry and homogeneous catalysis, on occasion of his 80th birthday.

Keywords:

1,3,5-Triaza-7-phosphaadamantane
Water-soluble ligands
Coordination chemistry
X-ray crystallography
Catalysis
Medicinal chemistry

ABSTRACT

This review paper covers the recent developments (2004–2009) on the tailored synthetic modifications and related coordination chemistry of the water-soluble cage-like aminophosphine ligand 1,3,5-triaza-7-phosphatricyclo-[3.3.1.1]decane (PTA), together with the new applications in the fields of catalysis, material science and medicinal chemistry.

© 2009 Elsevier B.V. All rights reserved.

Abbreviation: PTA, 1,3,5-triaza-7-phosphatricyclo-[3.3.1.1]decane; mPTA, 1-methyl-1,3,5-triaza-7-phosphatricyclo-[3.3.1.1]decane; dmPTA, 1,3-dimethyl-1,3,5-triaza-7-phosphatricyclo-[3.3.1.1]decane; dmoPTA, 3,7-dimethyl-1,3,7-triaza-5-phosphabicyclo[3.3.1]nonane; HdmoPTA, 3,7-H-3,7-dimethyl-1,3,7-triaza-5-phosphabicyclo[3.3.1]nonane; DAPTA, 3,7-diacetyl-1,3,7-triaza-5-phosphabicyclo[3.3.1]nonane; DAFTA, 3,7-diethyl-1,3,7-triaza-5-phosphabicyclo[3.3.1]nonane; pymePTA, 1-pyridylmethyl-3,5-diaza-1-azonia-7-phosphatricyclo[3.3.1.1]decane; PZA, phenyl-(1,3,5-triaza-7-phospha-tricyclo[3.3.1.1]^{3,7}]dec-6-yl)-methanol; PTN(Me), 7-methylphospha-3-methyl-1,3,5-triazabicyclo[3.3.1]nonane; PTN(Ph), 7-phenylphospha-3-methyl-1,3,5-triazabicyclo[3.3.1]nonane.

* Corresponding authors.

E-mail addresses: jbravo@uvigo.es (J. Bravo), mperuzzini@iccom.cnr.it (M. Peruzzini).

0010-8545/\$ – see front matter © 2009 Elsevier B.V. All rights reserved.

doi:10.1016/j.ccr.2009.08.006

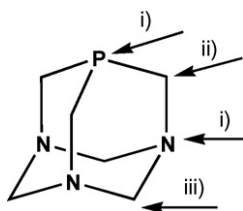


Chart 1. 1,3,5-Triaza-7-phosphaadamantane (PTA).

1. Introduction

This review follows after five years the first comprehensive report on the chemistry of 1,3,5-triaza-7-phosphatricyclo-[3.3.1.1]decane (PTA) published by some of us [1]. During the period of time covered by this review (2004–2009), the chemistry of transition-metal complexes containing one or more PTA ligands or derivatives has become very popular and many research teams have entered this field to explore new applications of this water-soluble phosphine and to expand the library of related water-soluble ligands introducing new synthetic modifications. These can be summarized (Chart 1) as: i) substitution at P or N atoms; ii) “upper rim” methylene functionalizations; iii) “lower rim” methylene functionalizations. The reactivity can lead (Scheme 1) or not (Scheme 2) to opening of the PTA cage either on the upper or on the lower rim. The new ligands, their coordination chemistry and related applications in catalysis and medicinal chemistry will be hereby reviewed.

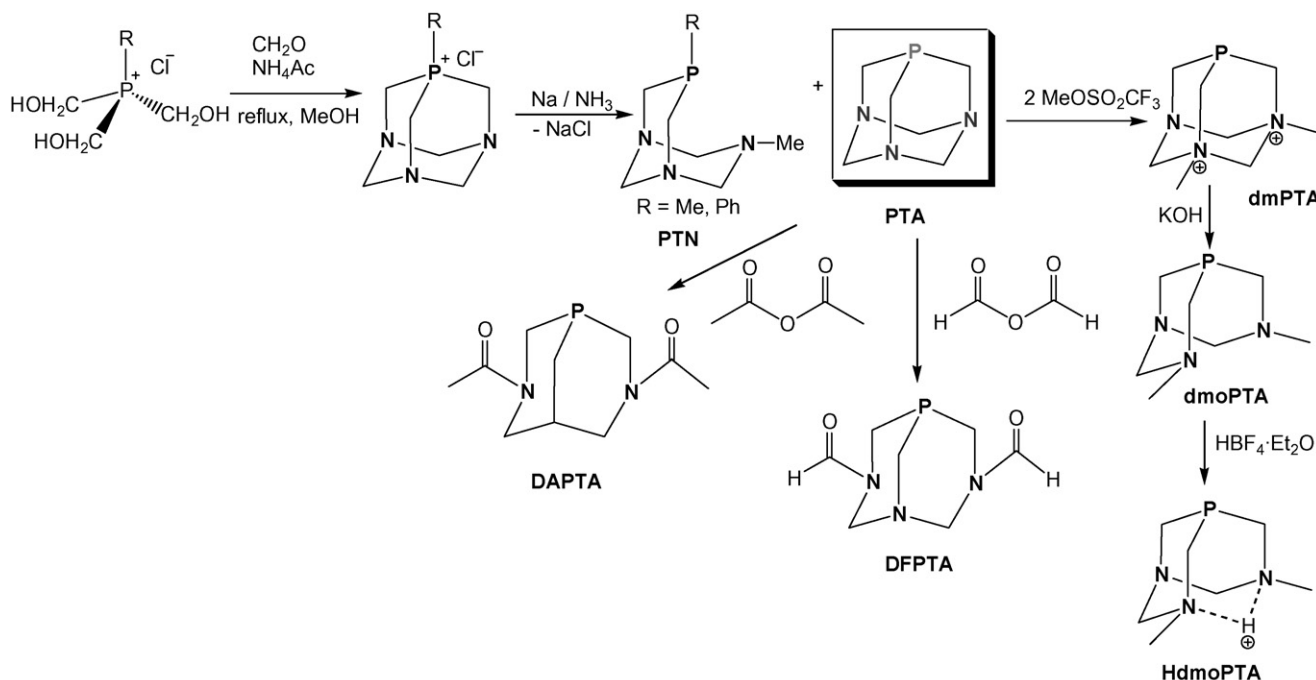
2. Ligand structural modifications

The complete understanding of electronic and steric effects of ligands is recognized nowadays as a pre-requisite for tailored design. Detailed studies on a variety of phosphorus ligands have included PTA. Suresh and co-workers [2] used a combined approach of quantum and molecular mechanics in a wide theoretical study

to estimate the stereoelectronic profile of a variety of phosphine ligands. This method allows the separation of the steric effect of a PR_3 ligand from its electronic effect and permits, by means of a stereoelectronic plot, to select the ligands in the design of a catalyst system in organometallic chemistry. Muller et al. [3] report the results of a kinetic study on the oxidative addition of SeCN^- to a series of phosphine ligands, showing that the rate of the reaction, following the kinetic law $k_{\text{obs}} = k_1[\text{SeCN}^-]$ is highly dependent on the electron density of the phosphorus center with k_1 varying by five orders of magnitude from 1.34×10^{-3} to 3.71×10^{-1} to $51 \text{ mol}^{-1} \text{ dm}^3 \text{ s}^{-1}$ changing from $\text{P}(\text{2-OMe-C}_6\text{H}_4)_3$ to PTA to PCy_3 , respectively.

PTA was used by He et al. [4] as an efficient base catalyst for the Morita–Baylis–Hillman reaction. Thus, reaction of 4-nitrobenzaldehyde with ethyl acrylate in THF– H_2O (4:1, v/v) in the presence of free PTA as catalyst (20 mol%) gives the desired addition product within 6 h after an initially rapid conversion. $^{31}\text{P}\{^1\text{H}\}$ NMR analysis of the reaction mixture shows that catalyst PTA ($\delta_{(\text{D}_2\text{O})} = -98.3 \text{ ppm}$) had disappeared and the new zwitterionic species $(\text{PTA})^+-\text{CH}_2-\text{CH}_2-\text{CO}_2^-$ emerges ($\delta_{(\text{D}_2\text{O})} = -37.6 \text{ ppm}$). The X-ray diffraction analysis of $(\text{PTA})^+-\text{CH}_2-\text{CH}_2-\text{CO}_2^-$ provides unambiguous evidence for the nucleophilic attack of PTA taking place at the P atom, and verifies the Michael addition step in the catalytic cycle [4c]. Moreover, PTA effectively catalyses a diastereoselective aza-MBH reaction between chiral *N*-thiophenyl imines and methyl vinyl ketone in good yields with moderate to excellent diastereoselectivities (>99% de) [5]. PTA is also an effective catalyst in the [3 + 2] cycloaddition of activated allenes with *N*-thiophosphoryl imines to give free amine 3-pyrrolines [6].

Direct reaction of PTA in methanol with KSeCN (Scheme 2) gives rapidly (<3 min) and almost quantitatively $\text{PTA}=\text{Se}$. The $^{31}\text{P}\{^1\text{H}\}$ NMR spectrum in D_2O displays a doublet at $\delta = -31.9 \text{ ppm}$ ($J_{\text{P-Se}} = 722 \text{ Hz}$). The structure of this compound was resolved by X-ray analysis showing that the PTA ligand retains its highly symmetrical rigid cage-like character with close to ideal tetrahedral angles around all atoms [7]. $[\text{mPTA}=\text{Se}]$ was obtained by reaction of Se powder with $[\text{mPTA}]\text{I}$ in a refluxing methanol/toluene (1:1) mixture. The limited solubility of the compound precluded a



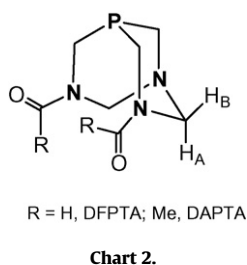
Scheme 1. Some examples of PTA functionalizations leading to cage opening.

Bis-methylation of PTA can be accomplished by reaction of PTA with 2 equiv of MeOTf in refluxing acetone, obtaining the dicationic compound *N,N'*-dimethyl-1,3,5-triaza-7-phosphaadamantane (dmPTA) as triflate salt (dmPTA)(OTf)₂ (Scheme 1) [12]. The white powder obtained is soluble in organic solvents and was characterized by NMR and IR spectroscopy and by X-ray diffraction analysis. ¹H NMR spectrum in D₂O shows a singlet at 3.16 ppm (6H) that agrees with the double methylation on two N atoms of PTA. The ³¹P{¹H} NMR spectrum in D₂O displays a singlet

N-alkyl-PTA halides [R-PTA]X (R = ⁿBu, ⁿPr, Et; X = I[−], Br[−]), undergo an unprecedented α-C–C bond cleavage within the alkyl arm of [R-PTA]X, generating the *N*-methyl-PTA (mPTA)X and the corresponding aldehyde, as demonstrated by NMR, GC, IR, FAB⁺-MS, and single-crystal X-ray structural analyses. Quantitative conversion of [R-PTA]⁺ to [mPTA]⁺ is achieved in aqueous solution and it is accelerated by heating. The PTA core and the halide counterion



Scheme 2. Some examples of PTA functionalizations maintaining to cage intact.



in [R-PTA]X play a determinant role, since no cleavage is detected for either [NBu₄]I or [BuPTA][BPh₄] [13].

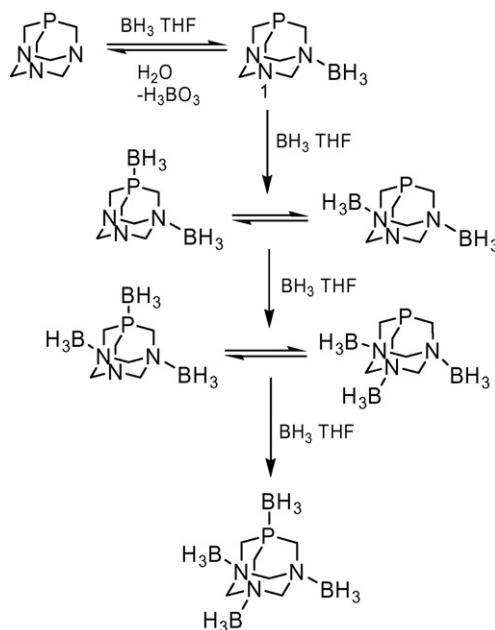
A demonstration of the possibility to open the PTA cage on the “bottom rim”, i.e. cleaving a N–C bond of the triazacyclohexane ring, was published by Darensbourg and co-workers, who reacted PTA with acetic anhydride to obtain the 3,7-diacetyl-1,3,7-triaza-5-phosphabicyclo[3.3.1]nonane ligand (DAPTA) and its oxide by acylation of PTA=O. DAPTA (Chart 2, R = Me) is remarkably more soluble than PTA (7.4 mol L^{−1} vs. 1.5 mol L^{−1}). Its coordination chemistry to Ni, Pd, Cr and W was also demonstrated (*vide infra*) [14a].

The di-*N*-formylated analogue of DAPTA, the open-cage 3,7-diformyl-1,3,7-triaza-5-phosphabicyclo[3.3.1]nonane (DFPTA, Chart 2) is obtained when “in situ” generated formic anhydride reacts with an aqueous solution of PTA at −5 °C [14b]. The product is soluble in water (1.1 M), insoluble in DMSO and sparingly soluble in halogenated hydrocarbons and alcohols, in marked contrast with DAPTA, which is soluble in most organic solvents and presents a higher water solubility (7.4 M). An intense (1670 cm^{−1}) and two smaller (2785 and 2801 cm^{−1}) IR stretching frequencies are typical of the formamide group. In contrast with what is observed in the solid state (*vide infra*), ¹H and ¹³C{¹H} NMR spectroscopic data indicate that the two C=O moieties are in *anti* conformation.

³¹P{¹H} NMR spectra displays the expected singlet at −74.2 ppm in CDCl₃. Colourless block crystals obtained by slow evaporation of a CH₂Cl₂ solution, were analyzed by X-ray diffraction. Although the structure of the phosphine is similar to that of DAPTA, two significant differences can be underlined: i) the average P–C bond distance (1.849 Å) is longer than the corresponding of DAPTA (1.728 Å); ii) The C(O)R moieties are *syn* in DFPTA (R = H) but *anti* in DAPTA (R = Me). The *anti* conformation of DFPTA was only observed in solution (*vide supra*) [14b].

Reaction of an acetone solution of PTA with 2-bromomethylpyridine gave the *N*-functionalized PTA derivative 1-pyridylmethyl-3,5-diaza-1-azonia-7-phosphatricyclo[3.3.1.1] decane bromide, [pymePTA]Br, shown in Scheme 2 [14]. The compound is soluble in halogenated solvents and is more soluble in water (2.4 M) than PTA. Its solid-state structure is similar to that of PTA with the average N–C bond distances involving the quaternary (1.53 Å) slightly longer than that around the others (1.45 and 1.46 Å) [14b].

The preparation of the borane N-adduct of PTA, PTA-BH₃ was almost simultaneously reported by Bolaño et al. [15] and Frost et al. [16] Addition of BH₃·THF to PTA in THF gave the aminoborane adduct as a white solid that was characterized by conventional spectroscopic techniques and its solid-state structure was resolved by X-ray crystallography [16]. The ³¹P{¹H} NMR resonance at δ ~ −90 ppm is deshielded with respect to PTA. The ¹¹B NMR spectrum displays a quartet at δ ~ −10 ppm (¹J = 98 Hz) which matches the values reported for other aminoboranes. The solid-state structure is practically identical to that of PTA with the (B)N–C(N) bond length at 1.505(9) Å, longer than the other N–C(N) bond lengths at 1.458(9) Å, as occurred with other PTA-modified compounds as PTA-H or mPTA [16].



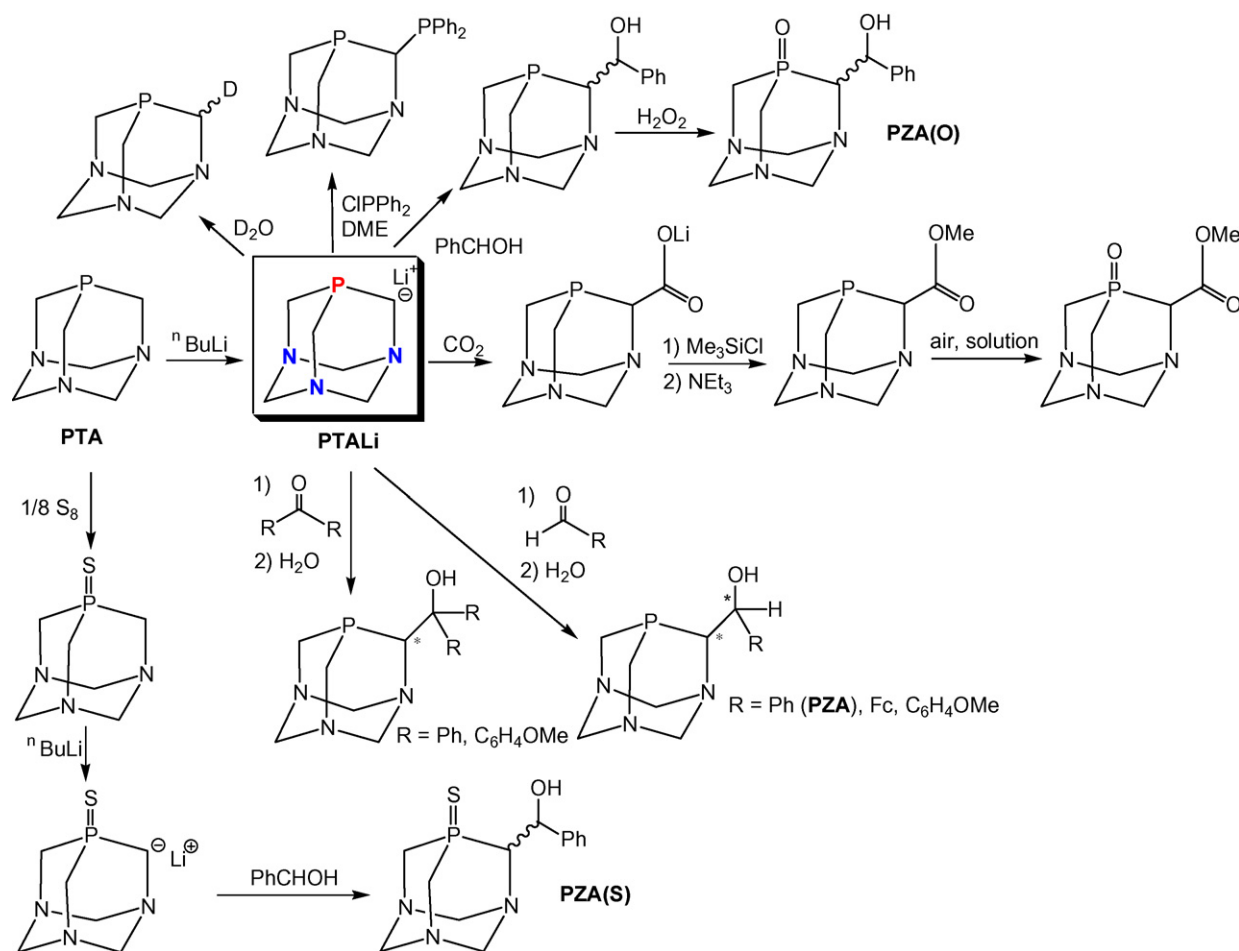
Scheme 3. Stepwise boronation of PTA.

Addition of BH₃·THF to O=PTA produces O=PTA-BH₃ similarly to PTA-BH₃ [16]. The ³¹P{¹H} NMR resonance, at δ ~ −10 ppm is deshielded with respect to O=PTA. The ¹¹B NMR spectrum displays a quartet at δ ~ −12 ppm (¹J = 95 Hz). The solid-state structure is similar to that of O=PTA with the P=O bond length slightly longer (1.490 Å vs. 1.476 Å). The B–N bond length is longer than the B–N bond distance in PTA-BH₃ due to the more positive nature of the phosphorus. DFT calculations performed on PTA-BH₃ and O=PTA-BH₃, predict an energy difference of 53.6 kJ mol^{−1} between N-bonded PTA-BH₃ and P-bonded H₃B-PTA indicating that nitrogen is the preferred site for boronation, and in agreement with the results obtained for alkylation (39.1 kJ mol^{−1} favouring N-alkylation) [16].

The reaction between PTA and BH₃·THF was monitored by ³¹P{¹H} NMR spectroscopy, results in a stepwise boronation to give the polyboranyl species N_x, P_y-B-PTA(BH₃)_(x+y) (x = 1–3, y = 0, 1) as shown in Scheme 3 [15]. Compounds PTA-BH₃ and O=PTA-BH₃ undergo hydrolytic cleavage of the B–N bond in both the solid state and solution [15,16]. PTA-BH₃ is stable against oxidation in solid state, but in solution gives O=PTA-BH₃ in the course of days, being more vulnerable than PTA, PTA-H⁺ or mPTA⁺ [16]. The presence of BH₃ also makes the P atom of PTA more susceptible to be methylated with MeI compared to free PTA [16].

“Upper rim” functionalizations of PTA (i.e. on the methylene carbons adjacent to P atom) have attracted recent interest as i) the steric and electronic properties of the ligand are thus modified in close proximity to the donor atom and ii) a chiral carbon atom in alpha-position to P is obtained, creating a new class of optically active water-soluble phosphines.

The first report on the “upper rim” modifications of PTA was published by Frost et al. [17] describing the fundamental step of lithiation of PTA to obtain the corresponding PTA-Li salt (Scheme 4) which could be further reacted with electrophiles to yield various derivatives (*vide infra*) [18]. Reaction of PTA with *n*-BuLi yields PTA-Li as an off-white highly pyrophoric powder that is insoluble in most common organic solvents. PTA-Li is regioselectively deuterated at the α-phosphorus methylene when it is reacted with D₂O (the P–CHD–N group displays an apparent quartet in the ¹³C{¹H} NMR spectrum at δ = 50.21 ppm, ¹J_{CD} ~ ¹J_{CP} ~ 21 Hz).

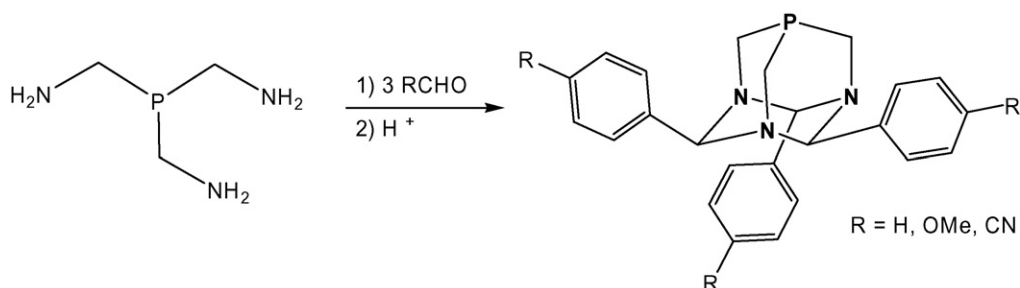


Scheme 4. Upper rim functionalization of PTA.

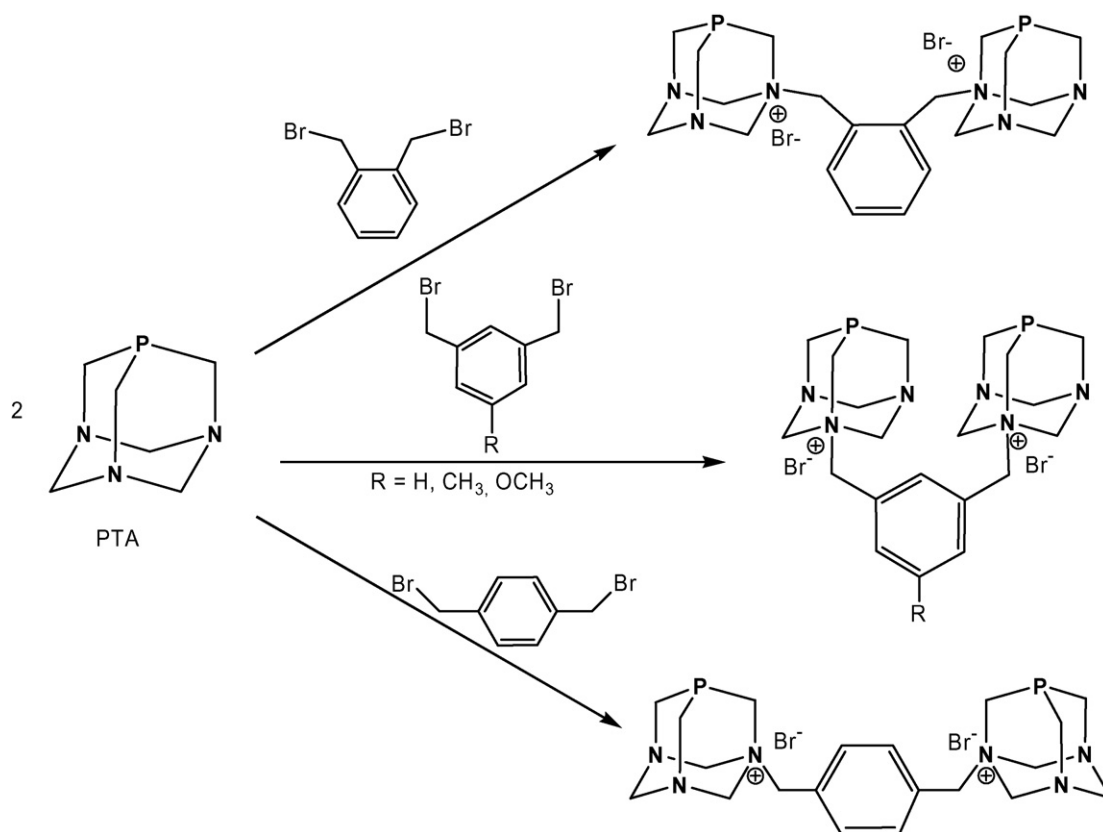
Reaction of PTA-Li with ClPPh_2 in 1,2-dimethoxyethane gives the racemic bidentate phosphine PTA- PPh_2 showing two $^{31}\text{P}\{^1\text{H}\}$ NMR doublets at -100.1 and -19.8 ($^2J_{\text{PP}} = 65$ Hz) corresponding to PTA and PPh_2 , respectively. This compound, obtained in *ca.* 10% yield after workup, is not soluble in water and slowly oxidizes in air giving $\text{O}=\text{PTA}-\text{PPh}_2$ (two doublets at -6.2 and -19.7 ppm, $^2J_{\text{PP}} = 40$ Hz, in the $^{31}\text{P}\{^1\text{H}\}$ NMR spectrum). Oxidation of both P atoms can be obtained by addition of H_2O_2 to PTA- PPh_2 yielding of $\text{O}=\text{PTA}-\text{P}(\text{O})\text{Ph}_2$ (two doublets at -1.4 and 34.3 ppm, $^2J_{\text{PP}} = 4$ Hz, in the $^{31}\text{P}\{^1\text{H}\}$ NMR spectrum). The crystal structure of PTA- PPh_2 shows that it crystallizes in the centrosymmetric space group $P2_1/c$, both *R* and *S* enantiomers being present. P-C-substituted bond distance is elongated [$1.890(4)$ Å] with respect to the average of those of the PTA ligand [1.856 Å], while the other two P-C distances are compressed [$1.815(5)$ and $1.832(4)$ Å].

Different electrophiles such as ketones, aldehydes and CO_2 were inserted into the C-Li bond of PTA-Li to produce a series of water-soluble β -phosphino alcohols, PTA- CR_2OH ($\text{R} = \text{Ph}$, $\text{C}_6\text{H}_4\text{OMe}$) bearing one stereocenter at the cage C atom, PTA- $\text{CH}(\text{R})\text{OH}$ ($\text{R} = \text{Ph}$, $\text{C}_6\text{H}_4\text{OMe}$, Fc) giving two stereogenic carbon atoms, and carboxylates PTA- CO_2X ($\text{X} = \text{Li}$, Me), respectively (Scheme 4) [18]. Some of these molecules were used as ligands for transition-metal fragments such as Ir(III) cyclopentadienyl (ligand PZA, Scheme 4) [18a] and Ru(II)-arenes [18b], showing in all cases κ^1 -P coordination (see Section 3.3).

Serendipitous separation of diastereomers was obtained in the case of PZA(O), synthesized from the reaction of PZA with H_2O_2 . From the reaction mixture in water only the *RS SR* diastereomer was collected as white crystals suitable for X-ray diffraction analysis. Interestingly, a intermolecular hydrogen bonding network is



Scheme 5. An example of lower rim modification of PTA.



Scheme 6. bis-PTA derivatives.

present in the solid state between the hydroxyl group of one PZA(O) and the P=O oxygen of the neighbouring molecule, not involving the triazacyclohexane N atoms (Fig. 1).

“Lower rim” modification of PTA by trisubstitution of the N-CH₂-N methylene groups of the triazacyclohexane ring with aryl groups (PTA-R₃) was obtained by condensation of P(CH₂NH₂)₃ with aldehydes under acidic conditions. The use of basic conditions leads to a 3-fold condensation reaction producing tris(iminomethyl)phosphines (Scheme 5) [19]. X-ray diffraction analysis of PTA-(R₃) (R=C₆H₄OMe) shows that the equatorial-equatorial-axial (*eea*) isomer is the only obtained, in agreement with the density functional theory calculations, which indicates that the *eea* isomer is the lowest in energy by ~3 kJ mol⁻¹ respect to the next (*eee*). NMR spectroscopy also indicates that only one isomer is present in solution in all cases.

Five new bis-phosphines obtained by linking two PTAs via the nitrogen atoms have been prepared. The *meta* substituted tolyl and anisyl derivatives have been studied by X-ray diffraction. The substitution pattern of the aromatic ring has a pronounced effect on the water solubility of the phosphines with the *ortho* compound being very water soluble (2000 mg mL⁻¹) while the *para* analogue is far less soluble (12.5 mg mL⁻¹). The *meta* phosphine and its tolyl analogue have water solubilities of 810 mg mL⁻¹, three times the value

of PTA. The anisyl version was determined to be much less soluble (121 mg mL⁻¹) indicating that the substituents on the ring greatly impact the water solubility of the compounds (Scheme 6) [20].

3. Transition-metal complexes of PTA and derivatives

3.1. Chromium, molybdenum and tungsten complexes

Complexes [M(CO)₅(DAPTA)] were obtained by photolyzing THF solutions containing M(CO)₆ (M=Cr, W) and DAPTA. κ^1 -P coordination was confirmed both by ³¹{¹H} NMR (−5.79 s and −47.7t, ¹J_{WP} 228.52 Hz, respectively) and X-ray crystal structure determination. M–P distances were W(1)–P(1)=2.492(3) and Cr(1)–P(1) 2.3562(19), in line with reported data [14a].

Only one molybdenum–PTA complex has been described, the quadruply bonded Mo(II)–Mo(II) complex, [Mo₂Cl₄(PTA)₄] (**1**) [21]. This blue-green compound is obtained by reaction of potassium octachlorodimolybdate(II) and PTA (Scheme 7).

The complex is air-stable and water soluble but decomposes rapidly in aqueous solution (*t*_{1/2} ~60 s). This stability is not improved by using degassed water saturated with nitrogen. The four PTA ligands are equivalent in solution as indicated by the presence of only one signal in the ³¹P{¹H} NMR spectrum. On the other

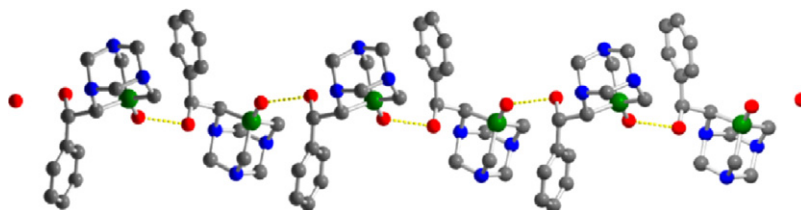
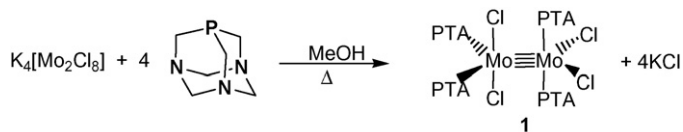
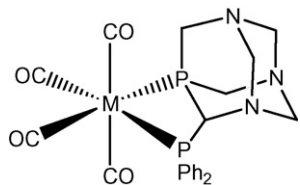


Fig. 1. View of the chain formed by P=O...HO-R hydrogen bonding along the *b* axis in PZA(O). H atoms omitted for clarity. Adapted from ref. [18a].



Scheme 7.



M = W (2), Mo (3)

Chart 3.

hand the two singlets of equal intensity displayed in the ^1H NMR spectrum of **1** in CDCl_3 corresponding to the PTA ligands, indicate that the $^2J_{(\text{PH})}$ is lost. No phosphine exchange is observed when an excess of PTA is added to a CD_2Cl_2 solution of **1**. Protonation of **1** by addition of 2.0 M HCl results on breaking the Mo–Mo bond. The solid-state structure of **1** determined by X-ray crystallography is described as two distorted trigonal bipyramidal Mo centers linked through an equatorial site and rotated $\sim 90^\circ$ with respect to one another. The Mo–Mo separation of 2.13 Å is consistent with a quadruple bond which is favoured by the eclipsed conformation of the ligands and the ability of the compound to have a δ bond.

Tetracarbonyl–molybdenum and tungsten complexes bearing the upper rim PTA-modified ligand PTA-PPh₂ (Chart 3), $[\text{M}(\text{CO})_4(\text{PTA-PPh}_2)]$, M = Mo (**2**), W (**3**), have been reported by Frost et al. [17].

The compounds have been prepared by reacting crude PTA-PPh₂ with $\text{cis-}[\text{M}(\text{CO})_4(\text{NHC}_5\text{H}_{10})_2]$ in degassed dichloromethane. The $^{31}\text{P}\{^1\text{H}\}$ NMR spectrum displays the expected pair of doublets at +37.3 (PPh₂) and –64.9 ppm (PTA), $^2J_{\text{PP}} = 23$ Hz for **2** and at +21.7 (PPh₂) and –89.5 ppm (PTA), $^2J_{\text{PP}} = 26$ Hz for **3**. Comparative electronic spectroscopy and electrochemistry studies between **1** and $[\text{Mo}_2\text{Cl}_4(\text{PPhPh}_2)_4]$ indicate the similar nature of PTA and PPhPh₂ from both an electronic and steric point of view. The solid-state structures of both **2** and **3** contain a distorted octahedral metal center with four CO ligands and the chelating PTA-PPh₂ ligand coordinated in a *cis* fashion. The PTA phosphorus is slightly closer to the metal [2.5040(3) (**2**) and 2.4949(11) Å (**3**)] relative to the PPh₂ phosphorus [2.5548(3) (**2**) and 2.5349(12) Å (**3**)].

For comparison to complex **3** a series of related compounds $[\text{W}(\text{CO})_4(\text{PPh}_3)(\text{PTA})]$ (**4**), $[\text{W}(\text{CO})_4(\text{PTA})_2]$ (**5**) and $[\text{W}(\text{CO})_4(\text{dppm})]$ (**6**) have also been prepared [17]. Each phosphorus in the complexes couples with ^{183}W nucleus, giving rise to satellites in the $^{31}\text{P}\{^1\text{H}\}$ NMR. The strain of the four-membered chelate ring in **3** relative to **4** makes the W–P coupling constants in **4** ca. 33 Hz larger than those of **3**. A comparison of the ν_{CO} region of the IR for a series of group 6 metal carbonyl complexes (Table 1) indicates that PTA-PPh₂ is more electron-donating than $\{(\text{PPh}_3)_2\}$, slightly more electron-donating than dppm (dppm = 1,2-bis(diphenylphosphino)methane), and comparable electronically to $\{(\text{PTA})_2\}$ or a mixture of $\{(\text{PTA})/\text{PPh}_3\}$.

3.2. Manganese and rhenium complexes

Although no manganese complexes containing P-bound PTA has been described, Frost et al. [22] reported the first N-coordinated PTA transition-metal complexes $[\text{MnX}_2(\text{PTA-}\kappa\text{N})_2(\text{H}_2\text{O})_2]$, X = Cl (**7**), Br

Table 1

IR ν_{CO} stretching frequencies of a series of $\text{cis-}[\text{M}(\text{CO})_4\text{L}_2]$ complexes [M = W and Mo; L₂ = (PTA)₂, (PPh₃)₂, PTA-PPh₂, dppm].

Complex ^a	ν_{CO} , cm^{-1}			
	A ₁	A ₂	A ₃	A ₄
$[\text{W}(\text{CO})_4(\text{PTA-PPh}_2)]$ (3)	2018 (m)	1916 (sh)	1899 (vs)	1881 (sh)
$[\text{W}(\text{CO})_4(\text{PPh}_3)(\text{PTA})]$ (4)	2017 (m)	1913 (sh)	1898 (vs)	1879 (sh)
$[\text{W}(\text{CO})_4(\text{PTA})_2]$ (5)	2018 (m)	1917 (sh)	1900 (vs)	1883 (sh)
$[\text{W}(\text{CO})_4(\text{PPh}_3)_2]$	2018 (m)	1939 (m)	1907 (sh)	1889 (vs)
$[\text{W}(\text{CO})_4(\text{dppm})]$ (6)	2018 (m)	1916 (sh)	1904 (vs)	1874 (m)
$[\text{Mo}(\text{CO})_4(\text{PTA})_2]^b$	2022 (m)	1930 (m)	1910 (vs)	1904 (sh)
$[\text{Mo}(\text{CO})_4(\text{PPh}_3)_2]^b$	2023 (m)	1927 (m)	1908 (vs)	1897 (m)
$[\text{Mo}(\text{CO})_4(\text{PTA-PPh}_2)]$ (2)	2022 (m)	1923 (sh)	1908 (vs)	1889 (m)
$[\text{Mo}(\text{CO})_4(\text{dppm})]^c$	2020 (m)	1920 (s)	1907 (vs)	1879 (vs)

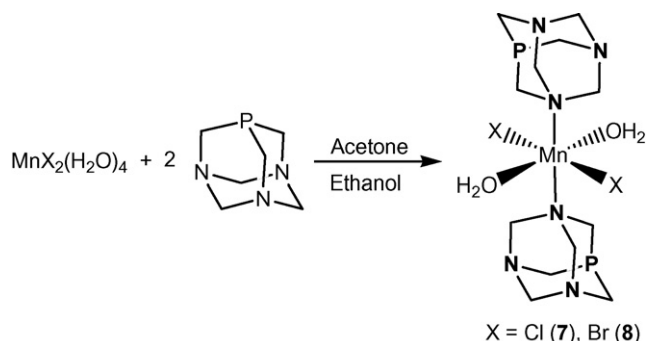
^a Spectra determined in CH_2Cl_2 .

^b Solvent: tetrachloroethylene.

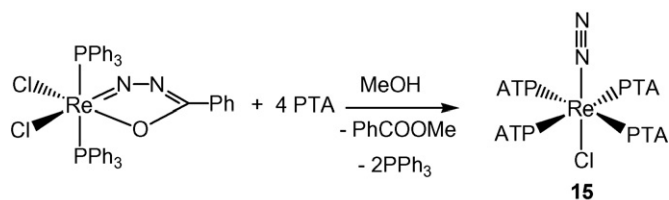
^c Solvent: $\text{ClCH}_2\text{CH}_2\text{Cl}$.

(**8**) (Scheme 8), from the straightforward reaction of hydrated MnX_2 salts and PTA. The N-coordination mode of the PTA ligand is not unexpected due to the *hard* nature of both the Mn(II) center and the N atoms of PTA complex. The solid-state structures of **7** and **8** indicate that both complexes are isomorphous, with the Mn(II) lying on an inversion center in an octahedral environment with two water, two halide, and two N-bound PTA ligands all in a mutually *trans* arrangement. EXAFS spectroscopy data of frozen (20 K) aqueous solution of compounds **7** and **8** suggest that ligand substitution is facile and a variety of substitution isomers are produced upon dissolution.

With the aim to develop new water-soluble precursors of rhenium for radiopharmaceutical applications, Marchi et al. [23] have prepared the new water-soluble Re(V) complexes $[\text{ReO}_2\text{Cl}(\text{PTA})_3]$ (**9**) and $[\text{ReNCl}_2(\text{PTA})_3]$ (**10**) by exchange of PPh_3 with PTA in dioxo- and nitrido-rhenium analogues. Both compounds have been characterized by X-ray diffraction studies showing an approximately octahedral geometry around the Re atoms. Molecules of **9** in the crystals are linked in chains by means of water bridges between oxygen atoms of two vicinal molecules. The stability of compounds **9** and **10** in water and physiological solution (0.154 mol L^{-1}) was tested by $^{31}\text{P}\{^1\text{H}\}$ NMR spectroscopy. The experiments seem to indicate that **9** and **10** undergo partial PTA dissociation which can be reverted by the elimination of water, followed by re-dissolution in organic solvent (CDCl_3). Reaction of **9** with sodium diethyldithiocarbamate gives the water-soluble complex $[\text{ReNCl}(\text{Et}_2\text{dtc})(\text{PTA})_2]$ (**11**) which presents an octahedral geometry with the Cl ligand *trans* to the $\text{Re}\equiv\text{N}$ multiple bond. The dinuclear Re(V) compound $[\text{Re}_2\text{N}_2\text{Cl}_3(\text{Et}_2\text{dtc})(\text{PTA})_4]$ (**12**) was unexpectedly obtained by recrystallization of **11** from a $\text{CH}_2\text{Cl}_2/\text{MeOH}$ mixture [23]. In this compound one molecule of $[\text{ReNCl}(\text{Et}_2\text{dtc})(\text{PTA})_2]$ coordinates with its nitrido ligand to the fragment $[\text{ReNCl}_2(\text{PTA})_2]$. The nitrido bridge is asymmetric and almost linear. $[\text{ReN}(\text{Et}_2\text{dtc})_2(\text{PTA})]$ (**13**) may be



Scheme 8.



Scheme 9.

prepared in two ways with similar yields: either by addition of one equivalent of $\text{Na}(\text{Et}_2\text{dtc})$ to a solution of **11** in CH_2Cl_2 , or by addition of two equivalents of $\text{Na}(\text{Et}_2\text{dtc})$ to a solution of **10**.

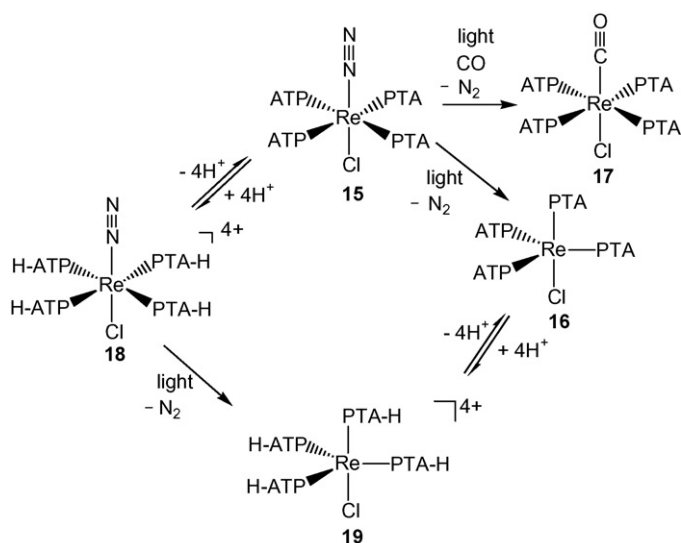
The moderately water-soluble $\text{Re}(\text{III})$ complex $[\text{ReCl}_3(\text{PTA})_2(\text{PPh}_3)]$ (**14**) was prepared by ligand-exchange reaction from $[\text{ReCl}_3(\text{NCMe})(\text{PPh}_3)_2]$ [23]. Compound **14** presents a *mer* arrangement of the three chlorine atoms, two PTA ligands in mutual *trans* positions, and a PPh_3 group *trans* to a Cl atom.

The first dinitrogen PTA complex *trans*- $[\text{ReCl}(\text{N}_2)(\text{PTA})_4]$ (**15**) was prepared by treatment of $[\text{ReCl}_2(\eta^2\text{-NNCOPh})(\text{PPh}_3)_2]$ with an excess of PTA in refluxing methanol in the dark (Scheme 9) [24]. The singlet at -74.8 ppm exhibited by its $^{31}\text{P}\{^1\text{H}\}$ NMR spectrum is indicative of the four equivalent PTA ligands and the N_2 in *trans* position to the Cl ligand. The N_2 ligand is bounded in an “end on” fashion as indicates the presence of a strong and sharp band at 1949 cm^{-1} in the IR spectrum due to $\nu(\text{N}\equiv\text{N})$.

Irreversible loss of N_2 from **15** by sunlight irradiation affords the unsaturated 16-electron complex $[\text{ReCl}(\text{PTA})_4]$ (**16**) according with photoexcitation of an electron from the HOMO to the LUMO which present $\text{Re}-\text{N}_2$ bonding or anti-bonding character, respectively. The pentacoordinate complex **16** can add carbon monoxide yielding the hydrosoluble carbonyl complex *trans*- $[\text{ReCl}(\text{CO})(\text{PTA})_4]$ (**17**) (Scheme 10).

Compound **15** can be fully and reversibly protonated on the N atoms of PTA in aqueous solution with HCl yielding *trans*- $[\text{ReCl}(\text{N}_2)(\text{PTA}-\text{H})_4]\text{Cl}_4$ (**18**) [24]. The N_2 ligand in the fully-protonated complex **18** is photo-labile producing the corresponding pentacoordinated compound $[\text{ReCl}(\text{PTA}-\text{H})_4]\text{Cl}_4$ (**19**) which can also be obtained by protonation of **16** (Scheme 10). NMR and IR spectroscopic studies of a sequential protonation of an aqueous solution of **15** shows that there is no spectroscopic differentiation between PTA and $\text{PTA}-\text{H}$ ligands, supporting fast H^+ scrambling within any of the *trans*- $[\text{ReCl}(\text{N}_2)(\text{PTA}-\text{H})_n(\text{PTA})_{4-n}]^{n+}$ ($n = 1-4$) species.

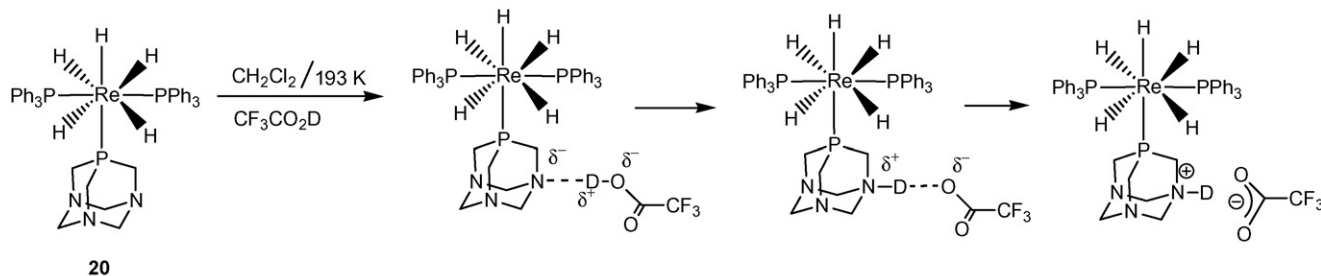
The first rhenium polyhydride complex containing PTA, $[\text{ReH}_5(\text{PPh}_3)_2(\text{PTA})]$ (**20**) was obtained by reaction of $[\text{ReH}_7(\text{PPh}_3)_2]$ with PTA in 1:1 molar ratio [25]. In spite of the presence of PTA, compound **20** is not soluble in water. This complex is highly fluxional in CD_2Cl_2 at room temperature due to fast scrambling of the five hydrides and shows a classical hydride nature both in the solid state and in solution. The X-ray diffraction analysis of



Scheme 10.

20 indicates a dodecahedral environment around the rhenium atom with the bulkier P donors occupying the less sterically hindered B sites of the dodecahedron. Stoichiometric protonation of **20** in CD_2Cl_2 results in the protonation of PTA yielding the cation $[\text{ReH}_5(\text{PPh}_3)_2(\text{PTA}-\text{H})]^+$. When an excess of $\text{HBF}_4\cdot\text{OEt}_2$ is added, a double protonation takes place giving the non-classical (T_1 of the hydride signal = 28 ms at 193 K) dication $[\text{ReH}_4(\eta^2\text{-H}_2)(\text{PPh}_3)_2(\text{PTA}-\text{H})]^{2+}$ which undergoes decomposition when the temperature is raised. IR study of the proton transfer reaction with CF_3COOD gives evidence for the formation of both the hydrogen bonded adduct $[\text{ReH}_5(\text{PPh}_3)_2\{\text{PTA}\cdots\text{DOC}(\text{O})\text{CF}_3\}]$ and the hydrogen bonded ion pair species $[\text{ReH}_5(\text{PPh}_3)_2\{\text{PTA}(\text{D})\cdots\text{OC}(\text{O})\text{CF}_3\}]$ along the reaction pathway eventually transferring a proton to one of the N atoms of PTA (Scheme 11) [25].

The cluster complex $[\text{Re}_6(\mu_3\text{-Se})_8(\text{PET}_3)_5(\text{PTA})](\text{SbF}_6)_2$ (**21**) was obtained as an orange solid by displacement of the labile acetonitrile ligand from $[\text{Re}_6(\mu_3\text{-Se})_8(\text{PET}_3)_5(\text{CH}_3\text{CN})](\text{SbF}_6)_2$ by PTA [26]. A singlet at $\delta -110.3$ ppm in the $^{31}\text{P}\{^1\text{H}\}$ NMR spectrum displayed by this compound in CD_2Cl_2 is the first observation of an upfield shift of the $^{31}\text{P}\{^1\text{H}\}$ resonance of PTA upon formation of a metal complex. X-ray diffraction studies of **21** show that the PTA cage does not have relevant distortions compared to the many reported metal-PTA complexes. Unexpected protonation of one N site of the PTA ligand to give $[\text{Re}_6(\mu_3\text{-Se})_8(\text{PET}_3)_5(\text{PTA}-\text{H})][\text{Re}_6(\mu_3\text{-Se})_8(\text{PET}_3)_5(\text{PTA})](\text{SbF}_6)_5$ (**22**) was observed when **21** was reacted with HgI_2 . The source of protons probably comes from trace amounts of water in the solvents by hydrolysis promoted by the $\text{Hg}(\text{II})$ ion. This protonation causes a noticeably downfield shift of PTA resonance in the $^{31}\text{P}\{^1\text{H}\}$ NMR spectrum (-106.5 ppm, CD_2Cl_2). The orange-red complex **22** contains two cluster units



20

Scheme 11.

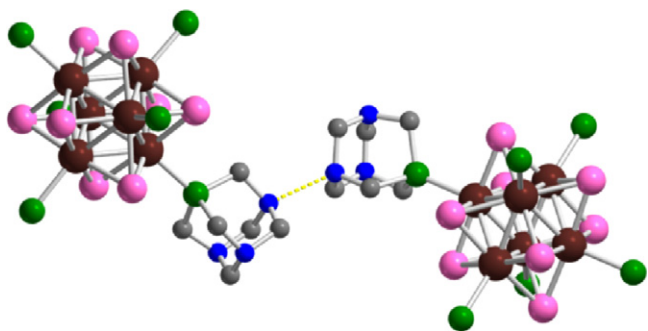


Fig. 2. Part of the crystal lattice of **22**, showing the chain formed by N-H...N hydrogen bonding. H atoms omitted for clarity. Adapted from ref. [26].

disposed in such a way that the two PTA ligands are pointing towards each other with a shortest N...N distance of 2.75(4) Å (Fig. 2).

If compound **21** is protonated with HBr the monoprotonated cluster species $[\text{Re}_6(\mu_3\text{-Se})_8(\text{PEt}_3)_5(\text{PTA-H})_2](\text{HBr})(\text{SbF}_6)_2\text{Br}_4$ (**23**) is obtained as an orange-red crystalline solid. Both protonations cause noticeable distortions on the cage structure: longer N–C bond lengths about the protonated N atom, and C–N(H)–C angles smaller than the angles about the non-protonated N atoms.

3.3. Iron, ruthenium and osmium complexes

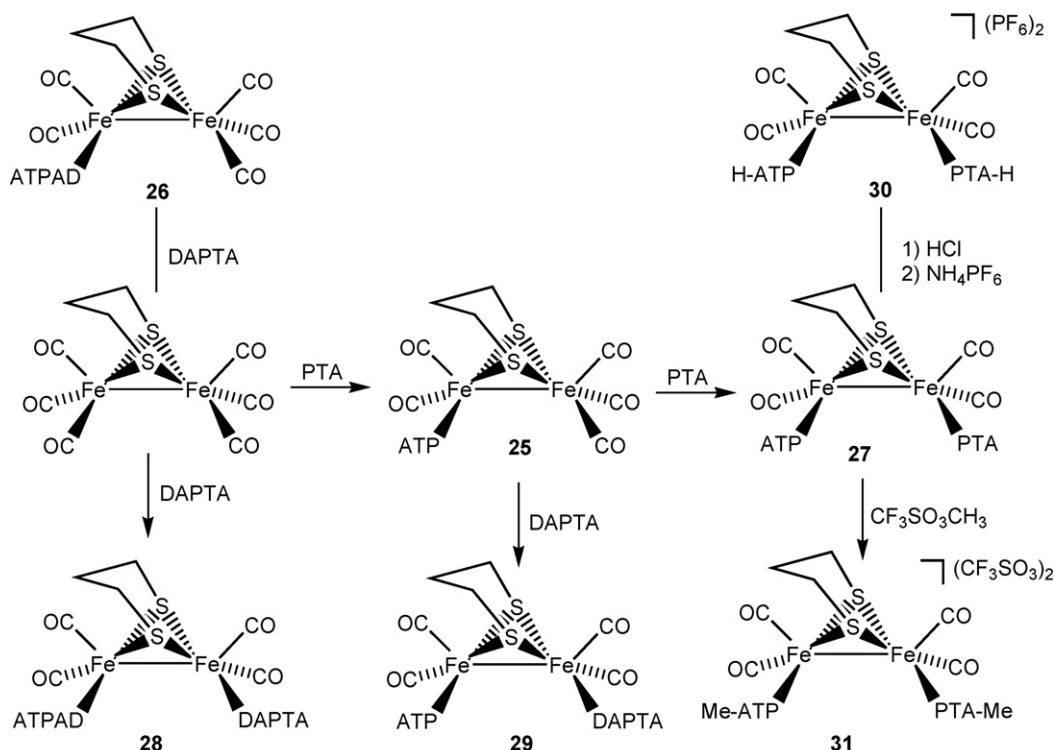
$[\text{Fe}(\text{NO})_2(\text{PTA})_2]$ (**24**) was prepared by refluxing a solution of $[\text{Fe}(\text{CO})_2(\text{NO})_2]$ and PTA in THF [27]. Compound **24** was obtained as a slightly water-soluble red solid. Both phosphorus atoms are equivalent as indicated by the presence of a singlet in the $^{31}\text{P}\{^1\text{H}\}$ NMR spectrum ($\delta = -25.5$ ppm). Its molecular structure shows a tetrahedral environment with the Fe atom on a crystallographic twofold axis. Compound **24** is a member of a family of iron nitrosyl complexes with various water-soluble ligands developed by

Berke et al. for use as NO donor prodrugs. Biophysical measurements using EPR and electrochemistry show that the behaviour as NO donors depends on the nature of the ligand, and those measurements indicate that compound **24** does not behave as NO donor.

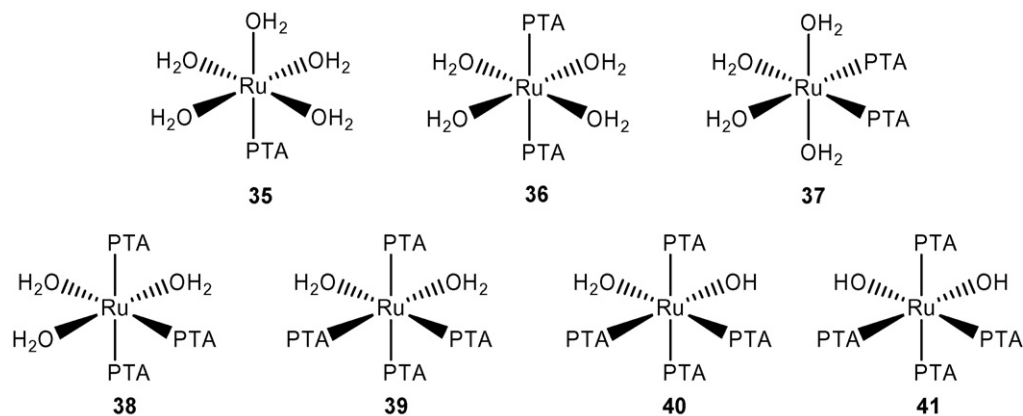
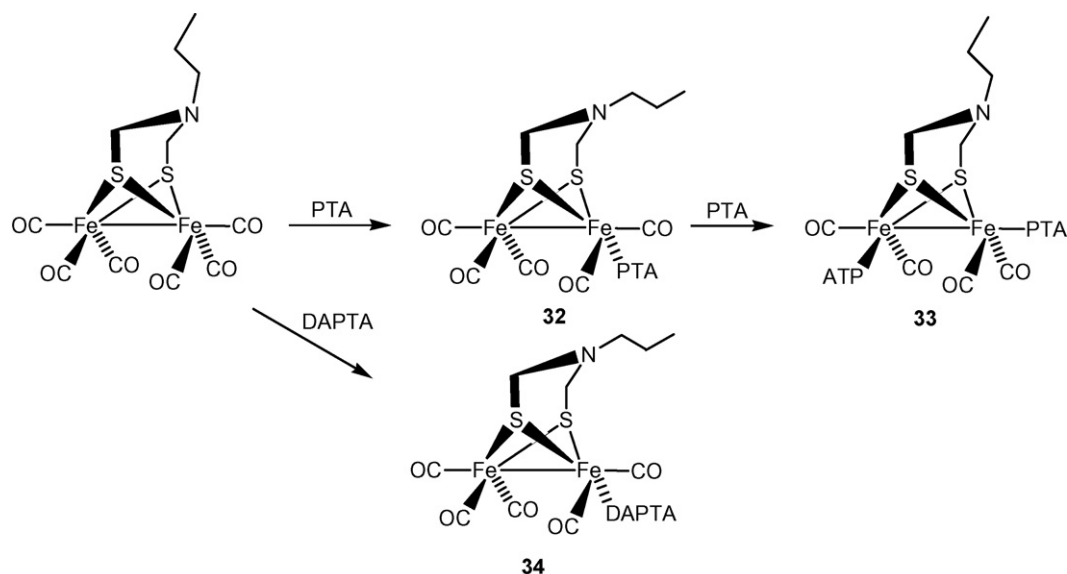
Diiron (μ -dithiolate) complexes with PTA or PTA-derivatives like PTA-H, mPTA or DAPTA were developed to improve hydrophilicity and water solubility on iron hydrogenase model complexes [28]. The complexes $[\{\text{Fe}(\text{CO})_3\}(\mu\text{-pdt})\{\text{Fe}(\text{CO})_2(\text{L})\}]$ [pdt = $-\text{S}(\text{CH}_2)_3\text{S}-$; L = PTA (**25**) [28c], DAPTA (**26**) [28d] and $[(\mu\text{-pdt})\{\text{Fe}(\text{CO})_2(\text{L})\}_2]$ [L = PTA (**27**) [28c] or DAPTA (**28**) [28d]] were obtained by replacing one or two CO ligands in $[(\mu\text{-pdt})\{\text{Fe}(\text{CO})_3\}_2]$ with the phosphine (Scheme 12).

Unsymmetrically PTA- and DAPTA-substituted complex $[\{\text{Fe}(\text{CO})_2(\text{L})\}(\mu\text{-pdt})\{\text{Fe}(\text{CO})_2(\text{L}')\}]$ [L = PTA, L' = DAPTA (**29**) [28d]] was prepared by the reaction of **25** with an excess of DAPTA in refluxing CH_3CN . The molecular structures of the PTA derivatives **25** and **27** show the PTA ligands in the basal positions of the thiolate-edge-bridged, square-pyramidal iron species. In complex **27** both PTA ligands are *transoid* to each other minimizing steric interactions. IR and NMR spectroscopic data show that protonation of **27** with $\text{HCl}/\text{NH}_4\text{PF}_6$ occurs at the tertiary N atom of the PTA ligand yielding the dicationic compound $[(\mu\text{-pdt})\{\text{Fe}(\text{CO})_2(\text{PTA-H})\}_2](\text{PF}_6)_2$ (**30**). In a similar way, treatment of **27** with the methylating agent $\text{CF}_3\text{SO}_3\text{CH}_3$ gives the PTA-methylated compound $[(\mu\text{-pdt})\{\text{Fe}(\text{CO})_2(\text{mPTA})\}_2](\text{CF}_3\text{SO}_3)_2$ (**31**) [28c].

Further attempts to prepare closer structural models of the diiron subsite were developed by Wang et al. [28a] by introducing not only water-soluble PTA or PTA-derivatives as ligands, but also a nitrogen heteroatom on the dithiolate bridge (Scheme 13). Thus, compounds $[\{\text{Fe}(\text{CO})_3\}(\mu\text{-adt})\{\text{Fe}(\text{CO})_2(\text{PTA})\}]$ (**32**), $[(\mu\text{-adt})\{\text{Fe}(\text{CO})_2(\text{PTA})\}_2]$ (**33**), and $[\{\text{Fe}(\text{CO})_3\}(\mu\text{-adt})\{\text{Fe}(\text{CO})_2(\text{DAPTA})\}]$ (**34**) (adt = $-\text{S}-\text{CH}_2-\text{N}(\text{CH}_2\text{CH}_2\text{CH}_3)-\text{CH}_2-\text{S}-$), were prepared by CO substitution in $[(\mu\text{-adt})\{\text{Fe}(\text{CO})_3\}_2]$ with PTA or DAPTA ligands. Complexes **32–34** are not soluble in neat water, but they show good



Scheme 12.



solubility in mixtures such as $\text{CH}_3\text{CN}/\text{H}_2\text{O}$ [28a]. X-ray diffraction analysis of both **32** and **33** show that they are structurally similar to compounds **25** and **27**, respectively. Protonation of compounds **29–31** with a strong acid only occurs at the bridging-N atom, rather than at the tertiary atom on the PTA or DAPTA ligands, as ^1H NMR and IR data indicate.

In recent years, most of the reports about new transition-metal complexes of PTA and derivatives concern the use of ruthenium, principally due to the catalytic and medicinal properties of such complexes. As aquo complexes are particularly suited to serve as catalyst precursors in aqueous organometallic catalysis, Kovács et al. [10] investigated the reaction of $[\text{Ru}(\text{H}_2\text{O})_6]^{2+}$ with PTA and mPTA in order to establish the composition of the species formed in solution. These studies required a careful control of pH to avoid hydrolysis of $[\text{Ru}(\text{H}_2\text{O})_6]^{2+}$ (above pH 6) and protonation of PTA (below pH 6.5) and most of them were performed around pH 6. Depending on the $[\text{PTA}]:[\text{Ru}]$ ratio, mixtures of several compounds were obtained (Chart 4).

Extensive $^{31}\text{P}\{^1\text{H}\}$ NMR studies have allowed the determination of spectroscopic features of the various Ru(II)-PTA complexes as shown in Table 2. At 2:1 PTA/Ru ratio, the main species is **35**. At higher ratios (15:1) compound **35** is gradually replaced by compounds **36** and **37** but the other compounds are present in very low (**38**) or negligible amounts (**39–41**).

mPTA derivatives *trans*- $[\text{Ru}(\text{H}_2\text{O})_4(\text{mPTA})_2](\text{tos})_4 \cdot 2\text{H}_2\text{O}$ (tos = *p*-toluenesulfonate) (**42**) and *trans-mer*- $[\text{Ru}_2(\text{H}_2\text{O})(\text{mPTA})_3]\text{I}_3 \cdot 2\text{H}_2\text{O}$ (**43**), were obtained by reaction of $[\text{Ru}(\text{H}_2\text{O})_6](\text{tos})_2$ with (mPTA)(tos) and (mPTA)I/KI respectively [10a]. X-ray structural

Table 2

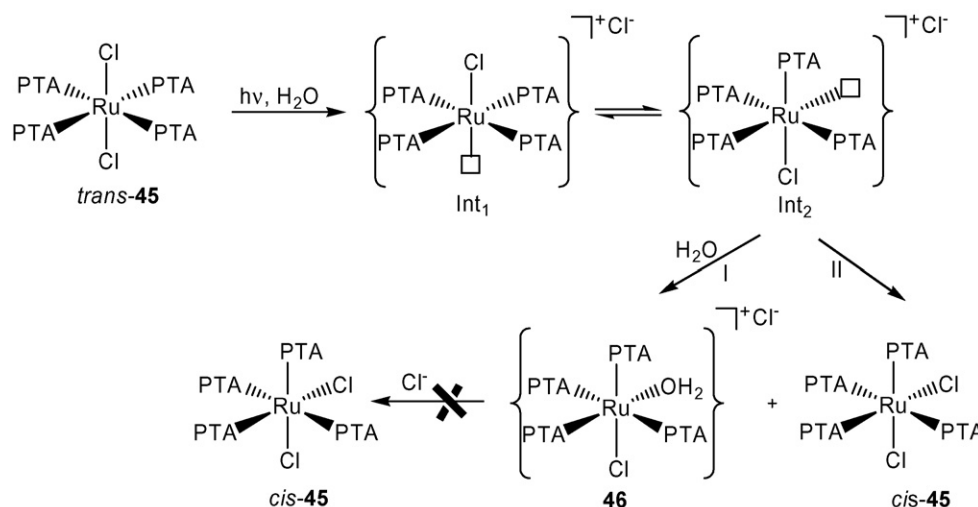
$^{31}\text{P}\{^1\text{H}\}$ NMR spectroscopic data of the species formed in the reaction between $[\text{Ru}(\text{H}_2\text{O})_6]^{2+}$ and PTA^a.

Compound	Chemical shift(s) (δ /ppm) and coupling constant(s) ($^2J_{\text{P-P}}/\text{Hz}$)
$[\text{Ru}(\text{H}_2\text{O})_5(\text{PTA})]^{2+}$ 35	−41.3 (s)
$[\text{Ru}(\text{H}_2\text{O})_4(\text{PTA})_2]^{2+}$ 36 , 37	−49.7 (s) ^b ; −50.1 (s) ^b
$[\text{Ru}(\text{H}_2\text{O})_3(\text{PTA})_3]^{2+}$ 38	−7.4 (t) {30.1}, −48.3 (d) {30.1}
$[\text{Ru}(\text{H}_2\text{O})_2(\text{PTA})_4]^{2+}$ 39 ^c	−16.5 (t) {27.0}, −46.4 (t) {27.0}
$[\text{Ru}(\text{H}_2\text{O})(\text{OH})(\text{PTA})_4]^+$ 40 ^c	−13.3 (dt) {30.6, 34.0}, −23.4 (dt) {26.0, 34.0}, −53.1 (dd) {26.0, 30.6}
$[\text{Ru}(\text{OH})_2(\text{PTA})_4]^+$ 41 ^c	−17.1 (t) {27.6}, −51.8 (t) {27.6}

^a Conditions: $[\text{Ru}] = 8.31 \times 10^{-2} \text{ M}$, $[\text{PTA}] = 1.25 \text{ M}$, D_2O , $T = 44^\circ \text{C}$, pH 6.29.

^b *cis*- and *trans*- $[\text{Ru}(\text{H}_2\text{O})_4(\text{PTA})_2]^{2+}$ could not be distinguished.

^c $[\text{RuX}_2(\text{PTA})_4]^{2+}$ ($\text{X} = \text{H}_2\text{O}$ or OH^-) gave closely similar $^{31}\text{P}\{^1\text{H}\}$ -NMR spectra; assignments are based on the changes of signal intensities upon variation of pH.



Scheme 14.

determination of **42** and **43** shows that, in both compounds, the coordination sphere of ruthenium is distorted octahedral. In compound **42**, the two phosphine ligands are in *trans* positions and the plane of the four water ligands dissects the molecule. In complex **43** the three mPTA ligands are in *mer* position leading to the weakest electrostatic repulsion among the charged ligands. The protonated PTA ruthenium complex *trans*-[Ru(H₂O)₄(PTA-H)₂](tos)₄·2H₂O (**44**) was obtained by reacting [Ru(H₂O)₆](tos) with PTA in water acidified (pH 4) with *p*-toluenesulfonic acid. The structural parameters determined by X-ray crystallography are similar to those of compound **42** [10].

The chemistry of compound [Ru(PTA)₄Cl₂] (**45**) was revisited by Mebi and Frost [29] and more recently by Girotti et al. [30], being a subject of some controversy. Thus, Mebi and Frost, in contrast with what was previously published, claim that reaction of RuCl₃ with PTA does not yield the *cis* (**cis-45**) but the *trans* isomer (**trans-45**) which undergoes isomerization in solution yielding the *cis* isomer. The *trans* isomer was isolated and structurally characterized by X-ray crystallography. The ruthenium center is in a distorted-octahedral environment. Isomerization was studied in chloroform, water and acidic (HCl) solution by ³¹P{¹H} NMR spectroscopy. In CDCl₃ the singlet at −49.29 ppm, corresponding to the *trans* isomer, is progressively replaced by two triplets at −23.40 and −57.64 ppm (²J_{PP} = 21.7 Hz) corresponding to the *cis* isomer. Equilibrium between both isomers is reached in a week (K_{eq} ~ 1.84). In D₂O the isomerization is almost complete over a period of a week with the singlet at −51.62 ppm (*trans* isomer) being replaced by two triplets at −24.0 and −54.9 ppm (²J_{PP} = 22.7 Hz) (*cis* isomer) and other signals of unidentified products. In acidic (2 mM HCl) solution the ³¹P{¹H} NMR spectrum shows that the signal correspondent to the *trans* isomer (−49.41 ppm) is totally replaced over a two-week period by two triplets of the *cis* isomer at −24.45 and −55.19 ppm (²J_{PP} = 22.7 Hz). Other signals tentatively assigned to [Ru(PTA-H)(PTA)₂Cl₃] [−4.54 (t), −43.88 (d) ppm, ²J_{PP} = 28.2 Hz] were also observed. On the other hand, Girotti et al. [30] found that the aforementioned *trans-cis* isomerization can be easily and quantitatively reached by visible light in CHCl₃. When the reaction is carried out in the dark at room temperature, the transformation does not occur. Besides, irradiation at 367 nm of a solution of the *cis*-product in CHCl₃ produces a complete conversion in about 20 min, showing the reversibility of the isomerization reaction. Photoaquation of the *trans-45* to give *cis*-[Ru(PTA)₄(H₂O)Cl]Cl (**46**) (95%) and *cis-45* (5%) is observed when a 1.5 mM solution in water is irradiated for 40 min. with visible light. A dissociative mechanism for this process is proposed (Scheme 14).

Reaction of the **trans-45** isomer with excess of sodium formate afforded the water-soluble ruthenium hydride *cis*-[Ru(PTA)₄H₂] (**47**) [29]. The ¹H and ³¹P{¹H} NMR spectra in D₂O are consistent with those previously reported. The IR spectrum shows a broad absorbance at 1800 cm^{−1} assigned to the ν(Ru–H) stretching mode. An aqueous solution of **47** does not show evidence of decomposition, ligand protonation or exchange over a week, but undergoes H/D exchange in D₂O affording *cis*-[Ru(PTA)₄D₂] as confirmed by the disappearance of the hydride resonance in the ¹H NMR spectrum and the isotopic shift of 497 cm^{−1} of the ν(Ru–D) absorbance with respect to the ν(Ru–H) band in the IR spectrum. Colourless block crystals of **47** were analyzed by X-ray diffraction. Six equiv of water co-crystallise with **47** and form hydrogen bonding with the nitrogen atoms of the PTA ligands [29].

Black crystals of [RuCl₄(PTA-H)₂]·4H₂O (**48**) were isolated when the crude product, obtained by reaction of excess of PTA with hydrated RuCl₃, was recrystallized from water solutions after 2 weeks standing on air [31]. The structure of **48** consists of slightly distorted octahedral molecules of the complex and clathrated water molecules in the 1:4 ratio. The phosphine ligands are *trans* to each other and the 3D architecture is mainly governed by the network of hydrogen bonding interactions between water molecules and the N-protonated ligand (Fig. 3).

The complex *trans*-[RuCl(L)(PTA-H)₂]Cl₂ (**49**) (L = 2-acetylpyridine N⁴,N⁴-dimethylthiosemicarbazone) was synthesized by reacting [RuCl₂(dmso)₄] with the thiosemicarbazone and PTA ligands in absolute ethanol [32]. The red compound obtained is highly water soluble (S_{25°C} ≥ 250 mg mL^{−1}) and it is claimed to be the first reported Ru(II) complex bearing a thiosemicarbazone and PTA ligands. Complex **49** shows two well-resolved MLCT transitions at 450 and 378 nm in its electronic absorption spectra attributed to Ru(4dπ) → π*(py) and Ru(4dπ) → π*(imine) transitions, respectively. The hydrazinic NNH proton signal (δ = 14.42 ppm in the ¹H NMR spectrum of the free thiosemicarbazone ligand), is absent in the complex, indicating the deprotonation of the ligand upon complexation. The ³¹P{¹H} NMR spectrum of **49** displays one singlet resonance at δ = −38.13 ppm indicating the presence of two equivalent PTA ligands. Comparative electrochemical studies between complex **49** and [Ru(L)Cl(PPh₃)₂] show a more positive oxidation response (+140 mV) in complex **49** in line with the poorer electron-donating ability of PTA compared to PPh₃ [32]. The crystal structure of **49** shows the ruthenium ion coordinated by the thiosemicarbazone ligand through the pyridine and imine N and the thiolate S atoms in the equatorial plane of a distorted octahedron. The fourth position is occupied by the Cl ligand and both axial positions are

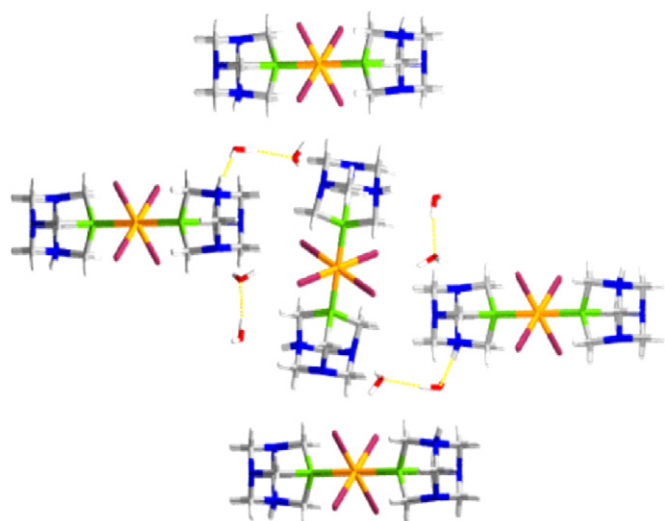


Fig. 3. Wireframe representation of the crystal lattice of **48**, showing the extensive hydrogen bonding network. Atom colour code: P, green; C, gray; N, blue; Cl, purple; H, white; Ru, orange. H bonding depicted in yellow. Adapted from ref. [31].

occupied by two PTA-H ligands whose N-protonated atoms are involved in hydrogen bonding to the two chloride contraanions [32]. $^{31}\text{P}\{^1\text{H}\}$ NMR studies of aqueous (D_2O) solutions of **49** at different pD values show that a solution of **49** in D_2O in the pD range 2.11–11.40, undergoes both protolytic reactions and hydrolysis of the Ru–Cl bond. Studies of antiproliferative activity in cancer cell lines show that **49** exerts a pH-dependent activity *in vitro* in micromolar concentrations (see Section 5).

The cycloruthenated compound *trans*-[Ru(C_6H_4 -2- $\text{C}_4\text{H}_4\text{N}$)(NCMe) $_3$ (PTA)](PF_6) (**50**) was synthesized by reacting one equiv of PTA to a solution of the cycloruthenated compound [Ru(C_6H_4 -2- $\text{C}_5\text{H}_4\text{N}$)(NCMe) $_4$](PF_6) at room temperature [33]. Compound **50** (Chart 5) exists as only one regioisomer as indicated by the ^1H and $^{31}\text{P}\{^1\text{H}\}$ NMR spectra. The single-crystal X-ray diffraction analysis reveals a distorted octahedral geometry around the Ru atom with the PTA ligand *trans* to the metalated arene. Compound **50** is sufficiently water soluble (3.2 mM) to permit to observe, by ^1H NMR in D_2O , that the MeCN ligands are not displaced by water. The activity as *in vitro* cell growth inhibitor of compound **50** was tested and, in contrast with similar cycloruthenated compounds bearing other phosphines (PMe_2Ph , PPh_3 , dppe), compound **50** displays a disappointingly very low activity (see Section 5).

The ruthenium(II) complexes *mer-trans*-[RuCl $_2$ (PTA) $_2$ { κ^2 (*P,N*)-FcPN}] (**51**) and *fac*-[RuCl $_2$ (PTA) $_2$ { κ^2 (*P,N*)-FcPN}] (**52**) bearing PTA and the chiral ligand (4*S*)-2-[(*Sp*)-2-(diphenylphosphino)ferrocenyl]-4-(isopropyl)oxazoline (FcPN) were prepared and their catalytic activity in asymmetric transfer hydrogenation of ketones has been explored (see Section 4) [34]. Complex **51** is obtained stereoselectively by reacting [RuCl $_2$ (PPh $_3$)]{ κ^2 (*P,N*)-FcPN} with PTA in CH_2Cl_2 at room temperature. $^{31}\text{P}\{^1\text{H}\}$ NMR spectrum shows a three set of signals (ABX spin system), namely a triplet at δ 43.6 ($^2J_{\text{PP}}$ = 28 Hz), and two doublet of doublets at δ –54.8 and –72.7 ppm

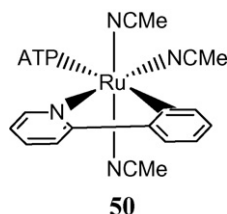


Chart 5.

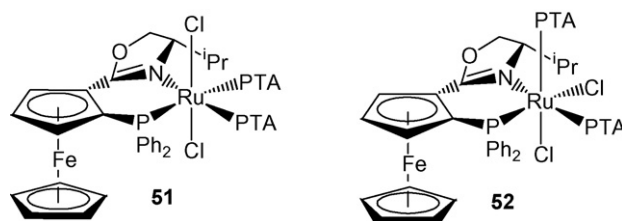


Chart 6.

($^2J_{\text{PP}}$ = 319 and 28 Hz, respectively). When a solution of this complex in MeOH is stirred at room temperature for 10 min. it affords the *fac*-isomer **52**. $^{31}\text{P}\{^1\text{H}\}$ NMR spectrum shows a doublet of doublets (PPh $_2$ group) at δ 37.1 ppm ($^2J_{\text{PP}}$ = 34 and 33 Hz) and two triplets (PTA) at δ –30.8 ($^2J_{\text{PP}}$ = 33 Hz) and –35.0 ($^2J_{\text{PP}}$ = 34 Hz) ppm (Chart 6).

A number of half-sandwich arene ruthenium complexes bearing PTA or PTA-derivatives were studied due to their applications in medicinal chemistry and catalysis. In order to explain the mono- and di-substitution reactions of PPh $_3$ when starting from the precursor [CpRuCl(PPh $_3$) $_2$], a theoretical study about the reaction of [CpRuCl(PPh $_3$) $_2$] with mPTA to obtain [CpRuCl(mPTA)(PPh $_3$)] $^+$ or [CpRuCl(mPTA) $_2$] $^{2+}$ was carried out using UFF molecular mechanics and DFT methods [35]. The results show that bis-substitution is energetically more demanding in the case of mPTA, as observed experimentally. The calculated free energies (ΔG at 298 K) in acetone for the reactions of monosubstitution and bis-substitution of PPh $_3$ by mPTA were –31.4 and +37.6 kcal mol $^{-1}$, respectively.

Frost and Mebi reported on the solid-state structure of the previously published compound [CpRuCl(PTA) $_2$] (**53a**) [36]. Two equiv of water cocrystallize with the piano-stool complex **53a** giving hydrogen bonding with the N atoms of PTA. The packing of the complex creates a channel with the water molecules pointing towards the center of the channel (Fig. 4). Reaction of an aqueous solution of **53a** with HPF $_6$ yields the PTA-protonated compounds [CpRuCl(PTA-H)(PTA)](PF_6) (**54**) and [CpRuCl(PTA-H) $_2$](PF_6) $_2$ (**55**) as a function of the amount of acid employed [37]. Both compounds were structurally resolved by X-ray analysis and they show very

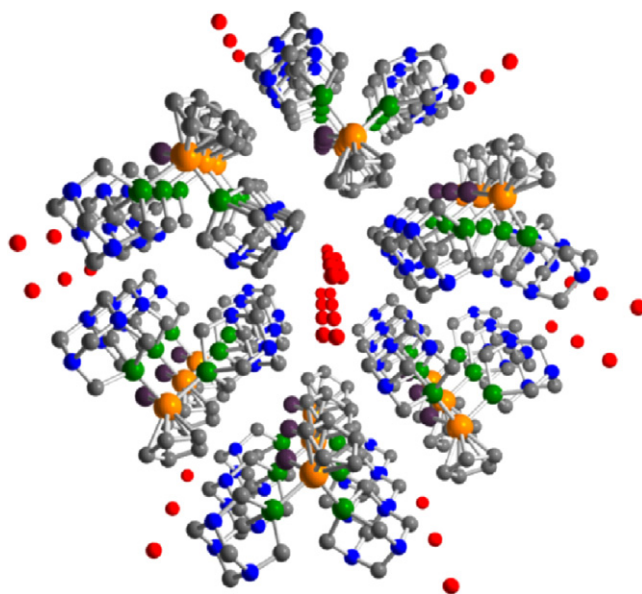
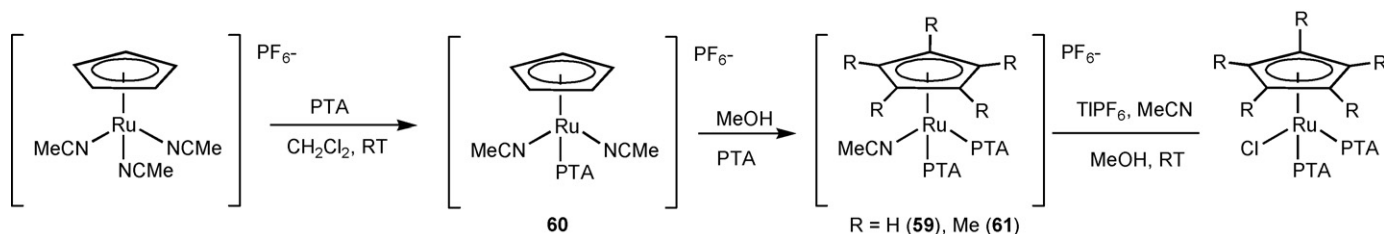


Fig. 4. Channels along the *c* axis containing water molecules in the crystal lattice of **53a**. H atoms omitted for clarity. Atom colour code: P, green; C, gray; N, blue; Cl, purple; Ru, orange. Adapted from ref. [36].



Scheme 15.

similar piano-stool structures, with the PTA ligands bound to the Ru atom through the phosphorus, as expected.

Reaction of **53a** with 1 equiv of AgOTf in dmsO does not produce the expected $[\text{CpRu}(\text{OTf})(\text{PTA})_2]$ (**56**) but a mixture of $[\text{CpRu}(\text{PTA})_2(\text{dmsO})]\text{OTf}$ (**57**) (singlet at $\delta = -28.13$ ppm in the $^{31}\text{P}\{^1\text{H}\}$ NMR spectrum in $\text{dmsO}-d_6$) and the bimetallic polymer $\{[\text{CpRu}(\text{PTA})_2(\text{dmsO})]\{\text{AgCl}_2\}\}_\infty$ (*vide infra*) (**58**). Conversely, the neutral bis-PTA complex **56** can be obtained by reaction of **53a** with $\text{Ti}(\text{OTf})$ in CHCl_3 , as an orange solid in good yield (85%) [38].

The cationic mono- and bis-PTA ruthenium complexes $[\text{CpRu}(\text{PTA})_2(\text{MeCN})(\text{PF}_6)]$ (**59**), $[\text{CpRu}(\text{PTA})(\text{MeCN})_2](\text{PF}_6)$ (**60**) $[\text{Cp}^*\text{Ru}(\text{PTA})_2(\text{MeCN})(\text{PF}_6)]$ (**61**, $\text{Cp}^* = \eta^5$ -pentamethylcyclopentadienyl) were prepared in good yields as depicted in Scheme 15. In addition, halogen exchange between a methanol solution of **53** and excess of KI, stirred at room temperature for 16 h, yields the water-soluble ($S_{25^\circ\text{C}} = 10 \text{ mg mL}^{-1}$) iodo complex $[\text{CpRuI}(\text{PTA})_2]$ (**62**) as an orange solid [39].

The complex $[\text{CpRu}(\text{CN})(\text{PTA})_2]$ (**63**) is prepared by reaction of **53a** with KCN in water at room temperature [40]. The complex is soluble in water ($S_{25^\circ\text{C}} = 280 \text{ g L}^{-1}$) and was characterized by IR and NMR spectroscopies. X-ray structure determination show that the complex is similar to the precursor complex except that the Cl^- ligand is substituted by cyanide. The organometallic polymer $\{[\text{Cp}(\text{PTA})_2\text{Ru}-(\mu\text{-CN})\text{-RuCp}(\text{PTA})_2]\{\text{Au}(\text{CN})_4\}\}_\infty$ (**64**) is obtained by reaction of **53a** with KCN and $\text{K}[\text{Au}(\text{CN})_4]$ in water at room temperature (Chart 7) [40].

This product can be alternatively prepared by reaction of **63** with $\text{K}[\text{Au}(\text{CN})_4]$ but in lower yields. The complex is air-stable in both solid state and solution and is water soluble (3.5 g L^{-1}). The $^{31}\text{P}\{^1\text{H}\}$ NMR spectrum in D_2O shows two singlets at $\delta -19.21$ and -21.82 ppm, corresponding to two magnetically inequivalent PTA ligands, but no coupling is observed between them. Recrystallization from a DMSO solution provided crystals suitable for X-ray diffraction (Fig. 5). The compound is a linear chain poly-

mer formed from alternating $[\text{CpRu}(\mu\text{-CN})\text{RuCp}]^+$ moieties and $[\text{Au}(\text{CN})_4]^-$ anions with bridging PTA ligands between the metal aggregates $[\text{d}(\text{Ru} \cdots \text{Au}) = 7.09(1) \text{ \AA}]$. The $\text{Ru}_2\text{-Au}$ chains form a 3D array by electrostatic interactions and hydrogen bonds between the $[(\text{PTA})_2\text{CpRu}(\mu\text{-CN})\text{RuCp}(\text{PTA})_2]^+$ and $[\text{Au}(\text{CN})_4]^-$ units. The bidimensional arrays are stacked in the lattice by a hydrogen-bonding network of water molecules. Complex **64** is a thermosensitive inorganic microgel. Dynamic light-scattering studies show that the polymer does not dissociate in water but associates to form stable microparticles that reversibly swell or shrink in response to external temperature changes.

The water-soluble bis-PTA half-sandwich complex $[\text{DpRuCl}(\text{PTA})_2]$ ($\text{Dp} = 1,2$ -dihydropentalenyl) (**65**) was obtained in an excellent yield (>98%) by refluxing excess of PTA and $[\text{DpRuCl}(\text{PPh}_3)_2]$ in toluene [41]. The $^{31}\text{P}\{^1\text{H}\}$ NMR spectrum in CDCl_3 shows a singlet at -27.3 ppm, 2 ppm downfield shifted from that of $[\text{CpRuCl}(\text{PTA})_2]$ (**53a**) and 7 ppm upfield shifted from the Cp^* analogue $[\text{Cp}^*\text{RuCl}(\text{PTA})_2]$ (**53b**). By contrast, the $^{31}\text{P}\{^1\text{H}\}$ NMR spectra of both **53a** and **65** in D_2O contain two sets of resonances with concentration-dependent intensities, indicating the existence of an equilibrium between chloride and aquo-complexes with equilibrium constants of 6.18×10^{-4} (**53a**) and 5.08×10^{-4} (**65**) (Scheme 16). The solid-state structure of **65** shows a typical piano-stool structure with two PTA ligands, a chloride, and a η^5 -coordinated C_8H_9^- ligand. The P-Ru-P bond angle (93.2°) is slightly smaller than that of the Cp analogue (96.8°) but similar to that of Cp^* analogue (93.3°) suggesting that Dp and Cp^* ligands have similar stereoelectronic influence on the metal center [41].

Mixed PPh_3/PTA and PPh_3/mPTA complexes similar to compounds **53a** and **62**, namely $[\text{CpRuCl}(\text{PPh}_3)(\text{PTA})]$ (**66**), $[\text{CpRuI}(\text{PPh}_3)(\text{PTA})]$ (**67**), $[\text{CpRuCl}(\text{PPh}_3)(\text{mPTA})]\text{OTf}$ (**68**),

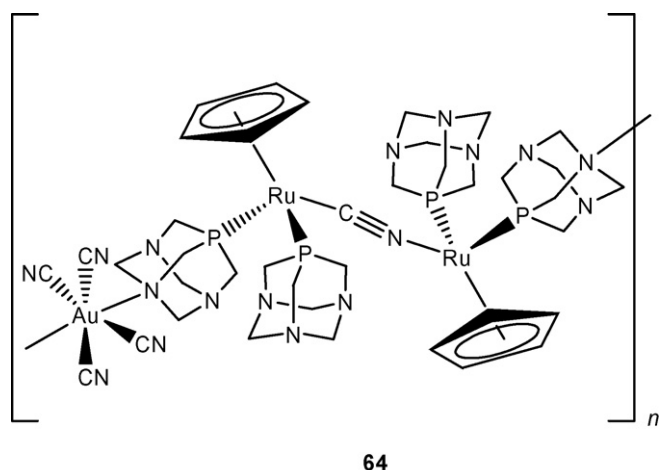


Chart 7.

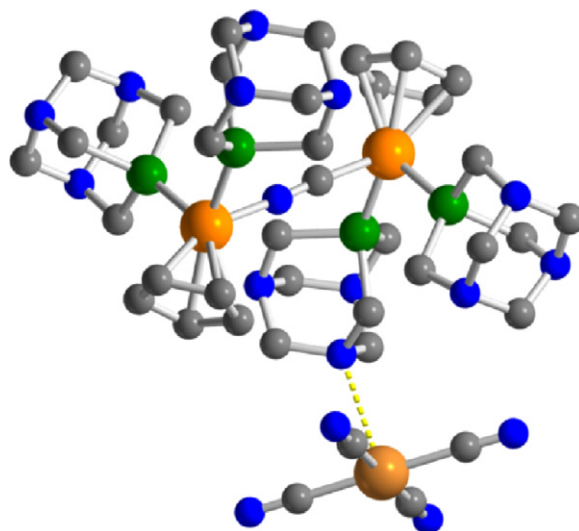
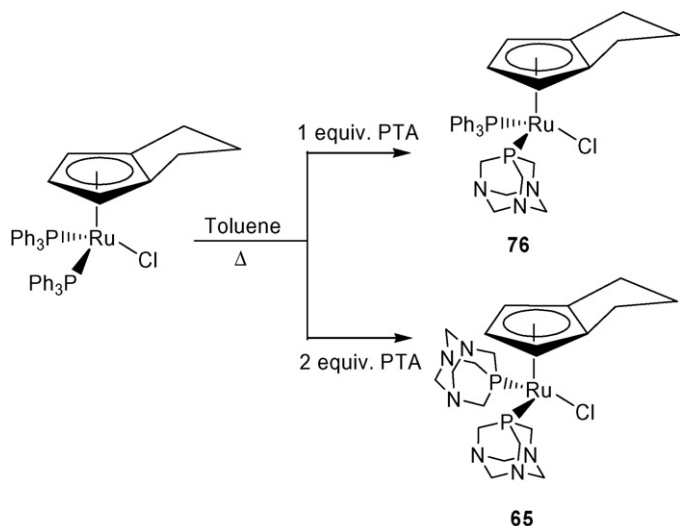


Fig. 5. Repeating unit in the X-ray crystal structure of **64**. H atoms omitted for clarity. Adapted from ref. [40].



Scheme 16.

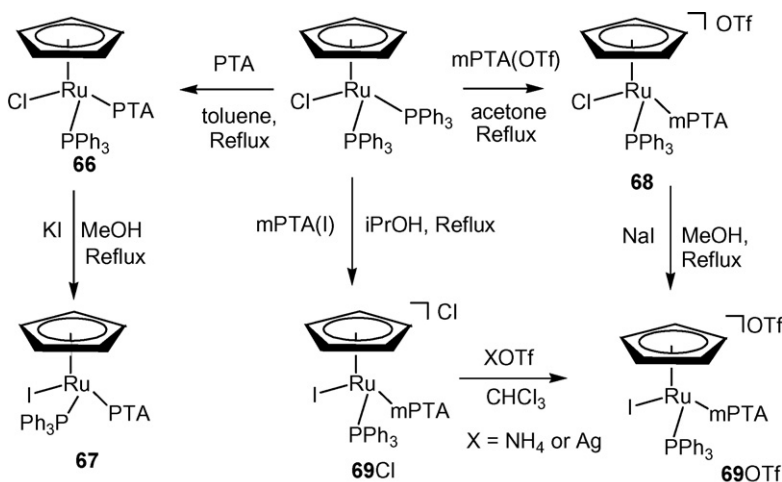
$[\text{CpRu}(\text{PPh}_3)(\text{mPTA})]\text{X}$ [$\text{X} = \text{Cl}$ (**69-Cl**), OTf, (**69-OTf**)], respectively, were prepared by Romero et al. [11a] to study the interaction with DNA (Scheme 17). The complexes are air-stable in both solid state and solution and do not undergo significant halide substitution in water. Substitution of PTA by PPh_3 strongly reduces the water solubility of the compounds. The chloride derivatives **66** and **68** are only slightly soluble in water and the Cl/I substitution makes compounds **67** and **69** practically insoluble in water. The existence of two doublets in the $^{31}\text{P}\{^1\text{H}\}$ NMR spectra of **66–69** clearly indicates the presence of two different phosphines. Substitution of the chloride by the iodide ligand shifts both doublets to high field, being the PTA resonance more susceptible to the Cl/I substitution. Compounds **66–69** are chiral-at-metal and the X-ray crystal structures for **66**, **67**, and **69-OTf** show the

expected piano-stool structures of a racemic mixture of the two possible enantiomers. Although the cone angle for PTA and mPTA is practically the same, the mPTA compound **69-OTf** shows a more pronounced octahedral distortion around the metal (P1-Ru-P2 angles: $100.12(8)^\circ$ for **69-OTf**; $97.31(4)^\circ$ for **67**).

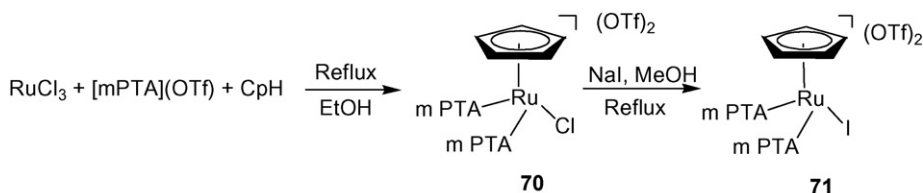
Attempts to obtain a bis-(mPTA) ruthenium compound by using the standard procedure of treating $[\text{CpRuCl}(\text{PPh}_3)_2]$ with excess of mPTA failed, the mixed PPh_3/mPTA compound being only obtained [11a]. Instead, $[\text{CpRuCl}(\text{mPTA})_2](\text{OTf})_2$ (**70**) was obtained by treating $\text{RuCl}_3 \cdot x\text{H}_2\text{O}$ with (mPTA)OTf and freshly cracked dicyclopentadiene, although in very poor yield (13%) (Scheme 18). The analogous iodide derivative (**71**) is easily obtained by chloride substitution via reaction with NaI. Singlets in the $^{31}\text{P}\{^1\text{H}\}$ NMR spectra at -10.74 (**70**) and -15.02 (**71**) ppm in D_2O , support the formulation proposed [11a]. An improved synthetic pathway for **70** and **71** has been published very recently [11b].

A modification on the Cp ring of compounds **53a** and **59** by introducing a hemilabile arm bearing a tertiary amine group was accomplished by Bolaño et al. [39] aiming to increase the catalytic performance in the selective hydrogenation of activated olefins. The synthesis of $[\{\text{Cp}(\text{CH}_2)_2\text{NEt}_2\}\text{RuCl}(\text{PTA})_2]$ (**72**) implies the reaction of the aminocyclopentadienyl ligand with $[\text{RuCl}_2(\text{PPh}_3)_3]$ followed by a metathesis reaction with excess of PTA (Scheme 19). Reaction of **72** with NH_4PF_6 in MeOH affords the N-coordinated complex $[\{\text{Cp}(\text{CH}_2)_2\text{NEt}_2\}\text{Ru}(\text{PTA})_2](\text{PF}_6)$ (**73**), but if this reaction is performed in the presence of a more coordinating solvent such as MeCN, the complex $[\{\text{Cp}(\text{CH}_2)_2\text{NEt}_2\}\text{Ru}(\text{MeCN})(\text{PTA})_2](\text{PF}_6)$ (**74**) is obtained, probing the hemilability of the N-arm.

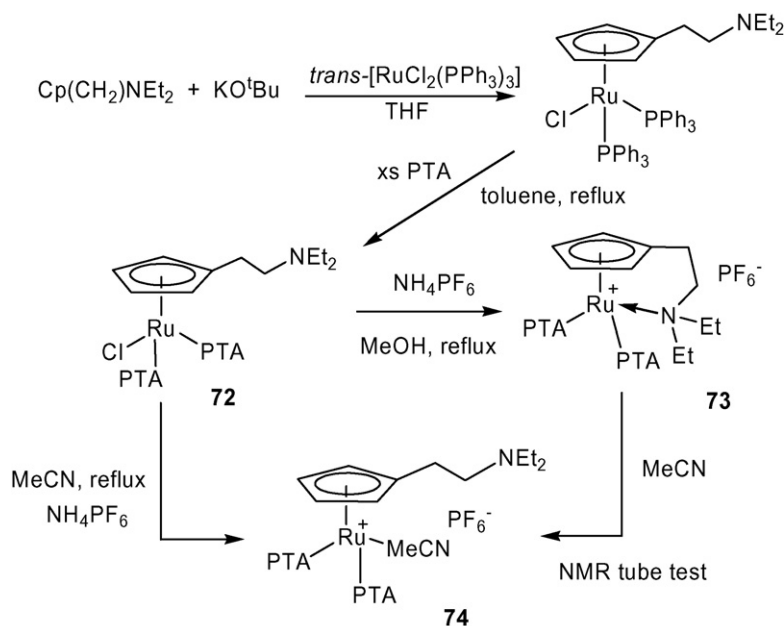
A dimeric version of **72** N-protonated at the amine group and on one PTA ligand for each dimeric unit, $[\{\text{Cp}(\text{CH}_2)_2\text{NHEt}_2\}\text{Ru}(\text{PTA})(\text{MeCN})(\mu\text{-}(\text{PTA-H})(\text{PTA}))\text{Ru}\{\text{Cp}(\text{CH}_2)_2\text{NHEt}_2\}(\text{PTA})(\text{MeCN})](\text{PF}_6)_5$ (**75**), was obtained by recrystallization from a diluted water solution of the crude product from the synthesis of **72**. The X-ray diffraction study shows that the two units of the dimer are connected by two PTA ligands sharing a proton laying on a special position, equally distant from the two N atoms



Scheme 17.



Scheme 18.



Scheme 19.

(Fig. 6). The coordination geometry about Ru can be described as a three-legged piano stool.

Another class of mixed PPh_3 /PTA half-sandwich ruthenium compounds, showing catalytic activity in transfer hydrogenation reactions (see Section 4), are $[\text{Cp}'\text{RuCl}(\text{PTA})(\text{PPh}_3)]$ [$\text{Cp}' = \text{Dp}$ (**76**), Ind (**77**)] [41]. Both complexes were prepared by refluxing equimolar amounts of $[\text{Cp}'\text{RuCl}(\text{PPh}_3)_2]$ and PTA in toluene. The $^{31}\text{P}\{^1\text{H}\}$ NMR spectra of the complexes each consist of two doublets due to coupling of the inequivalent phosphorous nuclei. Compounds **76** and **77** are insoluble in water but compound **76** dissolves in acidic solutions $[\text{HCO}_2\text{H}_{(\text{aq})}, \text{pH} \leq 3]$ due to the protonation of the PTA ligand and the formation of the cationic complex $[\text{DpRuCl}(\text{PTA-H})(\text{PPh}_3)]^+$, as is observed by the substantial shift of the PTA resonance (from -39.6 to -7.77 ppm) and a very small shift of the PPh_3 resonance (from 43.2 to 59.6 ppm) in their $^{31}\text{P}\{^1\text{H}\}$ NMR spectra. On the other hand, the indenyl compound **77** remains insoluble even in acidic solution. The solid-state structures of compounds

76 and **77** are very similar, consisting in three-legged piano-stool structures with the Ru atom bound to an η^5 -Cp' ligand along with one PTA, one PPh_3 and a chloride ligand. A slight increase in the P1–Ru–P2 bond angle is observed as the Cp' ligand changes: Cp 95.4° ; Dp 97.8° ; Ind 98.2° [41].

The cationic tris-phosphine indenylruthenium(II) complex $[(\text{Ind})\text{Ru}(\text{PTA})_2(\text{PPh}_3)]\text{Cl}$ (**78**) was obtained by reaction of $[(\text{Ind})\text{RuCl}(\text{PPh}_3)_2]$ with 2 equiv. of PTA in refluxing toluene. The $^{31}\text{P}\{^1\text{H}\}$ NMR spectra of **78** exhibit two sets of resonances, a triplet (48.9 ppm, PPh_3) and a doublet (-34.1 ppm, PTA), in accordance with the proposed formulation. Failing to obtain suitable crystals of **78**, the analogous compound $[(\text{Ind})\text{Ru}(\text{PTA})_2(\text{PPh}_3)](\text{SnCl}_3)$ (**78-Sn**) was synthesized by stirring a mixture of **78** and $\text{SnCl}_2 \cdot 2\text{H}_2\text{O}$. Both compounds are spectroscopically identical. The solid-state structure of **78-Sn** is the usual piano-stool structure presenting, as the unique remarkable aspect, that the two PTA ligands are not equivalent, with one Ru–P_{PTA} distance significantly shorter: 2.30 and 2.25 \AA [41]. The tris-PTA indenylruthenium(II) complex $[(\text{Ind})\text{Ru}(\text{PTA})_3]\text{Cl}$ (**79**) was obtained as a yellow solid soluble in water ($S_{20^\circ\text{C}} = 20 \text{ mg mL}^{-1}$) in a 53% yield by reacting $[(\text{Ind})\text{RuCl}(\text{PPh}_3)_2]$ with 3.5 equiv of PTA in refluxing toluene. The complex exhibits a single resonance in the $^{31}\text{P}\{^1\text{H}\}$ NMR spectrum at -26.7 ppm.

Tris-phosphine cyclopentadienyl ruthenium(II) complexes bearing PTA or mPTA ligands together with the water-soluble phosphine mTPPMS [$\text{mTPPMS} = \text{Ph}_2\text{P}(3\text{-OSO}_2\text{C}_6\text{H}_4)^-$] were prepared by Romerosa et al. [42] to try to improve the interaction of the $\{\text{CpRuCl}(\text{PR}_3)_2\}$ fragment with DNA. Reaction of $\text{Na}(\text{mTPPMS})$ with the bis-PTA derivative **53a** afforded $[\text{CpRu}(\text{mTPPMS})(\text{PTA})_2]$ (**80**). $\text{Na}[\text{CpRu}(\text{mTPPMS})_2(\text{PTA})]$ (**81**) and $[\text{CpRu}(\text{mPTA})(\text{mTPPMS})_2]$ (**82**) were synthesized by substitution of the chloride ligand in $\text{Na}_2[\text{CpRuCl}(\text{mTPPMS})_2]$ by PTA or mPTA, respectively. The $^{31}\text{P}\{^1\text{H}\}$ NMR spectra of **80** and **81** show the expected resonances corresponding to AM_2 spin systems. The three broad singlets observed for compound **82** are indicative of the magnetic inequivalence of both mTPPMS ligands, tentatively attributed by the authors to the steric crowding around the Ru atom.

Reaction of **66** or **68** with $\text{Na}(\text{mTPPMS})$ in refluxing MeOH produces the substitution of Cl ligand and formation of the first examples of half-sandwich CpRu complexes with

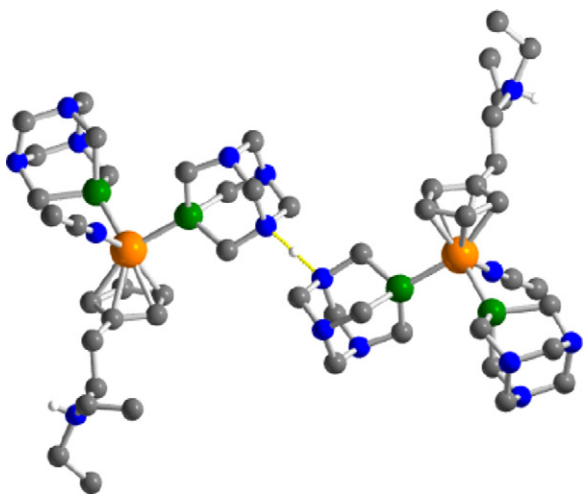


Fig. 6. Part of the crystal lattice of **75**, showing the dimer formed by two distinct molecules sharing a proton between two PTA ligands. H atoms on all ligands and PF_6^- counterions omitted for clarity. Adapted from ref. [39].

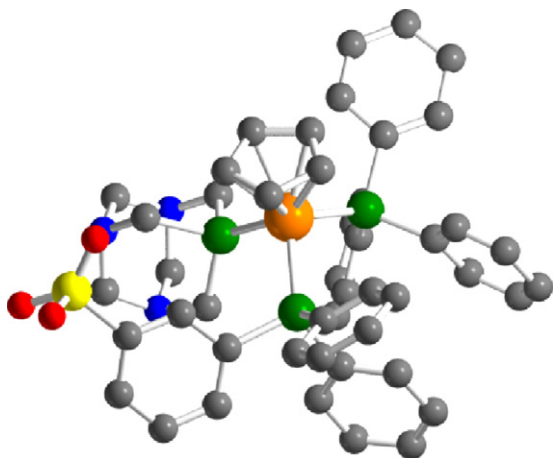


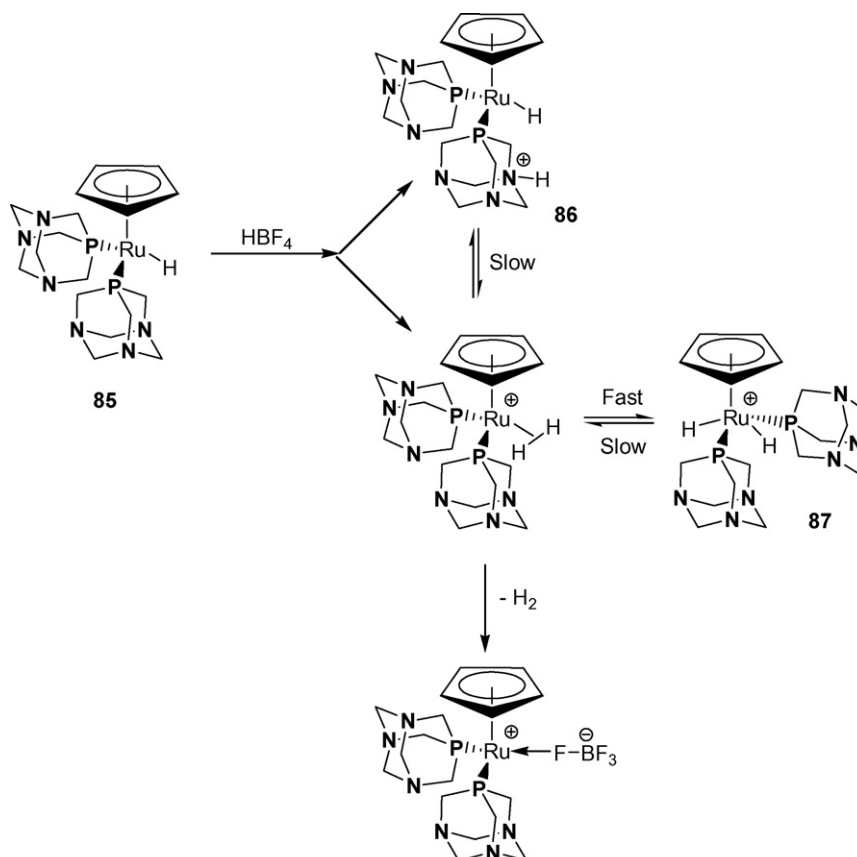
Fig. 7. X-ray crystal structure of $[\text{CpRu}(\text{mTPPMS})(\text{PTA})(\text{PPh}_3)]$ (**83**). H atoms omitted for clarity. Adapted from ref. [42].

three different phosphines $[\text{CpRu}(\text{mTPPMS})(\text{PTA})(\text{PPh}_3)]$ (**83**) and $[\text{CpRu}(\text{mTPPMS})(\text{mPTA})(\text{PPh}_3)](\text{OTf})$ (**84**). The appearance of an AXX' system in the $^{31}\text{P}\{^1\text{H}\}$ NMR spectrum of **83** accounts for the presence of the three different phosphines. On the other hand, compound **84** displays a broad triplet at -25.68 ppm (mPTA) and a broad resonance at 40.48 due to the fortuitous coincidence of the PPh_3 and mTPPMS signals not giving any fine structure at -60°C [42]. The solid-state structure of **83** is the first X-ray resolved for a Ru complex with mTPPMS or other sulfonated phosphine ligands (Fig. 7). The asymmetric unit contains two enantiomeric ruthenium complexes and two disordered water molecules. The arrangement of enantiomeric pairs along the asymmetric unit is supported by

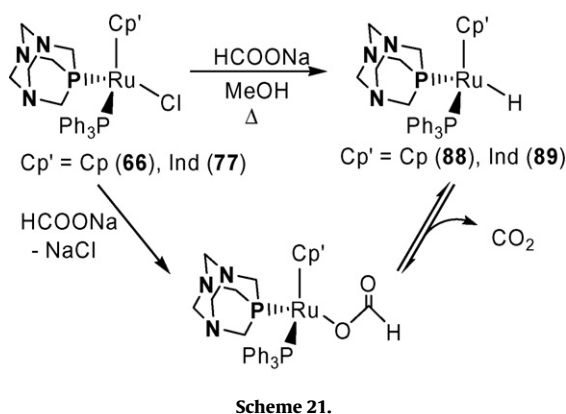
hydrogen bonds forming zigzag chains involving two double water bridges that connect two oxygen atoms of the same pendant sulfonate group to a pair of N atoms belonging to two PTA ligands from neighbouring complex molecules.

Complexes **80–84** are air-stable in aqueous solution. The water solubility spans from 0.6 mg mL^{-1} for **83** and **84** to 10 mg mL^{-1} for **80**, but a direct relationship between this property and the number of water-soluble ligands present in the complexes was not found although the presence of PPh_3 severely reduces the water solubility [42].

Reaction of **53a** with KOH in refluxing methanol gave the water-soluble hydride complex $[\text{CpRuH}(\text{PTA})_2]$ (**85**) ($S_{25^\circ\text{C}} = 20\text{ mg mL}^{-1}$). The hydride resonance in the ^1H NMR spectrum in CD_2Cl_2 is observed as a triplet at -14.36 ppm ($^2J_{\text{HP}} = 36.6\text{ Hz}$). In D_2O the signal shifts upfield to -14.61 ppm. X-ray diffraction analysis of **85** shows that the compound adopts a piano-stool structure with crystallographic parameters very similar to those of $[\text{CpRuH}(\text{PMe}_3)_2]$. All hydrogen atoms were located in the difference map and the DFT calculation of the Ru–H position is virtually identical to the experimentally determined Ru–H position [36]. Compound **85** is very stable in degassed water, but it decomposes quickly in presence of air. Compound **85** reacts with chlorinated solvents yielding the chloro-compound **53a** and undergoes H/D exchange with D_2O . An associative mechanism involving protonation by water of the hydride ligand was proposed [36]. In an attempt to understand the role of pH in hydrogenation catalysis, Mebi and Frost [37] investigated the aqueous phase speciation of **85** varying pH from 9.8 to 2.1 at 5°C . These studies show that compound **85** is in equilibrium with $[\text{CpRuH}(\text{PTA-H})(\text{PTA})]^+$ (**86**) (K_{eq} at $5^\circ\text{C} \sim 6 \times 10^6\text{ L mol}^{-1}$) and, presumably, with $[\text{CpRu}(\text{H})_2(\text{PTA})_2]^+$ (**87**). Scheme 20 depicts the cycle of protonation that is believed to occur in this system.



Scheme 20.



Half-sandwich ruthenium hydrides with formula $[\text{Cp}'\text{RuH}(\text{PTA})(\text{PPh}_3)]$ [$\text{Cp}' = \text{Cp}$ (**88**), Ind (**89**)] have been prepared by the reaction of the chloride derivatives **66** and **77** with sodium formate or sodium methoxide in refluxing methanol (Scheme 21) [41].

The ^1H NMR spectra of **88** and **89** show the characteristic Ru–H resonances at -13.2 ppm ($^2J_{\text{PTA-H}} = 36.0$ Hz, $^2J_{\text{PPh}_3\text{-H}} = 33.0$ Hz) for **88** and at -16.3 ppm ($^2J_{\text{PTA-H}} = 32.0$ Hz, $^2J_{\text{PPh}_3\text{-H}} = 29.2$ Hz) for **89**. Similarly to compound **85** (see above), compounds **88** and **89** undergo H/D exchange but, interestingly, compound **88** much more rapidly ($t_{1/2} = 127$ min for **85**, $t_{1/2} \ll 10$ min for **88**) in CD_3OD at 25°C , affording $[\text{Cp}'\text{RuD}(\text{PTA})(\text{PPh}_3)]$. Much slower H/D exchange was observed for **89** ($t_{1/2} \sim 5.5$ days) [41]. The solid-state structures of compounds **66** and **77** with a significant increase in the $\text{Cp}'\text{-ML}_2$ angle as the Cl is replaced by H due to both electronic effect and smaller steric requirements of H.

As indicated previously (see Section 2) the growing interest in obtaining new water-soluble ligands led to synthesize different PTA derivatives such as the *N,N*-dimethyl derivative dmPTA. The standard procedure of reacting this ligand with $[\text{Cp}'\text{RuCl}(\text{PPh}_3)_2]$ to obtain new water-soluble Cp–Ru complexes by substitution of PPh_3 for the new ligand gave instead $[\text{RuClCp}(\text{HdmoPTA})(\text{PPh}_3)](\text{OTf})$ (**90**) bearing an unexpected modification of the PTA ligand [12]. This modification implies the elimination of one methylene “lower rim” group of dmPTA to give the open version dmoPTA, as confirmed by NMR spectroscopy and X-ray diffraction studies (Scheme 22).

$^{31}\text{P}\{^1\text{H}\}$ NMR studies of the reaction depicted in Scheme 22, using different solvents (dry acetone- d_6 , with traces of water or acetone- d_6 with traces of CH_3OD) provided evidences that the new compound $[\text{Cp}'\text{RuCl}(\text{dmPTA})(\text{PPh}_3)](\text{OTf})_2$ (**91**) is firstly obtained then converted into **90** with a rate depending on the amount of water in the reaction. On the other hand, these studies suggest that the triazacyclohexane methylene group was removed after the substitution of one PPh_3 in the starting $[\text{Cp}'\text{RuCl}(\text{PPh}_3)_2]$ complex [12]. The structure of **90** is very similar to that of the parent complex

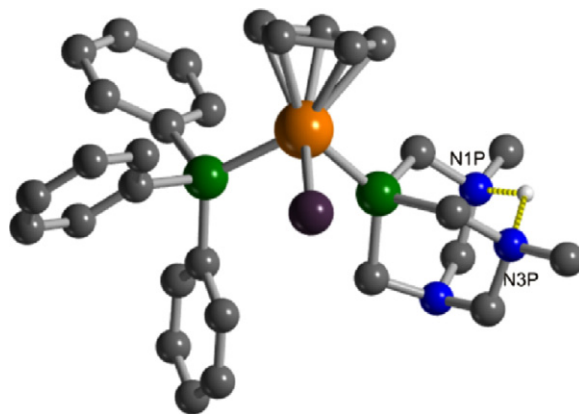


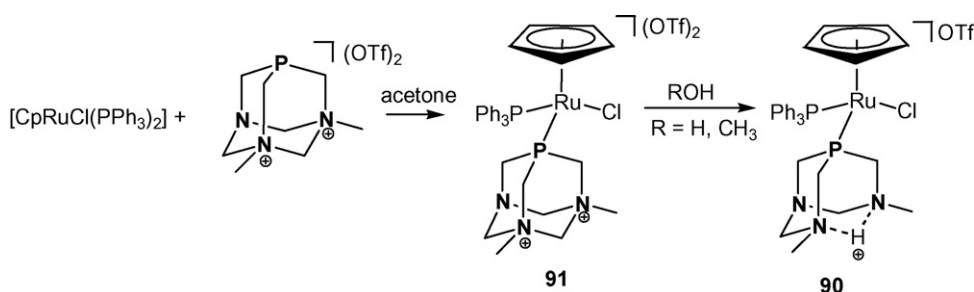
Fig. 8. X-ray crystal structure of the cationic part of $[\text{CpRuCl}(\text{HdmoPTA})(\text{PPh}_3)](\text{OTf})$ (**90**). H atoms on the ligands omitted for clarity. Adapted from ref. [12].

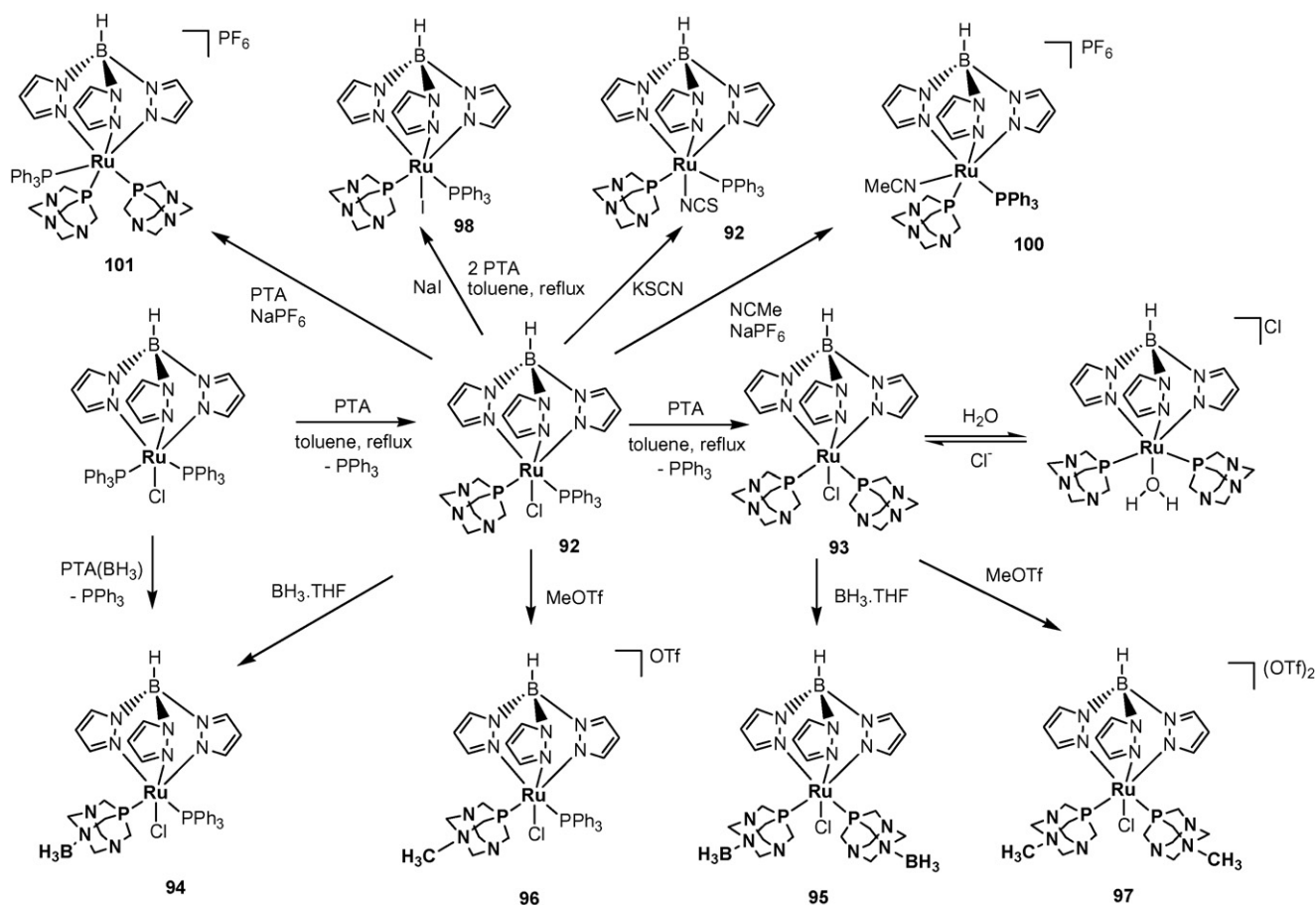
66 (Fig. 8). A relevant characteristic is the proton site, just between the nitrogen atoms N1P and N3P (Fig. 4) in a sharing situation supported by the short intramolecular contact $\text{N1P}\cdots\text{N3P} = 2.702(1)$ Å. A 3D network, through extensive hydrogen bonding involving PPh_3 , MeOH, and CF_3SO_3^- , forms the crystal structure [12].

A family of PTA and PTA-modified ruthenium complexes bearing the Cp-isoelectronic ligand hydridotris(pyrazolyl)borate (Tp), were recently prepared and, in some cases, their electrochemical and DNA binding properties were studied [43,44] (Scheme 23, see also Section 5).

The mono- and bis(PTA) complexes $[\text{TpRuCl}(\text{PPh}_3)(\text{PTA})]$ (**92**) and $[\text{TpRuCl}(\text{PTA})_2]$ (**93**) were prepared by treating $[\text{TpRuCl}(\text{PPh}_3)_2]$ in refluxing toluene in the molar ratio 1:1 or 1:2, respectively. Complex **93** can be also prepared by treating **92** with PTA. A similar reaction with the *N*-boronated PTA- BH_3 ligand gives the complexes $[\text{TpRuCl}(\text{PPh}_3)(\text{PTA-BH}_3)]$ (**94**) and $[\text{TpRuCl}(\text{PTA-BH}_3)_2]$ (**95**). Complexes **94** and **95** can also be prepared by direct boronation of **2** and **3** in THF with $\text{BH}_3\cdot\text{THF}$ at room temperature [44]. Monitoring of this reaction by $^{31}\text{P}\{^1\text{H}\}$ NMR spectroscopy shows no evidence for the formation of complexes with polyboronated-PTA ligands $[\text{PTA}(\text{BH}_3)_x]$, $x = 2, 3$. On the other hand, the parent compounds bearing the mPTA derivative $[\text{TpRuCl}(\text{PPh}_3)(\text{mPTA})]^+$ (**96**) and $[\text{TpRuCl}(\text{mPTA})_2]^{2+}$ (**97**) were prepared by methylation of the PTA ligands of **92** and **93** with MeOTf at -30°C in CH_2Cl_2 [43]. Water solubility of the modified-PTA complexes **94–97**, significantly decreases with respect to the parent compounds **2** and **3**. The chemical shift of the P atom of the modified PTA-ligands in the $^{31}\text{P}\{^1\text{H}\}$ NMR spectra appears in all cases at lower fields than the PTA ligand in the precursor complexes **92** and **93**.

Chloride metathesis on complex **92** by reaction with excess of NaI or KSCN in methanol gave the corresponding complexes $[\text{TpRuX}(\text{PPh}_3)(\text{PTA})]$ [$\text{X} = \text{I}$ (**98**); NCS (**99**)]. Complexes are soluble in water, alcohols and dichloromethane and insoluble in hexane





Scheme 23.

[43]. On the other hand, reaction of **92** with the chloride abstractor NaPF_6 in the presence of acetonitrile or PTA allows the formation of the cationic complexes $[\text{TpRu}(\text{NCS})(\text{PPh}_3)(\text{PTA})](\text{PF}_6^-)$ (**100**) and $[\text{TpRu}(\text{PPh}_3)(\text{PTA})_2](\text{PF}_6^-)$ (**101**). Complexes **100** and **101** are soluble in water, alcohols and dichloromethane and insoluble in diethyl ether and hexane. Elemental analysis and spectroscopic data for compounds **92**–**101** agree with the proposed formulations. IR spectra show the characteristic ν_{BH} band of the Tp ligand at $2456\text{--}2508\text{ cm}^{-1}$ (see Table 3).

Electrochemical studies on complexes **92**–**95** indicated partial κ^3 to κ^2 dechelation of Tp in some cases, and have allowed to measure the values of $E_{1/2}^{\text{ox}}$, which reflect the electron-donor character of the ligands $[\text{Tp (each arm)} > \text{PTA} > \text{PPh}_3 > \text{PTA}(\text{BH}_3)]$ (Table 4). The Lever electrochemical parameter E_L has also been estimated (Table 5).

X-ray diffraction studies of compounds **92**, **93** [43,44] and **99** [43] show that the Ru atom exhibits, in all complexes, a distorted octahedral coordination geometry with structural parameters similar to those of ruthenium(II) complexes bearing the Tp scorpionate ligand. Due to the higher *trans* influence for the phosphine ligands, the Ru–N bond distances *trans* to them are significantly longer than those *trans* to Cl (**92**, **93**) or NCS (**99**). Samples of complexes **92**, **96**, and **100** under physiological conditions (37°C , pH 7) indicate no appreciable decomposition after a period of 14 h [43]. In the case of compound **93**, although D_2O solutions are stable at room temperature for several days, its aquation takes place upon heating the solution to 60°C [44].

Protonation of $[\text{TpRuCl}(\text{PPh}_3)_2(\text{PTA})]$ (**92**) with an equimolecular amount of HBF_4 in CD_2Cl_2 at -30°C produces the protonation of one nitrogen of the coordinated PTA ligand leading to

$[\text{TpRuCl}(\text{PPh}_3)(\text{PTA-H})]\text{BF}_4$ (**102**) complex [45]. The $^{31}\text{P}\{^1\text{H}\}$ NMR spectrum exhibits two doublets at 42.4 (PPh_3) and -18.1 (PTA-H) ppm ($^2J_{\text{PP}} = 32\text{ Hz}$). The ^1H NMR spectrum shows two broad signals for the N– CH_2 –N protons at 4.82 and 4.52 ppm, and a broad signal at 3.94 ppm for the N– CH_2 –P protons. If the protonation is carried out with a 2:1 Ru/acid molar ratio at -30°C , the dinuclear complex $[\{\text{TpRuCl}(\text{PPh}_3)\}_2\{\mu\text{-}\kappa^2(\text{P},\text{P})\text{-PTA-H-PTA}\}]\text{BF}_4$ (**103**) is obtained, $^{31}\text{P}\{^1\text{H}\}$ NMR two doublets at 43.3 (PPh_3) and -21.1 (PTA-H-PTA) ppm ($^2J_{\text{PP}} = 32\text{ Hz}$); ^1H NMR, two broad signals for the N– CH_2 –N protons at 4.73 and 4.46 ppm, and a broad signal at 3.92 ppm for the N– CH_2 –P protons].

Reaction of $[\text{TpRuCl}(\text{PPh}_3)(\text{PTA})]$ (**92**) with I_2 at -30°C gives $[\text{TpRuCl}(\text{PPh}_3)(\text{PTA-I}_2)]$ (**104**) as an orange solid, [45] showing $^{31}\text{P}\{^1\text{H}\}$ signals as two doublets at 43.9 (PPh_3) and -16.2 (PTA-I_2) ppm ($^2J_{\text{PP}} = 30\text{ Hz}$) and ^1H NMR signal as two multiplets for the N– CH_2 –N protons at 4.46 and 4.25 ppm (AB spin system, $J_{\text{AB}} = 12\text{ Hz}$), and a multiplet at 3.95–3.85 ppm for the N– CH_2 –P protons. The crystal structure of this compound shows a distorted octahedral coordination geometry with parameters in the range of those found for other Ru(II) complexes. The I–I bond distance [$2.813(6)\text{\AA}$] is longer than the I–I distance either in gas phase (2.677) or in crystalline diiodine [$2.717(6)\text{\AA}$ at 110 K] showing the presence of a weak N...I–I interaction.

Complexes with modified PTA ligands $[\text{TpRuX}(\text{PPh}_3)(\text{PTA-R})][\text{Y}]$, ($\text{X} = \text{Cl}$, $\text{R} = \text{CH}_2\text{Ph}$ (**105**), $\text{CH}_2\text{CH}=\text{CH}_2$ (**106**), $\text{CH}_2\text{C}\equiv\text{CH}$ (**107**); $\text{X} = \text{I}$, $\text{R} = \text{CH}_2\text{Ph}$ (**108**), $\text{CH}_2\text{CH}=\text{CH}_2$ (**109**)), were obtained by reaction of $[\text{TpRuX}(\text{PPh}_3)(\text{PTA})]$ with organic halides RCH_2Y (Scheme 24) [45]. Slow evaporation of CH_2Cl_2 solutions of complex $[\text{TpRuI}(\text{PPh}_3)(\text{PTA-CH}_2\text{-CH}=\text{CH}_2)](\text{OTf})$ obtained via exchange of the I anion by OTf, yielded crystals suitable for X-ray diffraction

Table 3
Spectroscopic IR data of RuTp compounds (cm^{-1}).

Compound	ν_{BH}	Other relevant bands
[TpRuCl(PPh ₃)(PTA)] (92)	2475 (w)	
[TpRuCl(PPh ₃) ₂](PTA) (93)	2508 (w)	
[TpRuCl(PPh ₃)(PTA-BH ₃)] (94)	2478 (m); 2364 ^a (s); 2314 ^a (m); 2267 ^a (m)	
[TpRuCl(PTA-BH ₃) ₂] (95)	2482 (m); 2376 ^a (s); 2318 ^a (m); 2275 ^a (m)	
[TpRuCl(PPh ₃)(mPTA)](OTf) (96)	2483	ν_{OSO} : 1258
[TpRuCl(mPTA) ₂](OTf) ₂ (97)	2485	ν_{OSO} : 1259
[TpRu(PPh ₃)(PTA)] (98)	2466	
[TpRu(PPh ₃)(PTA) ₂](PF ₆) (101)	2488	ν_{PF6} : 842
[TpRu(NCMe)(PPh ₃)(PTA)](PF ₆) (100)	2491	ν_{PF6} : 840
[TpRu(NCS)(PPh ₃)(PTA)] (99)	2485	ν_{SCN} : 2113
[TpRuH(PPh ₃)(PTA)] (112)	2456 (m)	ν_{RuH} : 1920 (w)
TpRuH(PTA) ₂ (113)	2464 (m)	ν_{RuH} : 1866 (w)
TpRuH(PPh ₃)(PTA-BH ₃) (114)	2464 (m); 2368 ^a (m); 2319 ^a (m); 2271 ^a (w)	ν_{RuH} : 1940 (m)
[TpRuH(PPh ₃)(mPTA)](OTf) (115)	2476	ν_{OSO} : 1258; ν_{RuH} : 1931
[TpRuCl(PPh ₃)(PTA-H)](BF ₄) (102)	2480	ν_{BF4} : 1047
[{TpRuCl(PPh ₃) ₂ }{ μ - κ^2 (P,P)-PTA-H-PTA}](BF ₄) (103)	2480	ν_{BF4} : 1047
[TpRuCl(PPh ₃)(PTA-I ₂)] (104)	2468	
[TpRuCl(PPh ₃)(PTA-CH ₂ Ph)]I (105)	2479	
[TpRu(PPh ₃)(PTA-CH ₂ Ph)]I (108)	2479	
[TpRuCl(PPh ₃)(PTA-CH ₂ CH=CH ₂)]I (106)	2479	
[TpRu(PPh ₃)(PTA-CH ₂ CH=CH ₂)]I (109)	2479	
[TpRuCl(PPh ₃)(PTA-CH=CH ₂)]I (107)	2479	$\nu_{\text{C=C}}$: 2117
[TpRu(PPh ₃)(1-CH ₃ -4-Ph-PTA)]I (110)	2478	
[TpRu(PPh ₃){1-CH ₃ -4-{CH ₃ O(CH ₂) ₂ }-PTA}]I (111a)	2480	
[TpRu(PPh ₃){1-CH ₃ -4-{CH(CH ₃) ₂ O(CH ₂) ₂ }-PTA}]I (111b)	2477	

^a BH of PTA-BH₃.

studies. The Ru atom exhibits a distorted octahedral coordination geometry with parameters in the range of those found for other Ru(II) complexes.

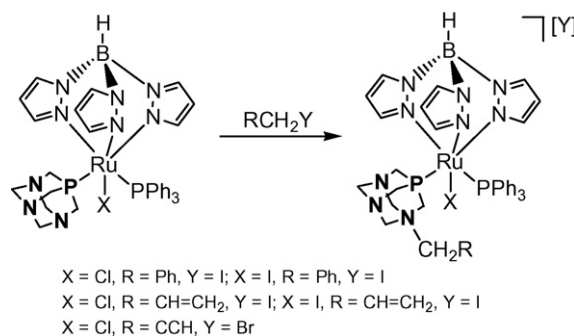
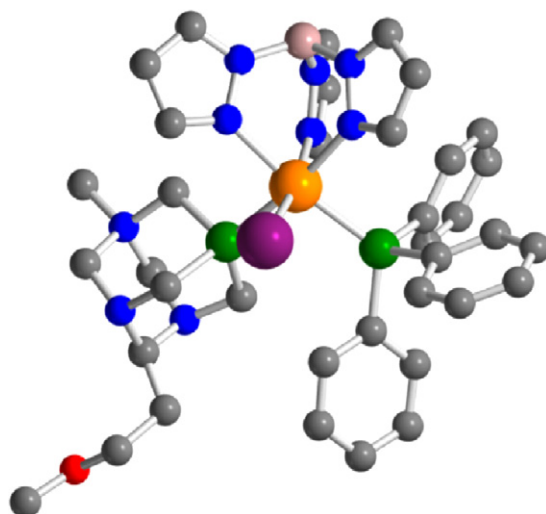
When solutions of compounds **108** and **109** in alcohols were refluxed for 9–13 h, new complexes **110**, **111a** and **111b** were obtained in which ring opening and C–H activation reactions were observed leading to unprecedented substituted 1-methyl-4-phenyl-PTA, 4-(2-methoxyethyl)-1-methyl-PTA and 1-methyl-4-[2-(propan-2-yloxy)ethyl]-PTA ligands, respectively [45]. Deuteration experiments have been performed leading to outline a reaction pathway closely related to that of the Duff-Sommelet reactions. X-ray crystal structure of **111a'** (OTf instead I, Fig. 9) cor-

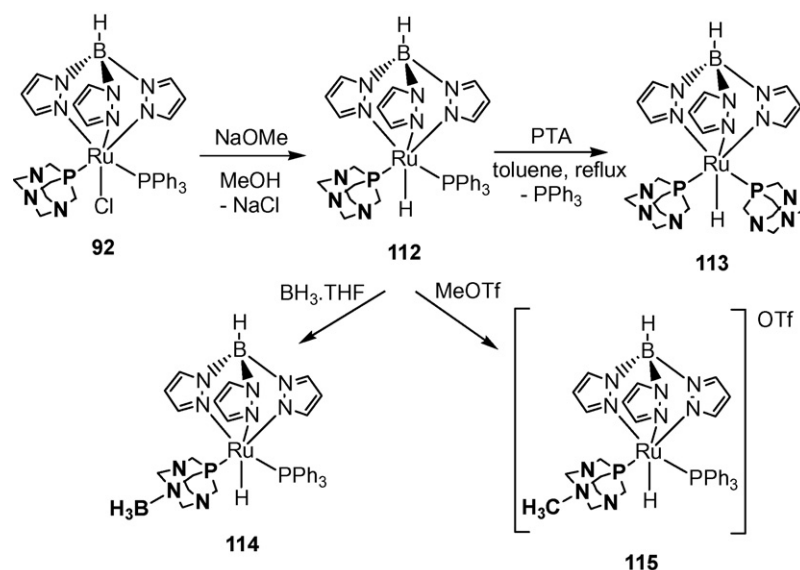
Table 4
Cyclic voltammetric data for TpRu complexes^a.

Complex	MeCN			dmso	
	$E_{1/2}^{\text{ox}}$	E_{p}^{ox}	E_{p}^{ox}	$E_{1/2}^{\text{ox}}$	E_{p}^{ox}
[TpRuCl(PPh ₃) ₂]	0.70 ^b	1.98 ^c		0.74	1.11
[TpRuCl(PPh ₃)(PTA)] (92)	0.70	1.26 ^d		0.70	1.13 ^e
[TpRuCl(PTA) ₂] (93)	0.66	1.23 ^f		0.61	1.14
[TpRuCl(PPh ₃)(PTA-BH ₃)] (94)	0.80	1.75, 1.87 ^g		0.77	–
[TpRuCl(PTA-BH ₃) ₂] (95)	0.89 ^h	1.15, 1.23 ^g		0.79	1.14

^a Potentials in V (± 0.02) vs. SCE, measured at 0.2 V s^{−1}.^b The reversible oxidation wave with a lower current intensity observed at $E_{1/2}^{\text{ox}} = 1.00$ V is ascribed to [κ^2 -Tp]RuCl(MeCN)(PPh₃)₂].^c Upon scan reversal, a cathodic reversible wave is detected at 1.26 V.^d Upon scan reversal, a cathodic reversible wave is detected at 0.89 V.^e Upon scan reversal, a cathodic reversible wave is detected at 0.85 V.^f Upon scan reversal, a cathodic reversible wave is detected at 1.03 V.^g Poorly defined.^h The reversible oxidation wave with a lower current intensity observed at $E_{1/2}^{\text{ox}} = 0.75$ V is assigned to [TpRuCl(MeCN)(PTA(BH₃))].**Table 5**
 E_{L} ligand parameter values estimated in this study^a.

Ligand	E_{L} [V] vs. NHE
Tp	0.14 ^b
PTA	0.34
PTA(BH ₃)	0.45

^a From Lever's equation $E_{1/2}^{\text{ox}} = S_{\text{M}} - (\sum E_{\text{L}}) + I_{\text{M}}$.^b Per ligating pyrazolyl arm.**Scheme 24.****Fig. 9.** X-ray crystal structure of the cationic part of **111a'**. H atoms on the ligands omitted for clarity. Adapted from ref. [45].



Scheme 25.

roborates the proposed structure with methoxy ethyl chain bound to C(5) of PTA and CH₃ bound to N(1) [45].

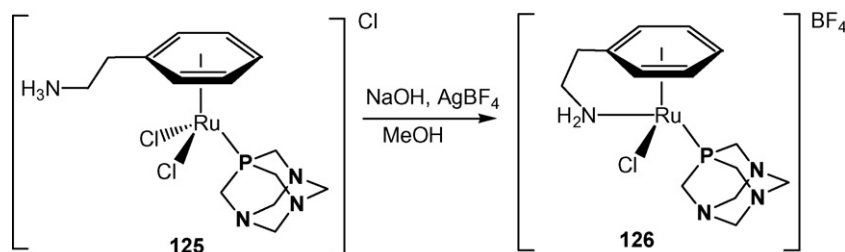
The hydrido[tris(pyrazolyl)borato]ruthenium(II) complex [TpRuH(PPh₃)(PTA)] (**112**) was prepared by chloride metathesis upon treatment of **92** with an excess of NaOMe in MeOH at room temperature [44]. [TpRuH(PTA)₂] (**113**) was prepared by treatment of complex **112** with PTA in refluxing toluene. Reaction of **112** with BH₃·THF provides a straightforward method to synthesise the new PTA-boronated hydrido complex [TpRuH(PPh₃)(PTA-BH₃)] (**114**) [44]. On the other hand, reaction of complex **112** with the methylating agent MeOTf yields the cationic complex [TpRuH(PPh₃)(mPTA)](OTf) (**115**) (Scheme 25).

All the hydrides were isolated as yellow solids and the spectroscopic data agree with the proposed formulation. The IR spectra show the characteristic ν_{BH} band of the Tp ligand (2456–2476 cm⁻¹), and a medium-intensity absorption at 1920–1940 cm⁻¹ attributed to ν_{RuH}. The ¹H NMR spectra of the compounds confirm the presence of the Tp ligand by showing the characteristic signals of the pyrazole hydrogen atoms of the Tp group, the number of these signals reflecting the number of identical co-ligands attached to the metal center. The ¹H NMR spectra of complexes **112**, **114** and **115** [43,44] show a high-field shifted doublet of doublets, each centered at ca. –14 ppm, due to coupling to two different phosphorus atoms, corresponding to a terminal hydrido ligand, whereas complex **113** displays a triplet at –16 ppm corresponding to the single hydrido ligand coupled to the two magnetically equivalent P atoms (²J_{PH} = 30.6 Hz). The water solubility of the mixed PPh₃/PTA hydrides is rather modest, but the bis(PTA) hydride **113** is readily soluble in water (S_{25°C} = 21 mg mL⁻¹) [44].

The discovery of antitumoral activity of ruthenium–arene–PTA complexes (RAPTA) has boosted significant synthetic efforts towards this class of compounds (see Section 5). One of the strategies developed to increase the activity of these compounds and to understand the activation mechanism, is to modify the η⁶-arene ligand by introducing different substituents. Chart 8 summarizes some RAPTA-type compounds developed by Dyson and co-workers, including derivatives bearing mPTA or DAPTA ligands [46–49]. The synthetic approach used to prepare these compounds is generally the direct reaction of the dimer [Ru(η⁶-arene)(μ-Cl)Cl]₂ with PTA or modified PTA ligands. Complex **126** is an exception and was prepared by deprotonation with a strong base and subsequent chloride abstraction with AgBF₄ (Scheme 26).

The ³¹P{¹H} NMR spectra of these compounds are very simple, only exhibiting a singlet resonance. For some of them X-ray crystal structures have been determined (**116b**, **126**, **132**) and are usually very similar, displaying the characteristic three-legged piano-stool geometry. In the case of the chelating compound **126** the structure was also calculated by theoretical methods showing an excellent agreement with the X-ray data. The structure is similar to those of the compounds shown in Chart 2 with a η⁶-arene ligand slightly tilted due to chelation. Other important parameters which have been measured for this class of compounds include the pK_a values (Section 5) [50].

The dicarboxylate RAPTA derivatives [Ru(C₂O₄)(η⁶-C₁₀H₁₄)(PTA)] (**133**) and [Ru(C₆H₆O₄)(η⁶-C₁₀H₁₄)(PTA)] (**134**) have been synthesized by reaction of the dimer [Ru(η⁶-p-cymene)(μ-Cl)Cl]₂ with an excess of the silver dicarboxylate followed by treatment with stoichiometric amounts of PTA (Scheme 27) [51].



Scheme 26.

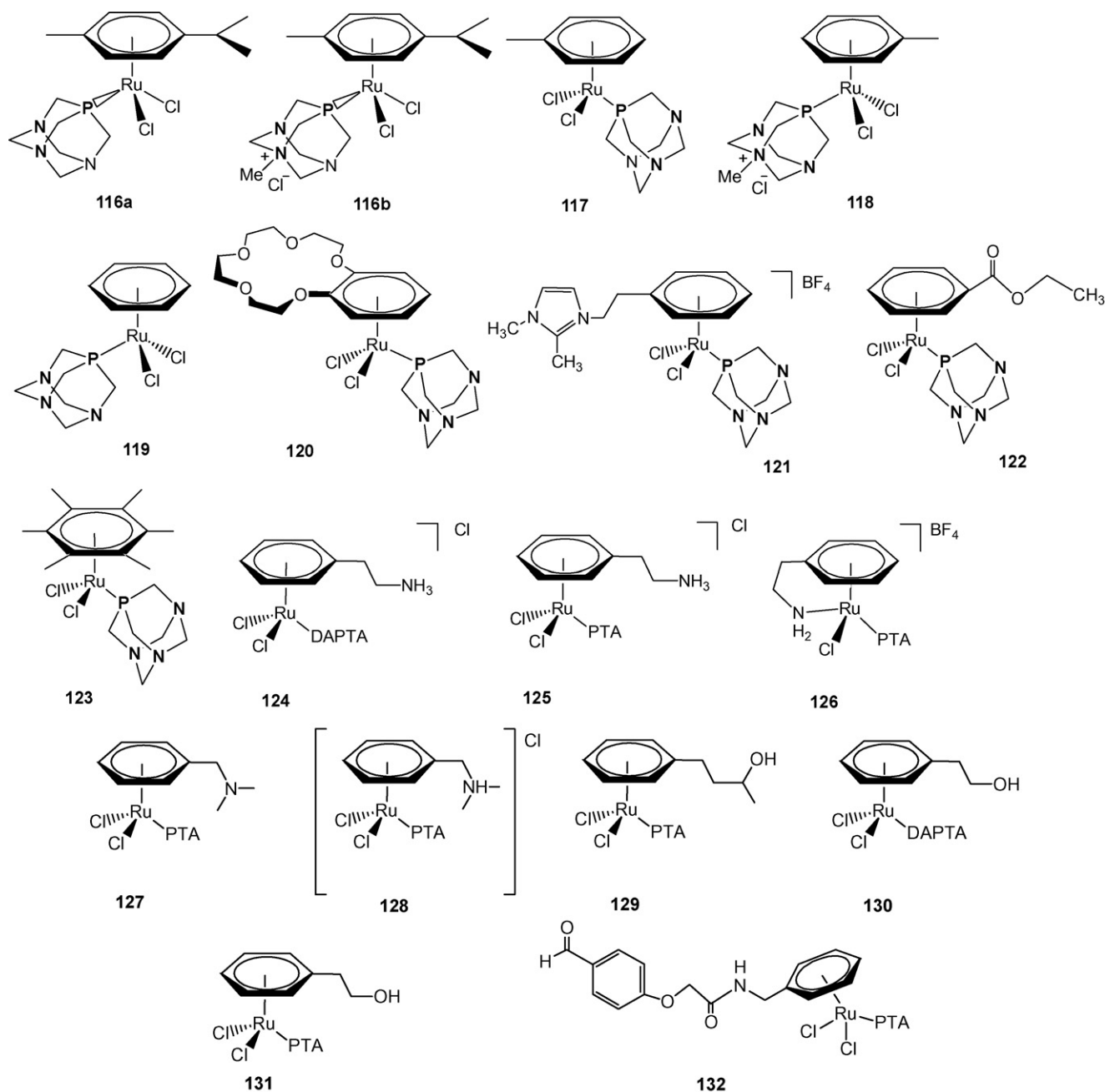
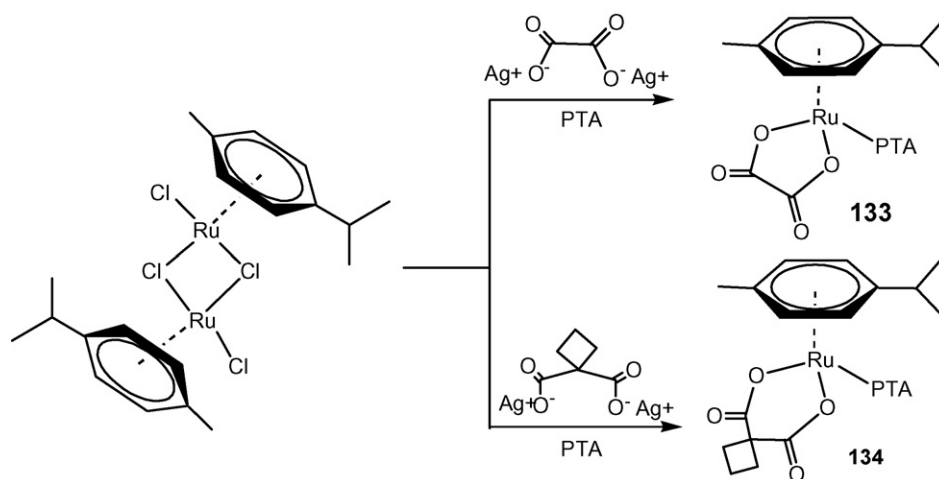


Chart 8.

The $^{31}\text{P}\{^1\text{H}\}$ NMR spectra of both complexes present a singlet shifted to lower frequency compared to $[\text{RuCl}_2(\eta^6\text{-C}_{10}\text{H}_{14})(\text{PTA})]$ **116a** due to the deshielding effect of the carboxylate groups. The solid structure of **133** shows the typical piano-stool disposition with the bond angle O1–Ru–O2 of $78.43(7)^\circ$ characterized by the strain of the five-membered ring. Monitoring the stability of both compounds in water by ^{31}P NMR spectroscopy and ESI-MS show that compound **133** does not undergo hydrolysis whereas compound **134** exhibits two peaks in the $^{31}\text{P}\{^1\text{H}\}$ NMR spectrum indicating possible hydrolysis products. UV–vis and $^{31}\text{P}\{^1\text{H}\}$ NMR spectroscopic studies suggest a stability trend **133** > **134** > $[\text{RuCl}_2(\eta^6\text{-C}_{10}\text{H}_{14})(\text{PTA})]$. The pK_a values for **133** and **134** (Table 21, Section 5) are significantly lower than those of $[\text{RuCl}_2(\eta^6\text{-C}_{10}\text{H}_{14})(\text{PTA})]$ indicating that they are stable as neutral species at lower pH values [51].

The tendency to self-aggregate of various neutral and cationic RAPTA complexes as a function of their chemical nature was evaluated by PGSE (pulse field gradient spin-echo) NMR experiments in acetone- d_6 [52]. The study shows that protonated RAPTA complexes have a remarkable tendency to form dicationic species through hydrogen bond interactions.

Cationic RAPTA complexes **135**–**138** [53] bearing a series of β -diketonato ligands were prepared by treatment of the corresponding chloride precursors with PTA in the presence of an excess of either NaBF_4 or NaBPh_4 (Scheme 28). The products were obtained as either yellow or yellow-orange solids having a singlet ranging from -28.08 to -30.60 ppm in the $^{31}\text{P}\{^1\text{H}\}$ NMR spectra. X-ray analyses of **135BF** $_4$, **135BPh** $_4$, **136BPh** $_4$, **137BF** $_4$ and **138BF** $_4$ show a three-legged piano-stool geometry, with the corresponding β -diketonato ligand and the Ru center forming a six-membered

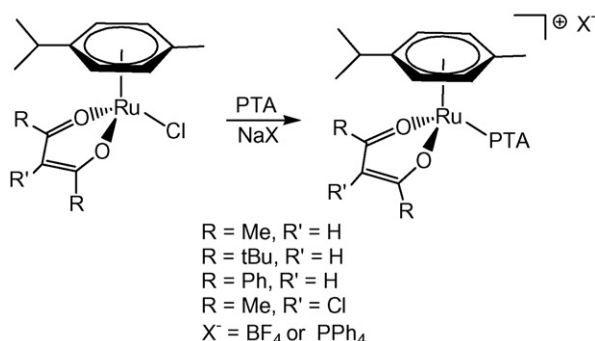


Scheme 27.

chelate ring. Interestingly, replacement of the BPh₄ counteranion by BF₄ in **135** results in an increase of the Ru-arene distance by 2.2 pm, indicating that the p-cymene ring is less strongly coordinated, in accordance with the ¹H NMR data for the resonances of the aromatic protons, which show a marked shift to higher frequencies, approaching those of the free p-cymene.

These compounds exhibit very good stability against hydrolysis under physiological conditions, the most stable complex being **136**BF₄, bearing the sterically demanding ^tBu₂acac β-diketonato ligand [53].

Reactions of the upper-rim PTA-modified ligands PTA-CRR'OH with [Ru(η⁶-arene)Cl₂]₂ in CH₂Cl₂ gave the new compounds [(arene)RuCl₂(PTA-CRR'OH)] (R = R' = C₆H₅ **139**; R = R' = C₆H₄OCH₃ **140**; R = C₆H₄OCH₃, R' = H **141**) in moderate to good yields [18b]. These complexes exhibit modest water solubility, 5.4 g L⁻¹ for [(η⁶-C₆H₅CH₃)RuCl₂(PTA-C(C₆H₅)₂OH)] (**139**) and a slightly higher 14.1 g L⁻¹ for [(η⁶-C₆H₆)RuCl₂(PTA-C(C₆H₄OCH₃)₂OH)] (**140**). The ³¹P{¹H} NMR spectra of [(η⁶-C₆H₆)RuCl₂(PTA-C(C₆H₄OCH₃)₂OH)] and [(η⁶-C₆H₅CH₃)RuCl₂(PTA-C(C₆H₄)₂OH)] give a single resonance at -31.3 and -31.0 ppm, respectively. The diastereomeric compound [(η⁶-C₆H₆)RuCl₂(PTA-CH(C₆H₄OCH₃)OH)] (**141**) contains two ³¹P{¹H} chemical shifts at -33.1 and -32.3 ppm for the major and minor diastereomer, respectively. The structures of the three ruthenium arene complexes show the PTA-CHRR'OH ligands bind the metal center through the phosphorus atom (Fig. 10). Addition of either CsCO₃ or NaOH produces a shift in the ³¹P{¹H} resonance of ~8–10 ppm. This fact is attributed to a deprotonation of the OH functionality and the subsequent chelating P,O behaviour of the ligand [18b].



Scheme 28.

As substitution of PTA by PPh₃ increases the reactivity of some CpRu complexes with DNA, mixed PTA/PPh₃ RAPTA derivatives were obtained [54]. The mixed-phosphine complex [Ru(η⁶-p-cymene)Cl(PTA)(PPh₃)]BF₄ (**142**) was synthesized in good yield by substitution of the labile CH₃CN ligand in [Ru(η⁶-p-cymene)Cl(CH₃CN)(PPh₃)]BF₄ with PTA in CH₂Cl₂ at room temperature. In a similar way, the corresponding RAPTA complex (**143**) bearing a hydroxyl-functionalized η⁶-arene, C₆H₅CH₂CH₂OH, is prepared by ligand substitution of the chloride ligand in [Ru(η⁶-C₆H₅CH₂CH₂OH)Cl₂(PPh₃)], to give **143** in high yield. As expected the ³¹P{¹H} NMR spectra of **142** and **143** show doublets at ca. 30 ppm (PPh₃) and ca. -42 ppm (PTA), with a ²J_{PP} coupling constant of 54 Hz indicative of the coordination of both phosphines to the ruthenium center. The solid-state structure of **142** exhibits the typical 'piano-stool' geometry around the ruthenium atom and has a close resemblance to that of the related bisphosphine complex, [Ru(η⁶-p-cymene)Cl(PPh₃)₂]BF₄ [Ru-P = 2.3649(6), 2.4042(6) Å], and [Ru(p-cymene)Cl₂(PTA)], although the Ru-P bond length is slightly elongated [2.3201(14) Å vs. 2.297(3) (average over two independent molecules) in [Ru(p-cymene)Cl₂(PTA)] [54].

Substitution of one chloro ligand by PTA in the N-heterocyclic carbene complex [RuCl₂(p-cymene)L] (L = 1-butyl-3-methylimidazol-2-ylidene) can be easily obtained adding 1 equiv of PTA to an aqueous solution of [RuCl₂(p-cymene)L] (L = 1-butyl-

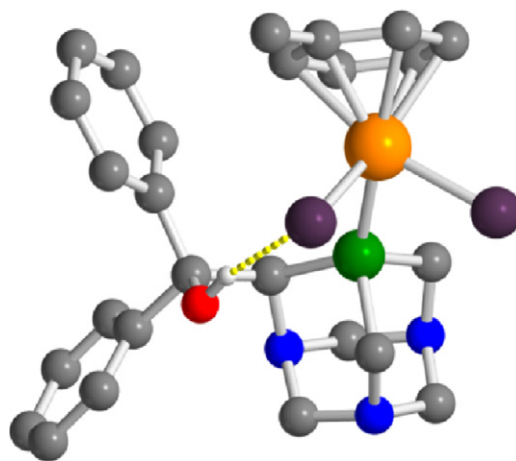


Fig. 10. X-ray crystal structure of **139**. H atoms on the ligands omitted for clarity. Intramolecular O-H...Cl hydrogen bonding shown as dotted line. Adapted from ref. [18a].

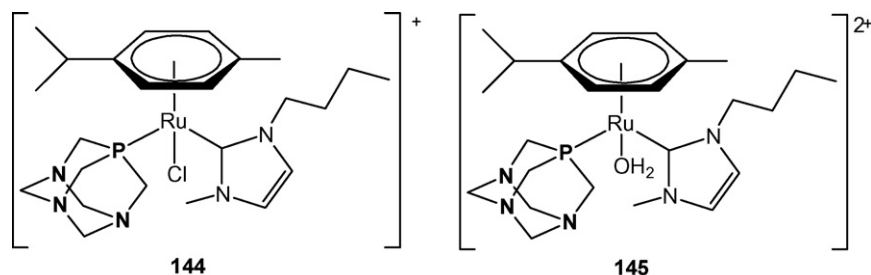
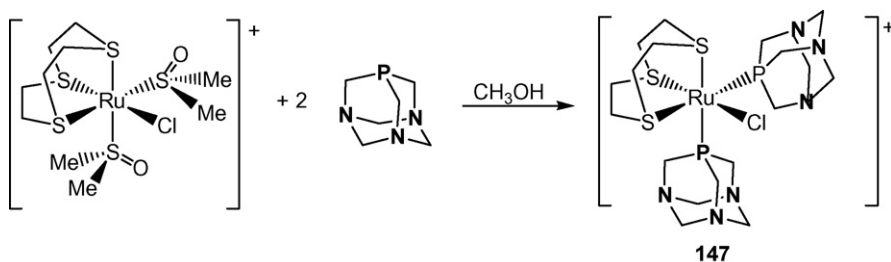


Chart 9.

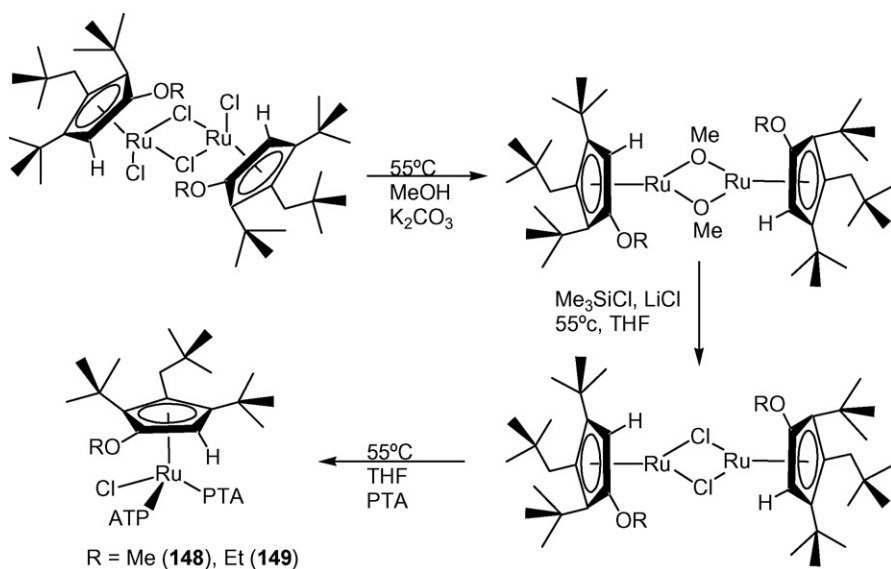


Scheme 29.

3-methylimidazol-2-ylidene) [55]. $[\text{RuCl}(p\text{-cymene})\text{L}(\text{PTA})]\text{Cl}$ (**144**) is obtained (Chart 9) together with small quantities of the dicationic $[\text{Ru}(p\text{-cymene})(\text{H}_2\text{O})\text{L}(\text{PTA})]^{2+}$ (**145**). The complexes were not isolated but they were identified by $^{31}\text{P}\{^1\text{H}\}$ NMR from the presence of singlet resonances at -35.5 and -36.1 ppm and from signals at 165.4 and 165.6 ppm in the ^{13}C NMR spectra. The strong peak at 566 Da in the ESI-TOF mass spectrum showed **144** as the single species in solutions containing 0.1 M KCl. Compound **144** is very active and selective catalyst for the hydrogenation of olefins and oxo compounds and for the redox isomerization of allyl alcohol (Section 4) [55].

The aromatic ring in RAPTA compounds may be replaced by the sulfur macrocycle 1,4,7-trithiacyclononane ([9]aneS₃) without changing the anticancer activity *in vitro* too significantly [56]. Thus, the neutral $[\text{RuCl}_2(\text{PTA})(\text{[9]aneS}_3)]$ (**146**) and the cationic $[\text{RuCl}(\text{PTA})_2(\text{[9]aneS}_3)][\text{OTf}]$ (**147**) compounds have been prepared in high yields by reaction of $[\text{RuCl}_2(\text{dmsO})(\text{[9]aneS}_3)]$ or

$[\text{RuCl}(\text{dmsO})_2(\text{[9]aneS}_3)][\text{OTf}]$ with PTA (Scheme 29). Their $^{31}\text{P}\{^1\text{H}\}$ NMR spectra show singlets at -33.41 and -33.45 ppm, respectively, against -36.63 ppm for $[\text{RuCl}_2(\text{PTA})(\eta^6\text{-}p\text{-cymene})]$ in CDCl_3 . Both solid-state structures exhibit the expected distorted octahedral geometry around the metal [56]. Two independent molecules of **146** were identified in the asymmetric unit with Ru–P bond lengths $[2.290(3)$ Å and $2.279(2)$ Å] similar to those observed in $[\text{RuCl}_2(\text{PTA})(\eta^6\text{-}p\text{-cymene})]$ whilst the two Ru–P bond lengths in **147** $[2.317(2)$ and $2.315(2)$ Å] are similar to those found in $[\text{Cp}^*\text{RuCl}(\text{PTA})_2]$. In both complexes, the three Ru–S bond lengths are remarkably different: those *trans* to Cl are significantly shorter $[2.233(3)\text{--}2.275(3)$ Å (**146**); $2.295(2)$ Å (**147**)] than that *trans* to the PTA phosphorus donor $[2.365(3)$ and $2.349(3)$ Å (**146**); $2.395(2)$ and $2.372(2)$ Å (**147**)]. The symmetry of each complex in solution (Cs) is higher than in the solid state owing to rapid conformational equilibration of the [9]aneS₃. In aqueous solution complex **146** undergoes chloride exchange to give the corresponding aquo



Scheme 30.

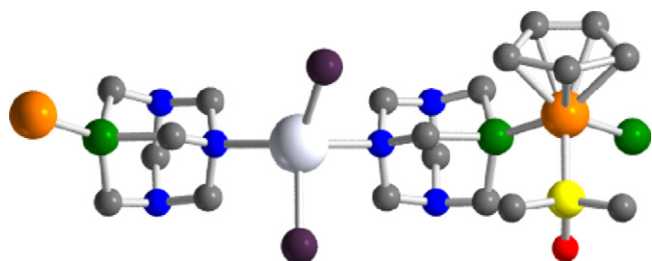


Fig. 11. X-ray crystal structure of the linear chain in **58**. H atoms on all ligands omitted for clarity. Adapted from ref. [38].

species. This process is rapidly reversed in the presence of free chloride, and coordination of phosphate to the aquo species is proposed to occur in phosphate-buffered solutions at physiological pH [56].

Aiming at finding new ruthenium compounds with high antiproliferative properties, Dutta et al. have recently reported on two compounds (**148**–**149**) which are not only two orders of magnitude more active than a close model structure but also show excellent activities in a cisplatin-resistant cancer cell line [57]. Thus, compounds $[(\text{Cp}^*\text{OR})\text{RuCl}(\text{PTA})_2]$ [$\text{Cp}^*\text{OR} = \eta^5\text{-1-alkoxy-2,4-di}(t\text{-butyl})\text{-3-neopentyl cyclopentadienyl}$; R = Me (**148**), Et (**149**)] were prepared as shown in Scheme 30 below. The planar chirality of the ring makes the two P atoms of the PTA ligands chemically different as indicates the presence of two doublets at the $^{31}\text{P}\{^1\text{H}\}$ NMR spectrum in $\text{C}_6\text{D}_5\text{CD}_3$ [−38.14 (d, $^2J_{\text{PP}} = 35$ Hz) and −48.22 (d, $^2J_{\text{PP}} = 35$ Hz) for **148** and −37.84 (d, $^2J_{\text{PP}} = 36$ Hz) and −47.64 (d, $^2J_{\text{PP}} = 36$ Hz) for **149**]. The X-ray analysis of **148** displays the expected three-legged piano-stool geometry with two PTA and one chloro ligand coordinated opposite to the π -ligand. Both compounds can be dissolved in toluene and diethyl ether, whereas $[\text{CpRuCl}(\text{PTA})_2]$ is not soluble in these solvents [57].

The bimetallic neutral coordination polymer $[\{\text{CpRu}(\text{PTA})_2(\text{dmsO}-\kappa\text{S})\}\{\text{AgCl}_2\}]_\infty$ (**58**) is the first known case of a water soluble ($S_{25^\circ\text{C}} = 12 \text{ mg mL}^{-1}$), air-stable, heterobimetallic polymeric structure based on two metal-containing moieties ($[\text{CpRu}]^+$ and $[\text{AgCl}_2]^-$) bridged by PTA, in an unprecedented N,P coordinating mode (Fig. 11) [38].

Complex **58** is quantitatively obtained when 1 equiv of NH_4Cl is added to a reaction mixture containing $[\text{CpRuCl}(\text{PTA})_2]$ (**53**) and AgOTf in dmsO, whereas in absence of NH_4Cl a mixture of **57** and

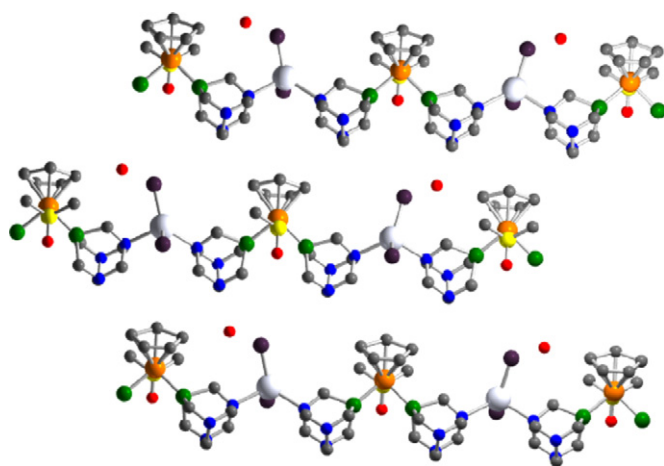
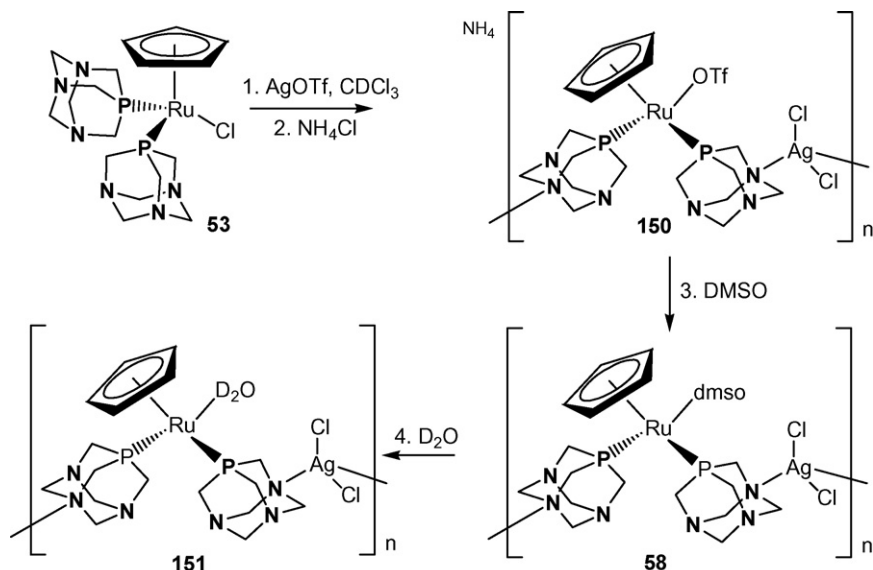


Fig. 12. Linear chains in the crystal lattice of **58**. H atoms on all ligands omitted for clarity. Atom colour code: Ru, orange; Ag, silver; P, green; C, gray; N, blue; S, yellow; Cl, purple; O, red. Adapted from ref. [38].

58 is obtained. If the same reaction is performed in CDCl_3 , an $\eta^1\text{-O}$ -coordinate triflate completes the coordination sphere of the Ru atom giving the complex $(\text{NH}_4)[\{\text{CpRu}(\text{OTf})(\text{PTA})_2\}\{\text{AgCl}_2\}]_\infty$ (**150**) characterized by a singlet at −20.85 ppm in the $^{31}\text{P}\{^1\text{H}\}$ NMR spectrum. A solution of **58** in D_2O reversibly exchanges the dmsO ligand to give the aquo complex $[\{\text{CpRu}(\text{D}_2\text{O})(\text{PTA})_2\}\{\text{AgCl}_2\}]_\infty$ (**151**) (singlet at −20.83 ppm in D_2O in the $^{31}\text{P}\{^1\text{H}\}$ NMR spectrum, Scheme 31) [38].

The solid structure of **58** was authenticated by X-ray crystallography. The compound forms a linear chain polymer by alternating $[\text{CpRu}(\text{dmsO}-\kappa\text{S})]^+$ cations and $[\text{AgCl}_2]^-$ anions, with bridging PTA ligands as tethering units between the two metal aggregates ($d_{\text{Ru}\cdots\text{Ag}} = 6.52(1) \text{ \AA}$). The PTA is behaving as a bidentate ligand, bonded to the ruthenium center through the P atom and to the dichloroargentate(I) moiety through one of the three nitrogen atoms contained in the adamantane cage. The crystal structure includes a molecule of water hydrogen bound to a PTA nitrogen atom belonging to a different polymer chain ($d_{\text{O}\cdots\text{N}} = 2.919(2) \text{ \AA}$) (Fig. 12).

Dynamic light-scattering (DLS) experiments carried out on complexes **58**, **150**, **151** indicate that the polymeric structure is retained



Scheme 31.

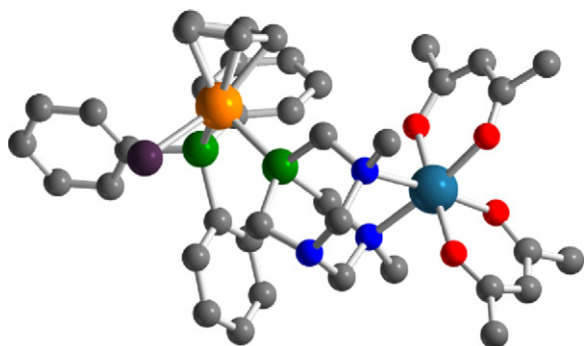


Fig. 13. X-ray crystal structure of $[\text{CpRuCl}(\text{PPh}_3)\text{-}\mu\text{-dmoPTA-1}\kappa\text{-P: } 2\kappa^2\text{-N,N'-Co(acac-}\kappa^2\text{-O,O')}_2]$ (**153**). H atoms omitted for clarity. Adapted from ref. [58].

in various solvents (dmso for complex **58**, dynamic diameter 247 nm; CHCl_3 for complex **150**, dynamic diameter 312 nm; water for complex **151**, dynamic diameter 500 nm) [38].

The polymeric complex $[\text{CpRuCl}(\text{PTA})_2(\text{Ph}_3\text{B}_3\text{O}_3)]_n \cdot 3\text{CH}_2\text{Cl}_2$ (**152**), in which the nitrogen sites of PTA are involved in dative bonding to another atom, was serendipitously obtained in very low yield (<10%) when NaBPh_4 was reacted with $[\text{CpRuCl}(\text{PTA})_2]$ in the presence of 1-propanol, probably due to small amounts of $\text{Ph}_3\text{B}_3\text{O}_3$ impurities in the NaBPh_4 , or from adventitious water reacting with the tetraphenylborate anion generating triphenylboroxine [16]. This complex was also obtained in moderate yields (48%) by reaction of $[\text{CpRuCl}(\text{PTA})_2]$ with three equivalents of phenylboronic acid in dichloromethane, which affords large orange crystals of $[\text{CpRuCl}(\text{PTA})_2(\text{Ph}_3\text{B}_3\text{O}_3)]_n \cdot 1/2 \text{CH}_2\text{Cl}_2$ (**152**). Unlike the polymers obtained by Lidrissi et al., [38] this compound does not remain polymeric in aqueous solution. The presence of the boroxine produces a shielding of the Cp protons and a deshielding of those of PTA as observed from the ^1H NMR spectra of **152** compared to that of $[\text{CpRuCl}(\text{PTA})_2]$ [16]. Two signals in the ^{11}B NMR spectrum of **152** in acetone (29.3 and 21.3 ppm) reveal that **152** remains polymeric in acetone with two of the boron atoms of triphenylboroxine coordinated to one PTA and the remaining boron being uncoordinated. Dark orange crystals of **152** were obtained by slow diffusion of hexanes into a CH_2Cl_2 solution of **152**. The X-ray diffraction analysis of **152** shows $[\text{CpRuCl}(\text{PTA})_2]$ moieties linked together in linear chains by $\text{Ph}_3\text{B}_3\text{O}_3$, cocrystallized with half a molecule of CH_2Cl_2 [16]. Two of the three boron atoms in triphenylboroxine form N–B bonds, which affords a linear polymer, with the geometry about the coordinated boron sites significantly distorted from planar towards tetrahedral with O–B–O angles of $115.8(2)^\circ$ and N–B–C angles of $107.46(18)^\circ$.

The heterobimetallic complex $[\text{CpRuCl}(\text{PPh}_3)\text{-}\mu\text{-dmoPTA-1}\kappa\text{-P: } 2\kappa^2\text{-N,N'-Co(acac-}\kappa^2\text{-O,O')}_2] \cdot \text{H}_2\text{O}$ (**153**) is prepared by reaction of complex **90** with Co(acac)_2 in methanol [58]. The $^{31}\text{P}\{^1\text{H}\}$ NMR spectrum in CD_3OD shows two doublets at 52.71 and 51.56 ppm ($^2J_{\text{PP}} = 41.6 \text{ Hz}$), located downfield than those found in **91** [$\delta(\text{PPh}_3) = 46.00 \text{ ppm}$; $\delta(\text{HdmoPTA}) = -2.93 \text{ ppm}$], while the coupling constant is practically the same ($^2J_{\text{PP}} = 42.72 \text{ Hz}$). The greater shifting of the dmoPTA signal ($\Delta\delta = 54.49 \text{ ppm}$) compare to that of the PPh_3 ($\Delta\delta = 6.71 \text{ ppm}$) is claimed to be due to the bigger paramagnetic influence of the Co(II) bonded to dmoPTA through both $\text{CH}_3\text{-N}$ atoms. Powder magnetism measurements of **153** between 2 and 300 K showed that the values and the shape of the curve are as expected for isolated octahedral Co(II) ions with some trigonal distortions [58]. Crystals good enough for X-ray diffraction were obtained by slow evaporation from an acetone solution of **153** [58]. The Ru atom is in a highly distorted pseudooctahedral environment [$\text{P1-Ru-P2} = 99.04(11)^\circ$], similar to that observed for the precursor complex **90** (Fig. 13). The monodentate $[\text{CpRuCl}(\text{PPh}_3)](\text{dmoPTA-}$

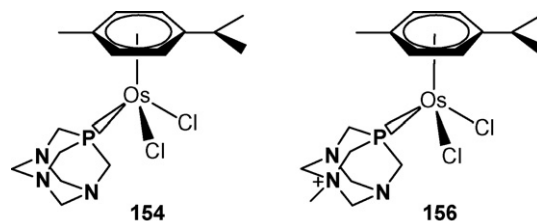


Chart 10.

$\kappa^1\text{P}$) entity acts as a bidentate ligand by its $\text{CH}_3\text{-N}$ atoms towards a Co atom, which completes its six-coordination geometry with four O atoms from two acac molecules. The ligands bonded to the metal form four stable six-membered chelated rings $[2(\text{Co-O-C-C-C-O}) + (\text{Co-N-C-P-C-N}) + (\text{Co-N-C-N-C-N})]$. Weak hydrogen bonds, $\text{C-H} \cdots \text{Cl}$ and $\text{N-H} \cdots \text{O}_{\text{water}}$, (ranging from 2.783 to 2.869 Å and from 2.644 to 2.801 Å, respectively) interconnect the heterometallic dinuclear units [58].

Osmium–PTA complexes such as $[\text{OsCl}_2(\eta^6\text{-p-cymene})(\text{PTA})]$ (**154**), $[\text{OsCl}_2(\eta^6\text{-p-cymene})(\text{PTA})_2]\text{Cl}$ (**155**), and mPTA complexes $[\text{OsCl}_2(\eta^6\text{-p-cymene})(\text{mPTA})]\text{Cl}$ (**156**), $[\text{OsCl}_2(\eta^6\text{-p-cymene})(\text{mPTA})_2]\text{Cl}_3$ (**157**) have been synthesized to compare the activity as anticancer drugs to their ruthenium analogues (complexes **154** and **156**, Chart 10) [49] and to study their reactivity with model DNA bases (in the case of **155** and **157**) [59] (see Section 5). The complexes were prepared from the direct reaction of the dimer $[\text{Os}(\eta^6\text{-p-cymene})(\mu\text{-Cl})\text{Cl}]_2$ with 2 or 4 equiv of the appropriate phosphine. The complexes are highly soluble in water and have been characterized by ^1H and $^{31}\text{P}\{^1\text{H}\}$ NMR spectroscopy and ESI-MS. The $^{31}\text{P}\{^1\text{H}\}$ NMR spectra are very simple, exhibiting singlets at -80.4 and -63.7 ppm for **154** and **156**, respectively, and at -79.6 and -64.8 ppm for **155** and **157**. The molecular structures of compounds **154–156** display the characteristic piano-stool geometry with structural parameters very similar to those of related compounds. $[\text{OsCl}_2(\eta^6\text{-benzene})(\text{PTA})]$ (**158**) [59] was prepared by treating the dimer $[\text{Os}(\eta^6\text{-benzene})(\mu\text{-Cl})\text{Cl}]_2$ (obtained in situ by dissolving $[\text{Os}(\eta^6\text{-benzene})\text{Cl}_2(\text{CH}_3\text{CN})]$ in water and removing the solvent under pressure) with two equiv of PTA in MeOH. The complex is a pale green solid and displays a singlet at -76.5 ppm in the $^{31}\text{P}\{^1\text{H}\}$ NMR spectrum in D_2O .

3.4. Cobalt, rhodium and iridium complexes

The first example of a cobalt complex bearing PTA, i.e. *mer*- $[\text{Co}(\text{NCS})_3(\text{PTA})_3] \cdot \text{EtOH}$ (**159**), was obtained by treating anhydrous CoCl_2 in ethanol with PTA followed by the addition of an acidic (HCl) solution of sodium thiocyanate in ethanol [60]. The unexpected oxidation of Co(II) to Co(III) by air, overcomes the common ability of PTA to act as a reductant of group 8–10 metal centers. The IR spectrum of **159** exhibits the typical absorptions for terminal N-bonded thiocyanate ligands and the $^{31}\text{P}\{^1\text{H}\}$ spectrum in $\text{DMSO-}d_6$ shows a triplet and a doublet at $\delta 8.9$ and -10.9 ppm ($^2J_{\text{PP}} = 38 \text{ Hz}$), respectively, indicative of the meridional configuration of the phosphines. The molecular structure of **159** exhibits a rather distorted octahedral environment about the Co center with three neutral P-bonded PTA and three N-bonded thiocyanate ligands in a meridional configuration [60].

The aquo cobalt complex *trans*- $[\text{Co}(\text{NCS})_2(\text{PTA}=\text{O})_2(\text{H}_2\text{O})_2]$ (**160**), having two molecules of N-coordinated oxide $\text{PTA}=\text{O}$, was obtained when an aqueous solution of $\text{Co}(\text{NO}_3)_2$ was reacted with $\text{PTA}=\text{O}$ [60]. Complex **160** is a water-soluble pink-orange solid which displays, besides the typical bands corresponding to the N-bonded thiocyanate ligands, a strong $\nu(\text{P}=\text{O})$ band at 1165 cm^{-1} in the IR spectrum. The crystal structure of **160** is composed of discrete monomeric units, with a Co(II) lying on an inversion cen-

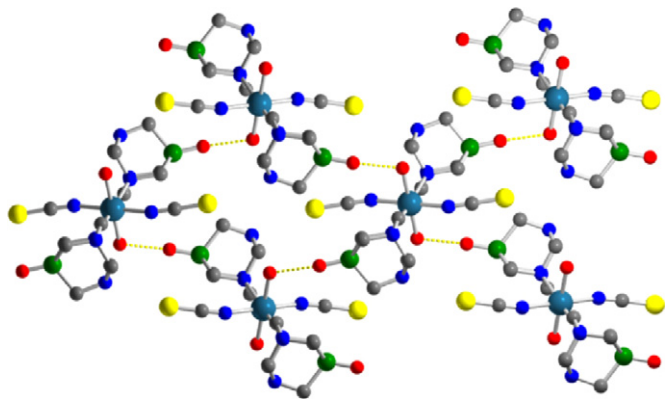
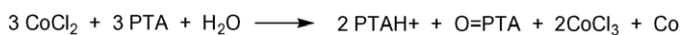


Fig. 14. Intramolecular HO–H...O=P hydrogen bonding (yellow dashed line) in the solid-state structure of *trans*-[Co(NCS)₂(PTA=O)₂(H₂O)₂] (**160**). H atoms omitted for clarity. Atom colour code: Co, steelblue; P, green; C, gray; N, blue; O, red; S, yellow. Adapted from ref. [60].



Scheme 32.

ter of a slightly distorted octahedral coordination geometry with the three types of ligands symmetrically equivalent and mutually *trans*-oriented. The structure presents an extensive intermolecular hydrogen-bonding interactions with water molecules acting as a double-hydrogen-bond donor to the PTA=O O atom [O–H...O 2.659(4) Å] and to one of the N atoms of the PTA core [O–H...N 2.830(4) Å] (Fig. 14).

When PTA and CoCl₂·6H₂O are dissolved in acetone and the solution is refluxed for 30 min, the complex [PTAH][Co(PTA=O)Cl₃] (**161**) [61] is obtained as a blue-green product. Oxidation of PTA was proposed by the authors to occur due to adventitious water and reduction of excess of Co(II) (Scheme 32).

If the reaction is carried out at room temperature, the compound [Co(H₂O)₃(PTA=O)(CoCl₃-PTA=O)₂] (**162**) is obtained [61]. The main part of the structure consists of an octahedral Co(II) center with three facial PTA=O ligands and three facial aquo ligands. In addition, two of the three PTA ligands are bound through a N atom to a tetrahedral CoCl₃[−] anion, yielding a zwitterionic complex (Fig. 15). Both complexes present bond lengths and angles consistent with other PTA complexes [61].

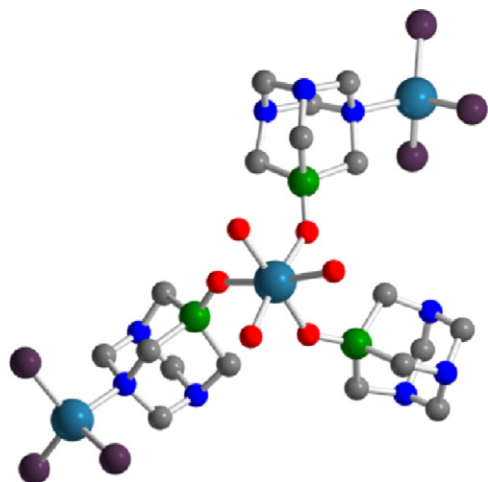


Fig. 15. X-ray crystal structure of [Co(H₂O)₃(PTA=O)(CoCl₃-PTA=O)₂] (**162**). H atoms omitted for clarity. Adapted from ref. [61].

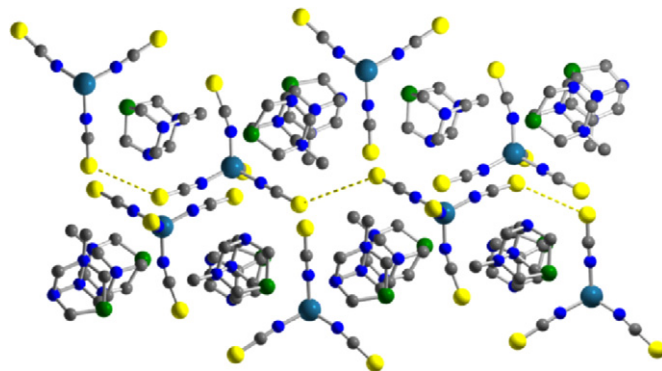
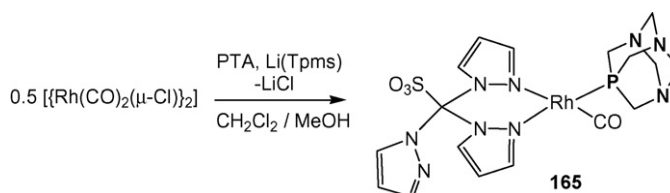


Fig. 16. Solid state packing of [(mPTA)₂{Co(NCS)₄}] (**163**). H atoms omitted for clarity. Atom colour code: Co, steelblue; P, green; C, gray; N, blue; S, yellow. Intermolecular S...S contacts depicted in yellow. Adapted from ref. [62].

The hybrid organic–inorganic compounds [(mPTA)₂{Co(NCS)₄}] (**163**) and [{EtPTA}₂{Co(NCS)₄}] (**164**) were obtained as blue air-stable solids by reaction of anhydrous CoCl₂, [R-PTA]I (R=Me, Et) and NaSCN [62]. Compounds **163** and **164** have been characterized by IR spectroscopy, FAB⁺-MS, EA and X-ray crystallography. The IR spectra of both compounds show the typical bands due to the [R-PTA] moieties, unshifted relatively to [R-PTA]I. The molecular structure of **163** [62] is composed of two symmetry inequivalent cage-like [mPTA]⁺ cations and one discrete [Co(NCS)₄]^{2−} anion with structural parameters comparable to those reported for other [mPTA]⁺ cations and [Co(NCS)₄]^{2−} anions. Interestingly, **163** presents a linkage of adjacent [Co(NCS)₄]^{2−} units through repeating weak intermolecular S...S [3.53(1) Å] contacts thus giving rise to 1D wave-like supramolecular chains. Such chains constitute the host matrix with cavities filled by the guest [mPTA]⁺ cations (Fig. 16). Complex **164** presents most of the structural features and bonding parameters similar to those of **163**, but the high degree of disorder of the crystal structure precluded a more detailed discussion [62].

The first water-soluble [Rh(Tpms)(CO)(PTA)] (**165**) transition-metal complex bearing PTA and Tpms [Tpms = tris(1-pyrazolyl)methanesulfonate] ligands [63] was obtained in high yield from [{Rh(CO)₂(μ-Cl)}₂], in a single pot, without the need for isolation of any intermediate. The synthetic strategy, in addition, directly employs Li(Tpms) and PTA without the use of CO or Tl(Tpms) salt (Scheme 33).

The ³¹P{¹H} NMR spectrum exhibits a doublet at −37.3 ppm (¹J_{RhP} = 151 Hz). Variable temperature ¹H NMR spectroscopy shows that, similarly to other Tpms complexes, a dynamic and fast pyrazolyl coordination exchange occurs at room temperature in CDCl₃, which is halted at −60 °C when the pyrazolyl groups become non-equivalent. In D₂O the ¹H NMR spectra shows the equivalence of the three pyrazolyl rings at 80 °C, and at room temperature the pyrazolyl exchange rate becomes comparable to the NMR time scale, implying that the exchange in D₂O is slower than in CD₃OD. A strong and sharp band at 2007 cm^{−1} confirms the presence of a terminal CO ligand. The crystal structure of **165** shows that the anionic tris(1-pyrazolyl)methanesulfonate group acts as a bidentate κ²-



Scheme 33.

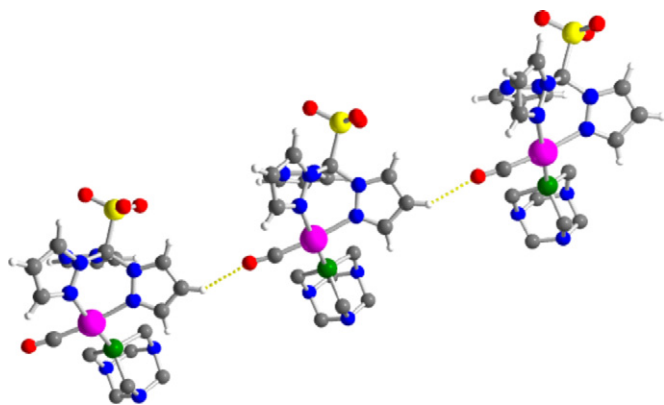


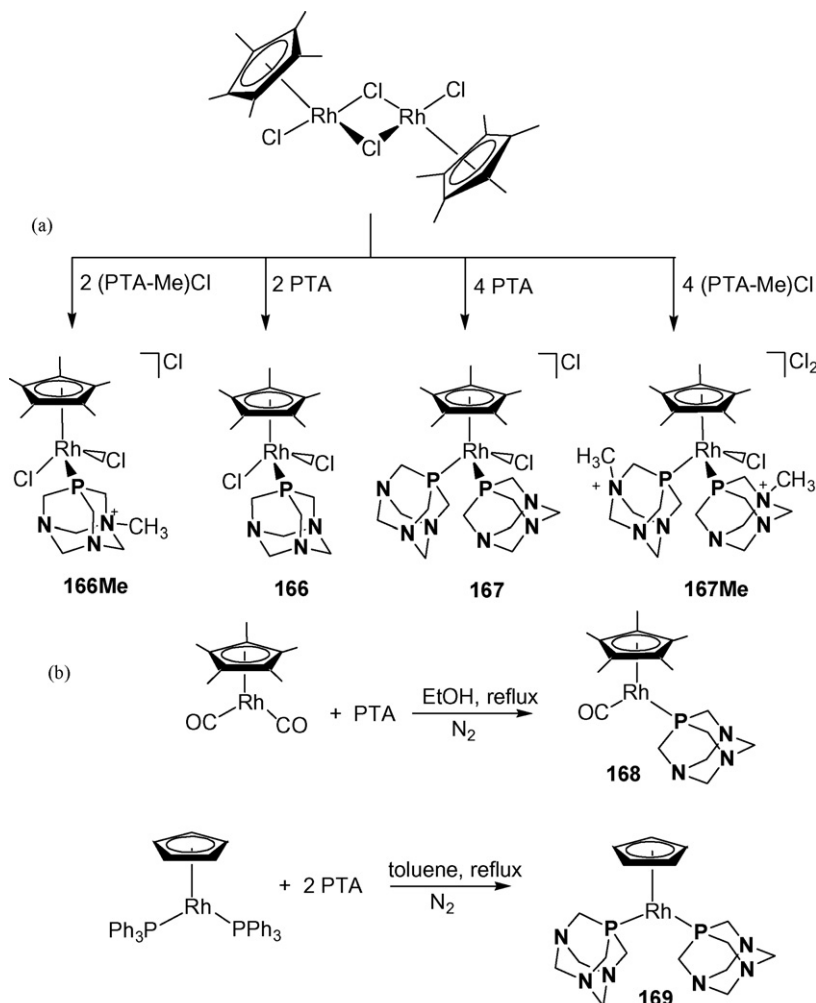
Fig. 17. Diagram of the C-H(pz)···O≡C hydrogen bonding in **165**. H atoms on PTA omitted for clarity. Adapted from ref. [63].

N,N-ligand, binding the Rh atom through the two pyrazolyl nitrogen atoms. PTA and CO complete the coordination sphere. Extensive inter-molecular hydrogen bonds are also formed, with d(H···A) distances ranging from 2.40 to 2.59 Å (Fig. 17). Cyclic voltammetry measurements of complex **165** show that PTA is a net electron-donor comparable to PMe₃, pyridine or acetonitrile [63].

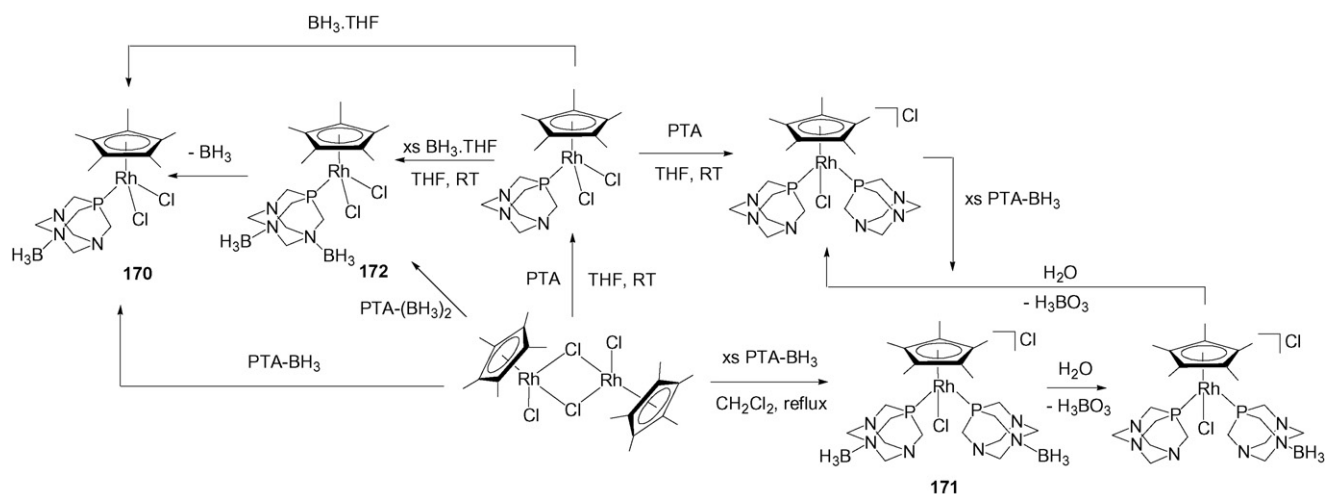
Direct reactions of the rhodium dimer $[(\eta^5\text{-C}_5\text{Me}_5)\text{Rh}(\mu^2\text{-Cl})_2]_2$ with 2 or 4 equiv of PTA [64] or (mPTA)Cl, [59] afford the highly water-soluble species $[(\eta^5\text{-C}_5\text{Me}_5)\text{Rh}(\text{PTA})\text{Cl}_2]$ (**166**),

$[(\eta^5\text{-C}_5\text{Me}_5)\text{Rh}(\text{PTA})_2\text{Cl}]\text{Cl}$ (**167Cl**), $[(\eta^5\text{-C}_5\text{Me}_5)\text{Rh}(\text{mPTA})\text{Cl}_2]\text{Cl}$ (**166Me**) and $[(\eta^5\text{-C}_5\text{Me}_5)\text{Rh}(\text{mPTA})_2\text{Cl}]\text{Cl}_2$ (**167Me**), respectively (Scheme 34a). Stirring **167Cl** with NaBPh₄ in MeOH easily substitutes the chloride counteranion by tetraphenylborate to give $[(\eta^5\text{-C}_5\text{Me}_5)\text{Rh}(\text{PTA})_2\text{Cl}]\text{BPh}_4$ (**167BPh₄**) [64]. Two Rh(I) complexes bearing $\eta^5\text{-C}_5\text{H}_5$ with either one or two PTA ligands, namely, $[(\eta^5\text{-C}_5\text{H}_5)\text{Rh}(\text{CO})(\text{PTA})]$ (**168**) and $[(\eta^5\text{-C}_5\text{H}_5)\text{Rh}(\text{PTA})_2]$ (**169**) were also synthesized (Scheme 34b) by substituting one CO or two PPh₃ ligands from suitable Rh(I) precursors $[\text{Cp}'\text{RhL}_2]$ (Cp' = Cp, Cp*; L = CO, PPh₃) [64]. The solution $^{31}\text{P}\{^1\text{H}\}$ NMR spectra of **166–169** exhibit doublet resonances at –32.37 ppm ($^1J_{\text{RhP}} = 141$ Hz) (**166**), –28.68 ppm ($^1J_{\text{RhP}} = 131$ Hz) (**167**), –24.7 ppm ($^1J_{\text{RhP}} = 150$ Hz) (**166Me**), and –28.2 ppm ($^1J_{\text{RhP}} = 140$ Hz) (**167Me**). The two rhodium(I) complexes $[(\eta^5\text{-C}_5\text{H}_5)\text{Rh}(\text{CO})(\text{PTA})]$ and $[(\eta^5\text{-C}_5\text{H}_5)\text{Rh}(\text{PTA})_2]$ exhibit typical doublet resonances in their solution $^{31}\text{P}\{^1\text{H}\}$ NMR spectra at –36.8 ppm ($^1J_{\text{RhP}} = 187.2$ Hz) and –25.32 (d, $^1J_{\text{RhP}} = 205.0$ Hz). The high magnitude of the $^1J_{\text{RhP}}$ is in line with the presence of a Rh(I) center.

Single crystals of **166**, **167Cl**, **167BPh₄** [64] and **167Me** [59] were obtained. The molecular packing of **166** is characterized by a small number of contacts, the shortest being between a nitrogen center of PTA and a methyl hydrogen of the $\eta^5\text{-C}_5\text{Me}_5$ ligand, 2.547 Å, and a longer contact between one chlorine substituent and a CH₂ group of PTA, 2.898 Å. Interestingly, the other Cl group has no other interactions apart from its bonding to the metal. Two different crystal structures have been obtained, which differ by the type of anion



Scheme 34.



Scheme 35.

and solvate contained within the lattice. The Rh–Cl and Rh–P bond distances in **166** and the two salts of **167** are essentially equivalent. The major difference between the mono- and bis-PTA species lies in the coordination of the η^5 -C₅Me₅ ring to the Rh center. In **166**, the two methyl substituents that eclipse the PTA ligand are lifted out of the C5 ring plane, by 5.49°. In contrast, the presence of two PTA units in **167** results in a lengthening of the Rh–Cp(centroid) distance as compared to **166** [1.861 Å vs. 1.804 Å] and in all of the methyl groups being bent above the C5 ring plane, ranging from 9.86° to 3.07°. The steric hindrance of the two phosphines in bis(mPTA) compound **167**Me [59] is reflected in the P–Rh–P angle being greater than 90° [95.75(7)°], and in the distortion of the Cp* ligand, showing deviation from the plane of the pentagon [0.35 Å for C21 and 0.3 Å for C24]. The complex **167**Me shows a large number of hydrogen bonds which link solvates (MeOH) with the anion and/or the cation [59].

Mono- and bis-(PTA-BH₃) complexes [Cp*RhCl₂(PTA-BH₃)] (**170**) and [Cp*RhCl(PTA-BH₃)₂]Cl (**171**) and the bis-boronated complex [Cp*RhCl₂{PTA-(BH₃)₂}] (**172**) were prepared by reaction of PTA-BH₃ or PTA-(BH₃)₂ with the dimer [Cp*RhCl(μ-Cl)]₂, respectively (Scheme 35) [65].

Alternatively, the compounds can also be obtained by direct (reversible) boronation of the parent Rh-PTA complexes [65]. Partial PTA deboronation of **172** (in solution and solid state) gives compound **170**. Presence of the aminoborane moiety was corroborated by IR bands of ν_{BN} at 1176, 1161 and 1164 cm⁻¹, respectively. The solid-state structure of [Cp*RhCl₂(PTA-BH₃)] can be described as a three-legged piano stool and shows that the boronation does not affect significantly the structural parameters in comparison with those of the parent compound [Cp*RhCl₂(PTA)] [Rh–P bond length 2.268(4) Å vs. 2.286(1) Å] [65].

The dihydride [Cp*RhH₂(PTA-BH₃)] (**173**BH₃) can be obtained by reaction of both **170** and [Cp*RhCl₂(PTA)] with an excess of NaBH₄ [65]. The compound is a brownish red solid, stable if kept under inert atmosphere (ν_{BN} = 1170, ν_{RH} = 1964 cm⁻¹). The two magnetic equivalent hydride ligands display a doublet at δ = –18.5 ppm (J_{RHP} = 155 Hz) in the ³¹P{¹H} spectrum which transforms into a doublet of triplets in the selective coupled ³¹P NMR spectrum ($J_{\text{PH(residual)}}$ = 43 Hz). The hydride signal (δ = –13.67 ppm, doublet of multiplets) exhibit a $T_{1(\text{min})}$ of 532 ms at 400 MHz, confirming the classical nature of the hydride ligands. Proton and carbon signals are fully assigned by 2D homo- and heteronuclear correlation experiments, and by computer simulation studies. The dihydride is unstable in chlorinated solvents, reverting to the chloride precursor, but it is stable in benzene, toluene and acetone for several days when stored under inert atmosphere.

Deboronation takes place by hydrolytic removal of BH₃ affording the rhodium dihydride [Cp*RhH₂(PTA)] (**173**) [65].

Reaction of **173**BH₃ with activated alkynes (phenylacetylene or ethyl propiolate) in C₆H₆ gives the π -alkene complexes [Cp*Rh(PTA-BH₃)(η^2 -CH₂=CHPh)] (**174**) and [Cp*Rh(PTA-BH₃)(η^2 -CH₂=CHC(O)OEt)] (**175**), as orange solids stable at room temperature if stored under inert atmosphere [65]. The presence of two doublets in both the ³¹P{¹H} NMR spectra in the ratios 1:4 and 1:9, respectively, is attributed to the presence of rotamers of the η^2 -alkene complexes. The absence of coalescence of the signals when temperature is raised to 80 °C suggests a high-energy rotational barrier of interconversion. The solid-state structure of **174** shows the typical piano-stool structure with all bond distances in the expected range (Fig. 18) [65].

The first examples of transition-metal complexes bearing the “lower rim” modified PTA ligands **PTA**_{R3} are [Rh(CO)Cl(PTA_{R3})₂] [R = Ph (**176**), C₆H₄OCH₃ (**177**), C₆H₄CN (**178**)] and can be obtained by reaction of [RhCl(CO)(PPh₃)₂] with appropriate amount of the ligand in benzene [19]. Compounds are off-white (**176**, **178**) or pale-yellow (**177**) solids displaying doublets in their ³¹P{¹H} NMR and strong ν_{CO} IR bands (CHCl₃) at 1979, 1978, and 1987 cm⁻¹, respectively. Modification of the triazacyclohexane ring of PTA alters the steric properties of the phosphine with minimal changes to the electronics. Comparison of ν_{CO} for a series of

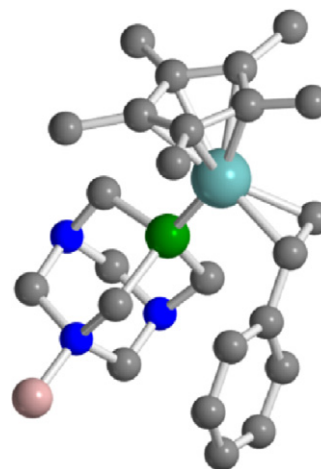


Fig. 18. Structure of [Cp*Rh(PTA-BH₃)(η^2 -CH₂=CHPh)] (**174**). H atoms omitted for clarity. Adapted from ref. [65].

Table 6 $\nu(\text{CO})$ stretching frequencies for $\text{trans-Rh}(\text{CO})\text{Cl}(\text{PTA}_{\text{R}_3})_2$ in CHCl_3 .

$\text{Rh}(\text{CO})\text{Cl}(\text{PR}_3)_2$	$\nu(\text{CO})$ (cm^{-1})
$\text{PR}_3 = \text{PPh}_3$	1979
$\text{PR}_3 = \text{P}(\text{CH}_2\text{OH})_3$	1960
$\text{PR}_3 = \text{PTA}_{\text{R}_3}$	
$\text{R} = \text{H}$	1963
$\text{R} = \text{C}_6\text{H}_5$	1979
$\text{R} = \text{C}_6\text{H}_4\text{OMe}$	1978
$\text{R} = \text{C}_6\text{H}_4\text{CN}$	1987

$\text{trans-Rh}(\text{CO})\text{Cl}(\text{PTA}_{\text{R}_3})_2$ complexes indicates that these ligands are similar electronically (Table 6) and less electron-donating than PTA [19].

The synthesis of the P-coordinated PTN(R) complexes from $[\text{RhCl}(\text{cod})]_2$ is straightforward ($\text{cod} = 1,5\text{-cyclooctadiene}$, Scheme 35) and affords the products $\kappa^1\text{-P-}[\text{RhCl}(\text{cod})\{\text{PTN}(\text{R})\}]$ ($\text{R} = \text{Me}$, **179a**; $\text{R} = \text{Ph}$, **179b**) as air- and moisture-stable yellow solids in high yields [66]. Complex **179a** is readily soluble in chlorinated solvents, toluene, and benzene and moderately soluble in water with $S_{(25^\circ\text{C})} = 3.80 \text{ mg mL}^{-1}$, at a value comparable to $[\text{RhCl}(\text{PTA})_3]$ and $[\text{Rh}(\text{acac})(\text{CO})(\text{PTA})]$ [1]. In contrast, the presence of the phenyl group on P significantly reduces the aqueous solubility for **179b**, $S_{(25^\circ\text{C})} = 0.74 \text{ mg mL}^{-1}$. Toluene solutions of **179** instantly produce black precipitates when heated beyond 100°C , whereas a sample of **179a** in D_2O heated to 80°C showed no change in the $^{31}\text{P}\{^1\text{H}\}$ spectrum after 5 h. Reaction of complexes **179** with 1 equiv of NaBARF_4 in dichloromethane affords the $\kappa^2\text{-P,N}$ complexes $[\text{Rh}(\text{cod})\{\text{PTN}(\text{R})\}](\text{BARF}_4)$ ($\text{R} = \text{Me}$, **180a**; $\text{R} = \text{Ph}$, **180b**, Scheme 35), which were isolated as air-sensitive bright yellow compounds. The neutral, air- and moisture-sensitive rhodium complex $\kappa^2\text{-P,N-}[\text{RhI}(\text{CO})\{\text{PTN}(\text{Me})\}]$ (**181**) is obtained directly by reacting the dimer $[\text{Rh}_2(\text{CO})_4\text{I}_2]$ with 2 equiv of PTN(Me) in dichloromethane or toluene and stirring for 1 h at room temperature, as shown in Scheme 36. The water solubility of **181** [$S_{(25^\circ\text{C})} = 0.2 \text{ mg mL}^{-1}$] is remarkably decreased from that of **180a**. ^1H - ^1H COSY and ^1H - ^{13}C HETCOR experiments were used to provide definitive assignments of the CH_2 groups of the ligand in **180a** and **180b**. Both the ^1H and ^{13}C NMR show that one set of the CH groups belonging to COD is shifted extremely upfield. These effects are attributed to the ring current generated by the π -system of the phenyl substituent. For **181**, the CO stretching frequency was

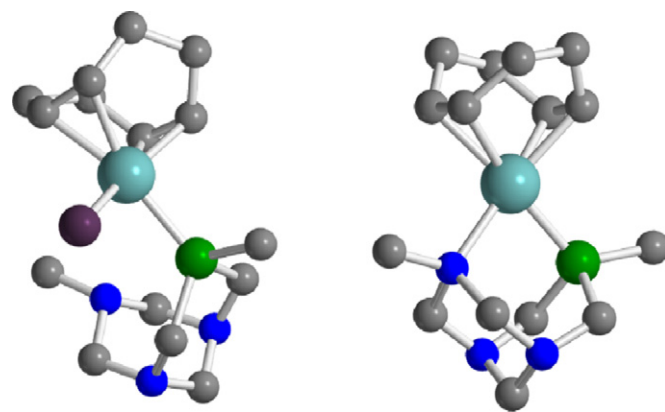
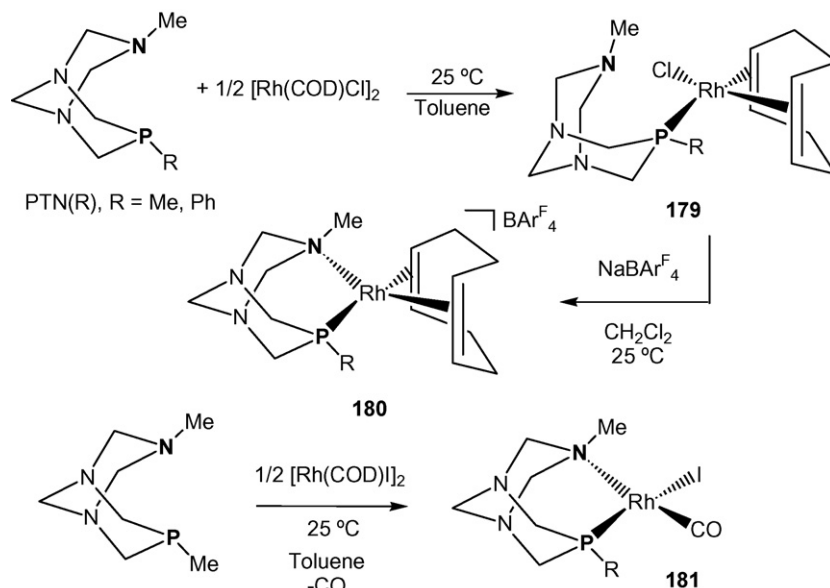


Fig. 19. X-ray crystal structures of $\kappa^1\text{-P-}[\text{RhCl}(\text{cod})\{\text{PTN}(\text{Me})\}]$ (**179a**) and $\kappa^2\text{-P,N-}[\text{Rh}(\text{cod})\{\text{PTN}(\text{Me})\}]^+$ (**180a**). H atoms omitted for clarity. Adapted from ref. [66].

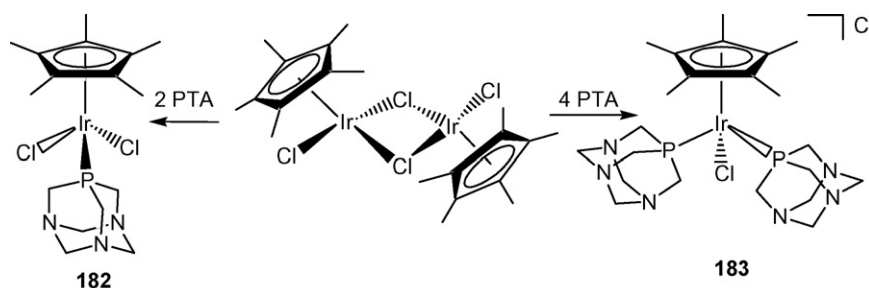
observed at 1989 cm^{-1} in CH_2Cl_2 and at 1974 cm^{-1} in KBr. The crystal structures for **179**, **180**, and **181** show that all compounds feature a square-planar geometry, two coordination positions being defined either by the centers of the C–C bonds of COD or, in the case of **181**, by iodide and CO ligands (Fig. 19). Compounds **179** contain a coordinated P donor and a dangling N(Me) group, the fourth coordination position being occupied by the chloride ligand, whereas the ligand adopts the $\kappa^2\text{-P,N}$ coordination mode in compounds **180** and **181** in keeping with the spectroscopic solution data.

The DFT studies reveal significant changes to the PTN ligand on passing from the P-mono- to the P,N chelating-coordination mode. Overall, it is evident that the PTN ligand has a preference for maintaining P-coordination to Rh. In contrast, a higher energy cost in terms of bond strain is associated with P,N-chelation, which suggests that the ligand may show hemilabile behaviour in the presence of polar solvents or other types of nucleophiles [66].

Water-soluble iridium(III) complexes $[\text{Cp}^*\text{IrCl}_2(\text{PTA})]$ (**182**) and $[\text{Cp}^*\text{IrCl}(\text{PTA})_2]\text{Cl}$ (**183**) were prepared by reaction of the iridium dimer $[\text{Cp}^*\text{Ir}(\mu\text{-Cl})\text{Cl}]_2$ with PTA (Scheme 37) [67]. The $^{31}\text{P}\{^1\text{H}\}$ NMR spectra of both complexes show singlets at -67.14 (CD_2Cl_2) and -74.22 (D_2O) ppm, respectively and their solid-state structure can be described as a typical piano-stool structure. The



Scheme 36.

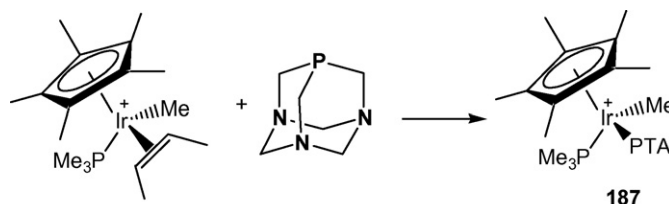


Scheme 37.

distance Ir–Cp* (centroid) for **183** [1.884(2) Å] is longer than for **182** [1.812(5) Å] partially due to greater steric influence of the second PTA group. A hydrogen bonding network is formed in **182** with the hydrogen atoms of the water solvate bridge both a chlorine [2.00(1) Å] and a nitrogen atom [2.22(1) Å], giving a weakly bound dimeric structure (Fig. 20).

Catalytic studies of hydrogenation of hydrogen carbonate with **182** show that the dihydride derivative [Cp*Ir(H)₂(PTA)] (**184**) is formed quantitatively under a pressure of hydrogen as shown by multinuclear NMR spectroscopy [67]. The presence of the two hydride ligands is indicated by the ¹H and ³¹P{¹H} NMR analysis showing a doublet in the hydride region of the corresponding ¹H NMR spectrum [δ = –18.4 ppm (¹J_{PH} = 30 Hz)], which is simplified into a singlet in the ¹H{³¹P} NMR spectrum, and a triplet in the ³¹P NMR spectrum [δ = –68.5 ppm (²J_{PH} = 30 Hz)]. On the other hand, an aqueous (D₂O/H₂O, 1:4) solution of **183** pressurised with 100 bar H₂ shows the presence of the cationic monohydride [Cp*Ir(PTA)₂H]⁺ (**185**), as evidences the presence of a triplet at δ = –17.9 ppm (²J_{PH} = 30 Hz) in the ¹H NMR spectrum (singlet by ³¹P–¹H decoupling). The ³¹P NMR spectrum shows a doublet δ = –76.3 ppm with ²J_{PH} = 30 Hz (reduces to a singlet by ¹H decoupling) [67].

Complex [Ir(cod)(PTA)₃]Cl (**186**), [68] was produced in high yield by reacting [Ir(cod)Cl]₂ with six equivalents of PTA in CH₂Cl₂. Almost immediately, the complex precipitated from the solution as an air-stable solid. The ³¹P{¹H} NMR spectrum of **186** in D₂O exhibits only one sharp singlet (δ = 86.8 ppm) thus indicating that the phosphines are fluxional on the NMR timescale. This behaviour is common with [Ir(cod)P₃]⁺ complexes and is likely due to a Berry pseudo-rotation. The structure of **186** may best be described as a distorted square-pyramid with P(1) occupying the axial site and P(2), P(3), and the COD ligand residing in the basal sites. This struc-



Scheme 38.

ture is similar to that of [Ir(cod)(PMe₃)₃]Cl being both the uniques describe as square pyramid for five-coordinate [Ir(cod)P₃]⁺ complexes; all others are trigonal bipyramidal [68].

As part of kinetic investigations on the mechanism of the C–H activation reactivity within a supramolecular host by an iridium guest, the water-soluble complex [Cp*Ir(Me)(PMe₃)(PTA)](OTf) (**187**) was prepared by reacting [Cp*Ir(Me)(OTf)(PMe₃)] with an stoichiometric amount of PTA (Scheme 38) [69]. The colourless solution obtained was lyophilized to give a white air-stable powder in high yield. The ³¹P{¹H} NMR spectrum of **187** in D₂O shows two doublets corresponding to both phosphines [δ –44.7 ppm (d, ²J_{PP} = 21.1 Hz, P(CH₃)₃), –77.9 ppm (d, ²J_{PP} = 21.1 Hz, PTA)] and the ¹⁹F NMR (D₂O) displays a singlet at δ –78.1 corresponding to the OSO₂CF₃ group. When the complex **187** was added to a solution of the host Na₁₂[Ga₄L₆] (L = catechol amide) no encapsulation occurred, indicating that the guest was too large to fit within the host cavity. Comparative kinetic studies with the parent complex Na₂[Cp*Ir(Me)(PMe₃)(TPPTS)] bearing the charged water-soluble triphenylphosphine tris-sulfonate sodium salt (TPPTS) allowed to propose a novel stepwise iridium guest dissociation mechanism that proceeds via a strongly bound ion pair intermediate [69].

The iridium(III) complex (κ^1 -P)-[Cp*IrCl₂(PZA)] (**188**) was synthesized by reacting the “upper rim” modified PTA ligand phenyl-(1,3,5-triaza-7-phospha-tricyclo[3.3.1.1^{3,7}]dec-6-yl)-methanol (PZA) with the dimer [Cp*IrCl(μ -Cl)]₂ in

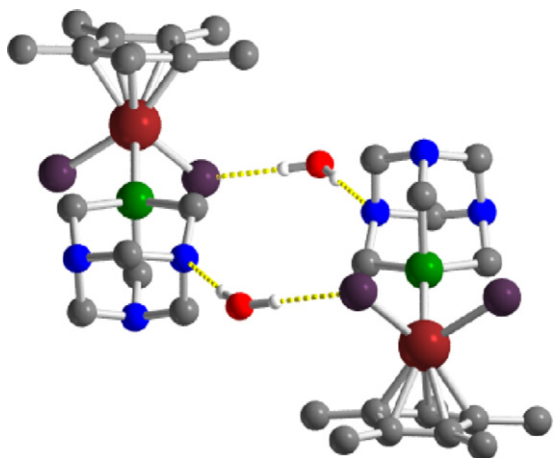


Fig. 20. Dimeric structure of **182** showing the weak H bonding between water molecules, the N atom of PTA and Cl ligands. Adapted from ref. [67].

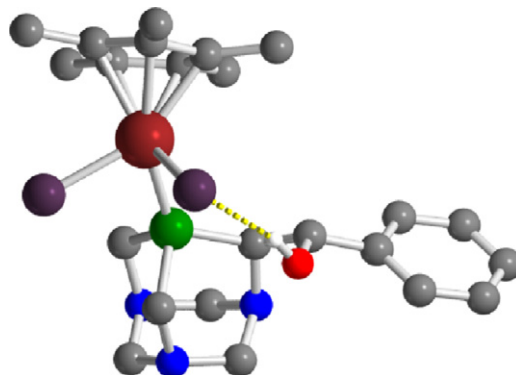
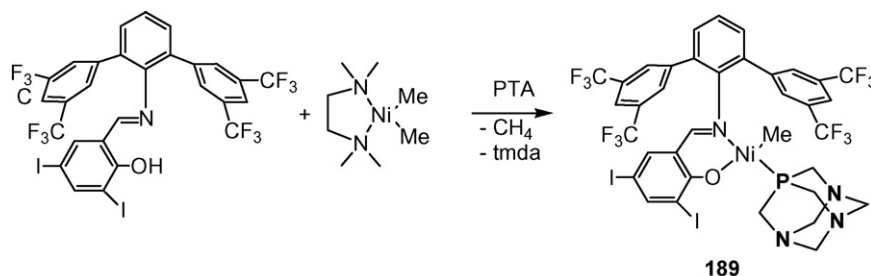


Fig. 21. X-ray crystal structure of (κ^1 -P)-[Cp*IrCl₂(PZA)] (**188**). H atoms (apart from OH) omitted for clarity. Adapted from ref. [18a].



Scheme 39.

CH_2Cl_2 . Complex **188** is only sparingly soluble in water ($S_{20^\circ\text{C}} = 1.8 \times 10^{-3} \text{ g mL}^{-1}$), as the corresponding PTA complex $[\text{Cp}^*\text{IrCl}_2(\text{PTA})]$ ($S_{20^\circ\text{C}} = 2.2 \times 10^{-3} \text{ g mL}^{-1}$) [18a]. The X-ray analysis of crystals obtained by slow concentration of a dichloromethane/ethanol solution of **188**, reveals the expected P coordination of the PZA ligand, with the Ir atom in a piano-stool coordination (Fig. 21). In a CD_2Cl_2 solution, the $^{31}\text{P}\{^1\text{H}\}$ NMR spectrum shows two singlets of comparable intensity at -59.3 and -72.3 ppm, indicating that both diastereomers are present as observed in the solid state [18a].

3.5. Nickel, palladium and platinum complexes

Only one nickel PTA complex was reported during the period covered by this review. The complex $[\text{Ni}(\text{salicylaldiminato-}\kappa^2\text{-N,O})(\text{Me})(\text{PTA})]$ (**189**) was reported by Mecking et al. [70] as a part of an study with other (salicylaldiminato)nickel(II) methyl complexes with different water-soluble ligands comparing their activity as catalyst precursors for ethylene polymerization. The complex is synthesized by reaction of solid PTA and $[(\text{tmeda})\text{NiMe}_2]$ with a cold toluene solution (-50°C) of the lipophilic salicylaldimine (Scheme 39). The product was isolated as a red solid and it is practically insoluble in water. The nickel(II)-bound methyl group displays a singlet in ^1H NMR (-1.5 ppm) and ^{13}C NMR spectra (-18.1 ppm) indicating that only one isomer is present, with respect to arrangement of L and the methyl ligand at the square-planar nickel center. For complex **189** no coupling between phosphorus and the Ni-bound methyl group is detected. The $^{31}\text{P}\{^1\text{H}\}$ NMR resonance of coordinated PTA is shifted from -100.3 ppm for free PTA to -51.7 ppm. Spectroscopic data similar to related complexes with solid-state structures resolved by X-ray diffraction suggest *trans* coordination of the methyl group to oxygen [70].

$[\text{Ni}(\text{cod})_2]$ was reacted with DAPTA in MeOH to obtain the tetra-substituted complex $[\text{Ni}(\text{DAPTA})_4]$ [14a]. $^{31}\text{P}\{^1\text{H}\}$ NMR showed a singlet at -28.3 . Solution IR showed strong terminal CO stretching frequency at 1643 cm^{-1} .

A Pd-DAPTA complex containing salicylaldimine was described by Darensbourg et al. [14a]. It was obtained by reaction of $[(\text{tmeda})\text{Pd}(\text{CH}_3)_2]$ in toluene at -30°C to which a solution of DAPTA in methanol was added dropwise. To this mixture, the salicylaldimine (L) in toluene at -30°C was slowly cannulated into the flask, and the solution was stirred for 30 min. The temperature was raised to room temperature, and the light red solution was further stirred overnight. After workup, complex $[\text{Pd}(\text{salicylaldiminato-}\kappa^2\text{-N,O})(\text{DAPTA})\text{Me}]$ was obtained. As in the case of Ni complex **189** featuring PTA, DAPTA was coordinated *trans*- to the N-donor arm of L.

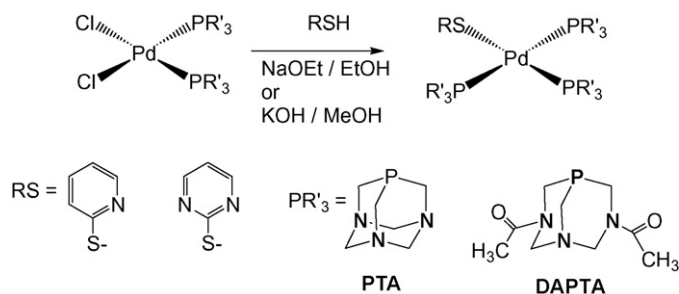
Complexes *trans*- $[\text{Pd}(\text{Ph})\text{X}(\text{PTA})_2]$ (X = I (**190**), Br (**191**)) were prepared by Grushin and Marshall [71] in their study for catalytic fluorination of bromobenzene. The complexes were prepared by treating $[\text{Pd}(\text{PPh}_3)_2(\text{Ph})\text{X}]$ with PTA in CH_2Cl_2 , and they show the expected singlets on the $^{31}\text{P}\{^1\text{H}\}$ NMR spectra [δ -68.3 and -66.3 ppm, respectively]. The structure of the iodo-derivative **190**

was resolved showing a square-planar coordination geometry about the Pt center, with two PTA ligands in mutually *trans*-position [71].

The chloride palladium(II) complex bearing the open-cage DAPTA ligand, i.e. *cis*- $[\text{PdCl}_2(\text{DAPTA})_2]$ (**192**) was easily prepared by reacting PdCl_2 directly with stoichiometric quantity of the phosphine, [72] and presents two $\nu(\text{Pd-Cl})$ and $\nu(\text{Pd-P})$ bands in the far-IR spectrum consistent with the *cis* geometry.

The palladium thiolato derivatives $[\text{Pd}(\text{SR})_2(\text{PR}'_3)_2]$ [SR = 2- $\text{SC}_5\text{H}_4\text{N}$ (**193**), 2- $\text{SC}_4\text{H}_3\text{N}_2$ (**194**); PR'_3 = PTA (**a**), DAPTA (**b**)] can be prepared in good yields by reaction of the chloride precursors with thiols in the presence of a base (Scheme 40) [72].

The $[\text{Pd}(\text{SR})_2(\text{PR}'_3)_2]$ complexes show only one $\nu(\text{Pd-P})$ and one $\nu(\text{Pd-S})$ bands in the far-IR spectrum, which suggests a *trans* configuration about the palladium that was confirmed by an X-ray crystallographic study of *trans*- $[\text{Pd}(2\text{-SC}_5\text{H}_4\text{N})_2(\text{PTA})_2]$ (**193a**) and *trans*- $[\text{Pd}(2\text{-SC}_5\text{H}_4\text{N})_2(\text{DAPTA})_2]$ (**193b**). The $^{31}\text{P}\{^1\text{H}\}$ NMR singlet resonances of the complexes are shifted to a higher field than those of the chlorido derivatives [72]. The DAPTA complexes show geminal H-H coupling for the NCH_2N and NCH_2P protons and, in addition, the P-H and H-H coupling patterns are identical to those observed in the free ligand. In addition, the ESI-MS mass spectra agree with the mononuclear structures of the four thiolate derivatives. No peaks due to any aggregation of metal-phosphine fragments comparable to gold(I) derivatives **248** (see below) are observed. Compounds **193–194** do not show any sign of decomposition even after several months at room temperature. They are insoluble in solvents such as methanol, ethanol, acetone and hexane, and they are partially soluble in CH_2Cl_2 , CHCl_3 , DMSO and H_2O . The solubility in H_2O is similar for all four complexes and is about 10 g L^{-1} . In the crystal structure of *trans*-**193a**, molecules associate through C-H...S interactions to form a chain motif along the *a* direction in contrast with the three-dimensional architecture found in the crystal structure of **193b** owing to the presence of C-H...O interactions (Fig. 22). Thermogravimetric analysis shows decomposition to metal around 750°C . This behaviour permits its use as “liquid metal” when deposited on tiles and heated around 800°C . The water solubility avoids the use of toxic organic solvents for this purpose [72].



Scheme 40.

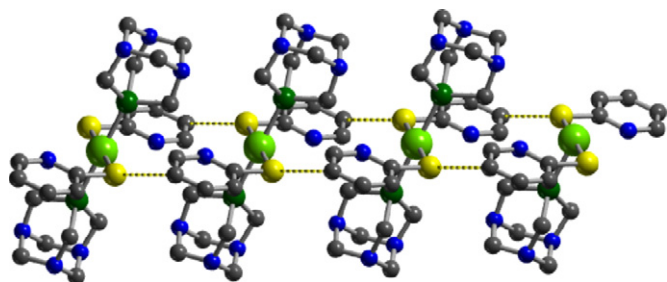
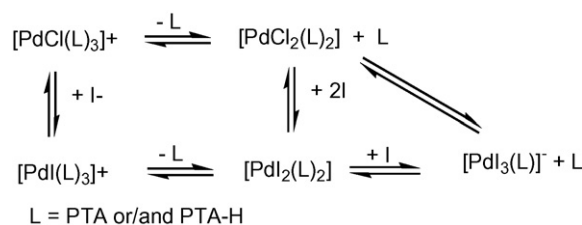


Fig. 22. X-ray crystal structure of $[\text{Pd}(\text{SC}_5\text{H}_4\text{N})_2(\text{PTA})_2]$ (**193a**) showing the C–H...S hydrogen bonding along the *a* direction in. H atoms omitted for clarity. Adapted from ref. [72].

The dimeric complex $[\text{Pd}(\text{dmba})(\mu\text{-Cl})_2]$ reacts at room temperature in CH_2Cl_2 with 2 equiv of PTA to yield the monomeric complex $[\text{Pd}(\text{dmba})\text{Cl}(\text{PTA})]$ (**195**) [73] (Scheme 41) in a very high yield. Complex **195** is an air-stable solid that decomposes above 220°C under a stream of N_2 . The ^1H NMR spectrum shows the PTA *trans*-to- NMe_2 ligand arrangement, as can be inferred from the small but significant coupling constants $^4J_{\text{PH}}$ (ranging from 2.4 to 2.7 Hz) of the NMe_2 and the CH_2N protons with the phosphorus atom. By use of 2D (HETCOR) and $^1\text{H}\{^{31}\text{P}\}$ NMR spectra, the assignment of the PTA ligand protons is unambiguously confirmed. Coordination at palladium is approximately square planar, with a bite angle of the cyclometalated ligand, C(1)–Pd–N(1), of $80.82(6)^\circ$. The PTA ligand is *trans* to the nitrogen atom due to the difficulty of coordinating a phosphine *trans* to an aryl ligand in palladium complexes (i.e. the destabilizing effect known as *transphobia*). In the crystal, a three-dimensional macromolecular network structure is observed built up by hydrogen bonding, which involves the PTA ligand, the coordinated chloride, dmbs, and even the metal center [73].

Trans- $[\{\text{PdI}_2(\text{PTA-H})_2\}\{\text{PdI}_3(\text{PTA})_2\}_2 \cdot 2\text{H}_2\text{O}]$ (**196**) was prepared by treating an aqueous solution of *cis*- $[\text{PdCl}_2(\text{PTA})_2]$ at pH ~ 3 , (perchloric acid) with an excess of NaI [74]. The cation in **196** can be formed via protonation of the PTA ligands and substitution of the chlorides by iodide, in combination with the usual isomerization to the *trans* isomer as expected for the larger I^- anion. One of the protonated PTA ligands may be substituted by iodide to form a triiodo complex in a pH-dependent reactivity. Treating $[\text{PdCl}(\text{PTA})_3]\text{Cl}$ with an excess of NaI in water (pH 6.2) results in the formation of an orange solution from which orange crystals of *trans*- $[\text{PdI}_2(\text{PTA})_2]$ (**197**) [74]. Other complexes that may form in the equilibria in the reaction between $[\text{PdCl}(\text{L})_3]^+$ and I^- under acidic or neutral conditions are shown in Scheme 42 [74].

The crystal structure of *trans*- $[\{\text{PdI}_2(\text{PTA-H})_2\}\{\text{PdI}_3(\text{PTA})_2\}_2 \cdot 2\text{H}_2\text{O}]$ (**196**) shows that the symmetrical *trans*- $[\text{PdI}_2(\text{PTA-H})_2]^{2+}$ cationic moiety lies on the inversion center in $P\bar{1}$ ($Z=1$), while the water and $[\text{PdI}_3(\text{PTA})]^-$ molecules occupy general positions. For both cation and anion, the geometry around the Pd(II) center is distorted square planar although as the iodide atoms of the anions show weak interactions with the Pd(II) of

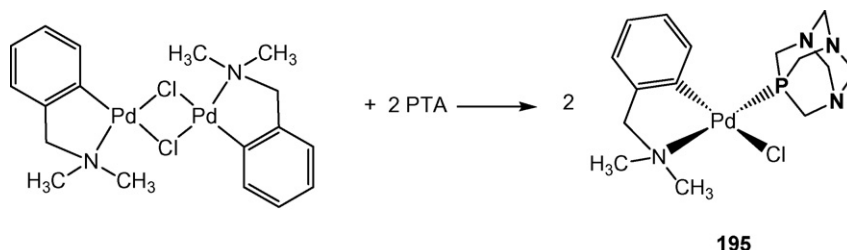


Scheme 42.

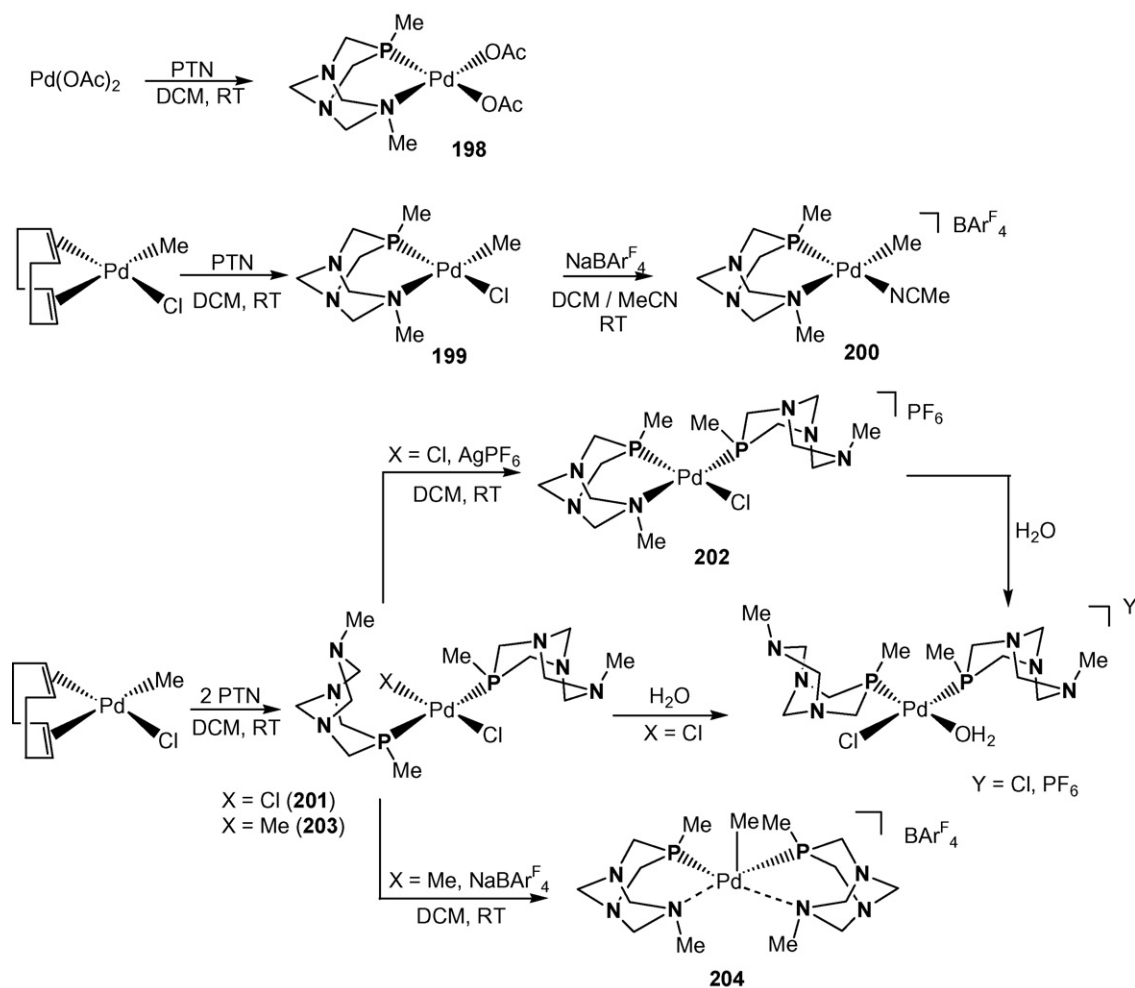
the cation $[\text{Pd-I}=3.550(30)\text{\AA}]$, its coordination can be considered as pseudo octahedral. This interaction, together with extensive hydrogen bonding, results in infinite chains of alternating cations and anions. In *trans*- $[\text{PdI}_2(\text{PTA})_2]$ (**197**), the Pd center adopts a slightly distorted square-planar geometry on the inversion center in $P2_1/n$ with the phosphine ligands in a *trans* orientation [74].

Palladium(II) complexes containing the water-soluble PTN ligand were prepared by reaction of the $\text{Pd}(\text{OAc})_2$, $[\text{Pd}(\text{cod})\text{Cl}_2]$ and $[\text{PdMe}(\text{cod})\text{Cl}]$ in either 1:1 or 2:1 ratio, respectively (Scheme 43) [75] and isolated as moderately air-stable solids. Complex $[\text{Pd}(\kappa^2\text{-}P,N\text{-PTN})(\text{OAc})_2]$ (**198**) is characterized by a singlet at -41.60 in the $^{31}\text{P}\{^1\text{H}\}$ spectrum in CD_2Cl_2 . ^1H signals of the $\text{CH}_3\text{-P}$ (1.30 d, $^2J_{\text{HP}}$ 13.5 Hz) and $\text{CH}_3\text{-N}$ groups (2.34 s) belonging to coordinated PTN, as well as those of $^{13}\text{C}\{^1\text{H}\}$ at 3.60 (d, $^1J_{\text{CP}}$ 25.7 Hz, $\text{CH}_3\text{-P}$) and 45.4 ppm (s, $\text{CH}_3\text{-N}$) are of diagnostic relevance. Complex **198** dissolves readily in water (377 mg mL^{-1} at 25°C), but with major decomposition. X-ray crystal structure of **198** shows that the coordination geometry of palladium is best described as square-planar, with one PTN-ligand coordinating to the metal atom in the $\kappa^2\text{-}P,N$ mode and in the *exo/exo* form conformation, occupying two *cis*-coordination sites at the metal center [75]. Complex $[\text{PdMe}(\kappa^2\text{-}P,N\text{-PTN})\text{Cl}]$ (**199**) was prepared by reaction of $[\text{Pd}(\text{cod})(\text{Me})\text{Cl}]$ with 1 equiv of PTN [75]. The ^1H NMR signal due to Pd–Me shows as a doublet at 0.50 ppm with a coupling constant $^3J_{\text{HP}}$ of 13.4 Hz, as expected for a *cis* Me–Pd–P geometry. Chelate behaviour of PTN can be inferred from the signals belonging to $\text{CH}_3\text{-P}$ (1.20 d, $^2J_{\text{HP}}$ 10.8 Hz) and $\text{CH}_3\text{-N}$ groups (2.40 s). Treatment of **199** with $\text{NaBAR}^{\text{F}}_4$ in a mixture of dichloromethane and acetonitrile, affords the monocationic complex $[\text{Pd}(\kappa^2\text{-}P,N\text{-PTN})(\text{Me})(\text{CH}_3\text{CN})](\text{BAR}^{\text{F}}_4)$ (**200**). The presence of ^1H singlet at 2.26 ppm and IR stretching bands at 2292 and 2319 cm^{-1} confirms the coordination of acetonitrile to Pd without disrupting the $\kappa^2\text{-}P,N$ coordination of the ligand [75].

A second family of palladium(II) complexes is prepared by reaction of the same Pd(II) precursors with 2 equiv. of PTN [75]. Starting from *cis*- $[\text{Pd}(\text{cod})\text{Cl}_2]$, complex *trans*- $[\text{Pd}(\kappa^1\text{-}P\text{-PTN})_2\text{Cl}_2]$ (**201**) was obtained as indicates a close inspection of the $^{13}\text{C}\{^1\text{H}\}$ NMR data, and the presence of a peak at m/z 489 corresponding to the $[\text{M-Cl}]$ molecular peak in the ESI-MS spectrum. The monocationic pale-yellow complex $[\text{Pd}(\text{PTN})_2\text{Cl}]\text{PF}_6$ (**202**) was obtained by chloride abstraction with AgPF_6 from complex **201**. The $^{31}\text{P}\{^1\text{H}\}$ NMR spectrum (acetone- d_6) of **202** shows two broad bands $[-25$ ($\kappa^1\text{-}P$) and -45 ppm ($\kappa^2\text{-}P,N$)], for the two inequivalent *cis*-disposed phosphorus nuclei. The crystal structure of **202** (Fig. 23) shows



Scheme 41.



Scheme 43.

a square-planar coordinated palladium atom with a $\kappa^2\text{-P,N}$ and a $\kappa^1\text{-P}$ coordinating PTN ligand. The $\kappa^1\text{-P}$ coordinated PTN exhibits an intramolecular $\text{P}(2) \cdots \text{N}(4)$ distance of 2.867(5) Å, which is significantly longer compared to the value found for the $\kappa^2\text{-P,N}$ coordinated ligand, indicating ring strain of the ligand upon coordination to the metal supporting the hemilabile behaviour observed when dissolving the complex in water [75].

The off-white complex $\text{trans-}[\text{PdMe}(\kappa^1\text{-P-PTN})_2\text{Cl}]$ (**203**) is obtained by reaction of $[\text{PdMe}(\text{cod})\text{Cl}]$ with 2 equiv of PTN [75]. Similarly to **201**, NMR data suggest that the two PTN ligands are *trans* to each other. Subsequent treatment of complex **203** with 1 equiv. of $\text{NaBAR}_4^{\text{F}}$ affords the monocationic complex $\text{trans-}[\text{PdMe}(\kappa^2\text{-P,N-PTN})_2][\text{BAR}_4^{\text{F}}]$ (**204**), yellow and highly insoluble in water as expected from the presence of BAR_4^{F} counter ion. The NMR data collected in CDCl_3 suggest a highly fluxional situation intermediate between $\kappa^1\text{-P}$ and $\kappa^2\text{-P,N}$ behaviour for PTN (See Scheme 43 above) [75].

The complex $\text{cis-}[\text{PtCl}_2(\text{PPh}_3)(\text{PTA})]$ (**205**) is obtained by the treatment of $\text{cis-}[\text{PtCl}_2(\text{PPh}_3)_2]$ with 1 equiv of PTA in dichloromethane and was characterized spectroscopically and by X-ray crystal structure determination [76]. The $^{31}\text{P}\{^1\text{H}\}$ NMR spectrum of **205** in CDCl_3 shows two coupled doublets ($^2J_{\text{PP}} = 18 \text{ Hz}$) with a $^1J_{\text{PTP}}$ for coordinated PTA of ca. 500 Hz smaller than for PPh_3 (3195 and 3750 Hz, respectively) although both phosphines are *trans* to chloride. Two PtCl stretching bands at 280 and 258 cm^{-1} also corroborate the *cis* geometry. The structure of **205** shows a distorted square-planar coordination geometry around the Pt atom, with angle distortion in agreement with the cone angles of the two phosphines ($\text{PTA} = 102^\circ$; $\text{PPh}_3 = 145^\circ$). Centrosymmetric dimers are formed by short interactions $\text{C}(\text{PTA})\cdots\text{H}\cdots\text{Cl}$ with $\text{H}\cdots\text{Cl}$ distances of 2.84 and 2.94 Å [76].

To enhance the hydrophilicity of different ascorbate–platinum complexes tested for antiproliferative activity *in vitro*, the complex $[\text{Pt}(\text{O}_2, \text{O}_3\text{-asc})(\text{PTA})_2]$ (**206**) (asc = ascorbate) was obtained by treating $[\text{Pt}(\text{PTA})_2(\text{NO}_3)_2]$ with 2 equiv of sodium ascorbate [77]. The asc ligand is coordinated to the Pt center by the two alcohol oxygens. The compound is soluble in water and its $^{31}\text{P}\{^1\text{H}\}$ NMR spectrum in D_2O shows two doublets with Pt satellites at $\delta -58.34$ and -58.71 ppm ($^1J_{\text{PPt}} = 3302$ and 3343 Hz), respectively.

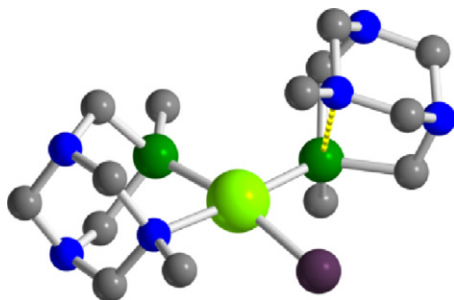


Fig. 23. X-ray crystal structure of $[\text{Pd}(\text{PTN})_2\text{Cl}]\text{PF}_6$ (**202**). H atoms omitted for clarity. Intramolecular contact shown as dotted line. Adapted from ref. [75].

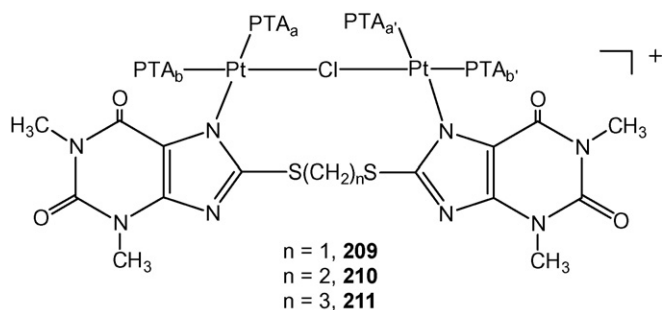


Chart 11.

The complex is stable in aqueous solution but reverts to the dichloride complex after 48 h in the presence of an excess (4 equiv) of added chloride [77].

The thiopurinic complexes (*SP*-4,2)-[PtCl(8-MTT)(PPh₃)(PTA)] (**207**) and *cis*-[Pt(8-MTT)₂(PPh₃)(PTA)] (**208**) were prepared from **205** by reaction respectively with 1 and 2 equiv of 8-MTTH [8-MTTH = 8-(methylthio)theophylline] and NaOH in a double phase mixture of dichloromethane and water [76]. The synthesis of **208** by reaction of **205** with 2 equiv of 8-MTTH was observed to proceed via a two-step process, starting from fast substitution of the chloride trans to PTA by MTT[−] (15 min), leading to **207**, as indicated by the 10 ppm upfield shift of the PTA signal (from −63.3 ppm in **205** to −73.8 ppm in **207**), followed by slow substitution of the residual chloride by the remaining equiv of deprotonated ligand MTT[−] [76]. The reaction of *cis*-[PtCl₂(PTA)₂] with NaOH and the ligands bis(*S*-8-thiotheophylline)methane (MBTTH₂), 1,2-bis(*S*-8-thiotheophylline)ethane (EBTTH₂), and 1,3-bis(*S*-8-thiotheophylline)propane (PBTTH₂), gave the binuclear complexes **209–211**, respectively (Chart 11) [76].

Compounds **209–211** display ³¹P{¹H} NMR spectra characterized by two groups of very close signals, assigned to PTA *trans* to chloride, and to PTA *trans* to N. The chloride-bridged structure is established by variable-temperature and 2D-³¹P{¹H} COSY NMR experiments showing a clear connection (⁴*J*_{Pa/Pa'} = ca. 8 Hz) between phosphorus nuclei bound to different Pt. Mixing a solution of the chloride of **209** with NaBPh₄ in MeOH produces the precipitation of the insoluble complex *cis*-[Pt(PTA)₂]₂(μ-Cl)(μ-N,N-MBTTH)(BPh₄) (**209BPh₄**) confirming the cationic nature of the complex **209** [76].

The reaction of 8-TTH₂ (8-thiotheophylline) with NaOH and *cis*-[PtCl₂(PTA)₂] in the biphasic system H₂O/CH₂Cl₂ at room temperature leads to the water-soluble complex [Pt(μ-S,N-8-TT)(PTA)₂]₂ (**212**) [78]. The ¹H NMR in combination with the IR spectroscopy, suggest that the N atom of the purine was deprotonated. A molecular weight of 1438 Da, measured by MALDI-TOF mass spectrometry, unequivocally identifies **2** as a binuclear complex [78].

The reaction of 8-MTTH [8-MTTH = 8-(methylthio)theophylline] with NaOH and *cis*-[PtCl₂(PTA)₂] in H₂O/CH₂Cl₂ in 1:1:1 molar proportion gave the complex *cis*-[PtCl(8-MTT)(PTA)₂] (**213**) while in 2:2:1 molar ratio gave *cis*-[Pt(8-MTT)₂(PTA)₂] (**214**) [78]. Complex **213** and **214** are soluble in H₂O as well as in organic solvents (CH₂Cl₂ and CHCl₃). The ³¹P{¹H} NMR spectrum for **213** displayed two doublets (*P*_A = −69.5 ppm; *P*_B = −58.4 ppm; ²*J*_{PP} = 20.5 Hz). The coupling constant between *P*_A and Pt was 2962 Hz, which is adequate for a P *trans* to a N, while the corresponding value for *P*_B (¹*J*_{PP} = 3369 Hz) was in agreement with a P *trans* to a Cl. Complex **214** showed a singlet at −68.8 ppm with a PtP coupling constant similar in value (3066 Hz) to *P*_A of complex **7** [78].

The *trans*-platinum thiolate complexes bearing PTA or DAPTA ligands *trans*-[Pt(SR)₂(P)₂] [P = PTA, SR = 2-thiopyrimidine (**215**),

Table 7

Pt–S and Pt–P stretching frequencies (cm^{−1}) of the complexes **215–218**.

Compound	ν(Pt–S)	ν(Pt–P)
215	392	281
216	391	275
217	369	282
218	361	278

2-thiopyridine (**216**); P = DAPTA, SR = 2-thiopyrimidine (**217**), 2-thiopyridine (**218**)] are obtained by reaction of the appropriate chloroplatinum(II) precursors with the thiol derivatives, in the presence of NaOEt in EtOH [79]. The four complexes are soluble in water and they are fully characterized using various spectroscopic techniques. PTA complexes **215** and **216** show singlet resonances with Pt-satellites in their ³¹P{¹H} NMR spectra. DAPTA complexes **217** and **218** show two singlet resonances each giving coalescence at higher temperature [Compound **217**: (CDCl₃, r.t.), δ −40.19 ppm (s, ¹*J*_{PtP} = 2721 Hz), −40.28 ppm (s, ¹*J*_{PtP} = 2724 Hz); (CDCl₃, 303 K), δ −40.14 ppm (s, ¹*J*_{PtP} = 2724 Hz); compound **218**: (CDCl₃, 253 K), δ −38.89 ppm (s, ¹*J*_{PtP} = 2701 Hz), −38.94 ppm (s, ¹*J*_{PtP} = 2701 Hz); (CDCl₃, r.t.), δ −38.73 ppm (s, ¹*J*_{PtP} = 2731 Hz)]. This behaviour can also be observed in the methyl resonances of DAPTA and indicates the presence of conformational isomers. The ¹*J*_{PtP} values as well as the presence of only one band each due to Pt–S and Pt–P stretching vibrations in the IR spectra confirm the *trans* configuration both in solution and in the solid state (Table 7) [79]. For complexes **215**, **216** and **218**, the *trans* configuration was confirmed by X-ray diffraction studies [79]. The molecular structures of **215** and **218** show the Pt atom on a crystallographic inversion center with two thiolate and two phosphine ligands mutually *trans* to each other (low quality of crystals of complex **216** precluded acceptable structural description). In the case of complex **218** the COCH₃ groups of the DAPTA ligands are *anti* with respect to each other, as in the free phosphine [79].

As part of a study on the reactivity between the metalloligand [Pt₂(μ-S)₂(PPh₃)₄] with platinum(II) chloride moieties with the aim of detecting any metal scrambling by ESI-MS spectrometry, the trinuclear dicationic adduct [Pt₂(μ-S)₂(PPh₃)₄Pt(PTA)₂]²⁺ (**219**) was isolated as tetraphenylborate salt [80]. The compound is air-stable and soluble in chlorinated hydrocarbon solvents. The ³¹P{¹H} NMR spectrum of the complex shows two phosphine signals in a 2:1 ratio due to the PPh₃ resonances, together with PTA (δ −64.5). The PPh₃ ligands show ¹*J*_{PtP} coupling constants of 3247 Hz, while PTA shows ¹*J*_{PtP} coupling constant of 2916 Hz [80].

Reaction of the thiocarbamate esters 4-RC₆H₄NHC(S)OMe [R = H, Cl, OMe, NO₂, Me] with *cis*-[PtCl₂(PTA)₂] in the presence of a base affords the Pt(II) complexes *trans*-Pt[SC(OMe)=NC₆H₄R]₂(PTA)₂ (**220–224**) as colourless or pale-yellow solids [81]. Despite the presence of two PTAs, complexes **220–224** are insoluble in water. Complex **220** is insoluble in all common solvents and it was only characterized by EA and IR spectroscopy (ν_{CN} = 1601, 1579 cm^{−1}). *Trans* configuration and deprotonation of the thiocarbamate esters are confirmed for compounds **221–224** by spectroscopic techniques. The *trans* square-planar structure for complex **224** was confirmed by X-ray methods [81].

The PTA complexes *cis*-[PtX₂(PTA)₂] (X = Br (**225**), I (**226**)) were prepared by reacting the corresponding *cis*-[PtX₂(cod)] precursor with two equivalents of PTA in CH₂Cl₂ [82]. The ³¹P{¹H} NMR spectra show a singlet with platinum satellites. The ¹*J*_{PtP} value of the bromo derivative (3432 Hz) clearly show a *cis* phosphine configuration. Although the relatively small ¹*J*_{PtP} value of the iodo-derivative (2509 Hz) seemed to indicate that in solution [PtI₂(PTA)₂] adopted a *trans* geometry, the known ³¹P{¹H} NMR data for *trans*-[PtI₂(PTA)₂] (δ −73.1 ppm; ¹*J*_{PtP} = 2316 Hz) eliminate

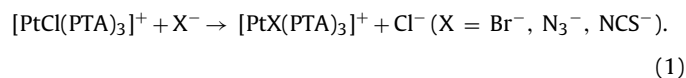
Table 8

Equilibrium constants for formation of $[\text{PtX}(\text{PTA})_3]^+$ ($\text{X} = \text{Br}^-$, N_3^- , NCS^-) complexes at 25 °C and pH 5.6 [83].

X	K_{eq}
Br^-	3.3(7)
N_3^-	11(2)
NCS^-	20(2)

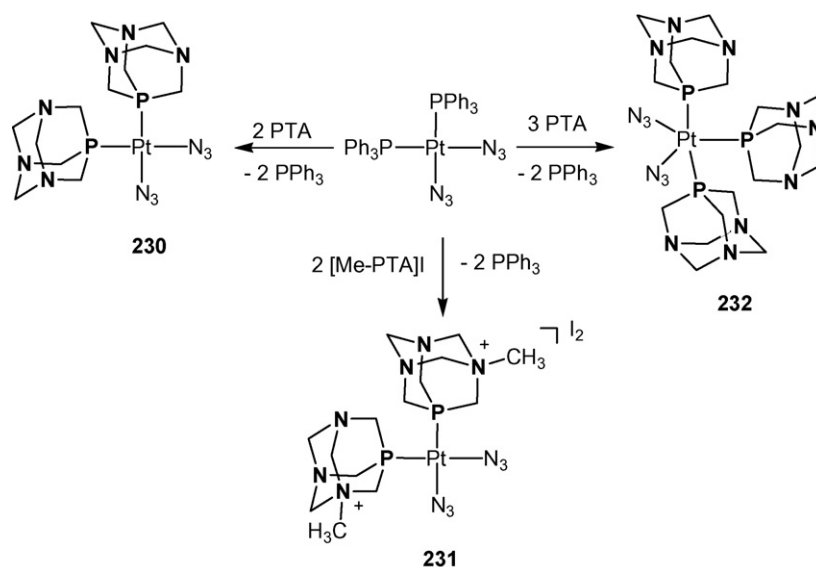
this possibility [82]. The coordination geometry about the platinum atom in both $[\text{PtBr}_2(\text{PTA})_2]$ and $[\text{PtI}_2(\text{PTA})_2]$ is slightly distorted square planar with the two phosphines in *cis* disposition. The deviation from ideality is due to steric repulsion of the PTA ligands as demonstrated by the P–Pt–P angles of 94.95° in the bromide and 99.53° in the iodide compounds. In compound **226**, the iodide ligand does not dissociate in water, as indicated by the recrystallization from aqueous HCl and by being inert in the presence of saturated KCl solutions [82].

Reaction of aqueous solutions of $[\text{PtCl}(\text{PTA})_3]\text{Cl}$ with NaNCS , LiBr or NaN_3 gives the complexes $[\{\text{Pt}(\text{NCS})(\text{PTA})_3\text{NCS}\}]_3 \cdot 5\text{H}_2\text{O}$ (**227**), $[\text{PtBr}(\text{PTA})_3]\text{Br}$ (**228**), and $[\text{Pt}(\text{N}_3)(\text{PTA})_3]\text{N}_3$ (**229**) in moderate yields (Equation 1) [83].



The complexes are characterized by NMR, IR and UV–vis spectroscopies, and the structure of **227** was determined by X-ray crystallography showing Pt in a distorted square-planar structure with two PTA ligands *trans* to each other and the other PTA bound *trans* to the nitrogen of the NCS ligand. The compound crystallizes with three platinum cations, three NCS cations and five solvent water molecules in the asymmetric unit. There are strong hydrogen bond interactions between the water molecules and the SCN^- counteranion and the PTA ligands. The equilibrium constants for formation of **227–229** were determined by absorbance spectra recorded between 200 and 500 nm (Table 8) [83].

Four- and five-coordinated diazido-platinum(II) complexes *cis*- $[\text{Pt}(\text{N}_3)_2(\text{PTA})_2]$ (**230**), *cis*- $[\text{Pt}(\text{N}_3)_2(\text{mPTA})_2]\text{I}_2$ (**231**) and $[\text{Pt}(\text{N}_3)_2(\text{PTA})_3]$ (**232**) were obtained by reaction of *cis*- $[\text{Pt}(\text{N}_3)_2(\text{PPh}_3)_2]$ with stoichiometric amounts of PTA or $[\text{mPTA}]\text{I}$ (Scheme 44) [84].

**Scheme 44.**

Complexes **230–232** are air-stable as solids and in water solution. They are readily soluble in water and polar solvents, but insoluble in Et_2O , C_6H_{14} and CCl_4 . *Cis*-phosphine configuration for **230** and **231** is deduced from $^{31}\text{P}\{^1\text{H}\}$ NMR studies [δ –59.1 and –47.2, singlets with Pt-satellites ($^1J_{\text{PtP}} = 3139$ and 3153 Hz), respectively]. The penta-coordinated complex **232** shows a fluxional behaviour in solution as observed by variable temperature $^{31}\text{P}\{^1\text{H}\}$ NMR experiments [84]. The X-ray crystal structure of **230** shows a slightly distorted square-planar geometry with the phosphine and the end-on azide ligands in the *cis*-orientation [84]. There is an extensive hydrogen bonding with the terminal N_3 azide atom and the N-atoms of the PTA ligands. Additional contacts involve N atoms of one of the azides as well as O5 water oxygen with PTA methylene hydrogen atoms. The intercalated crystallization water molecules form infinite water clusters composed of alternatively linked cyclic decamers and pentamers with an average $\text{O} \cdots \text{O}$ contacts of ca. 2.79 Å similar to that found in the structure of ice (Fig. 24).

Bis(tetrazolato) complexes *trans*- $[\text{Pt}(\text{N}_4\text{-CR})_2(\text{PTA})_2]$ [$\text{R} = \text{Ph}$ (**233**), 4- ClC_6H_4 (**234**), 3- NC_5H_4 (**235**)] were obtained by reaction of **230** with the appropriate organonitrile NCR which is accelerated by microwave irradiation (120–135 °C for 1 h) [84] (Scheme 45).

The complexes are stable in the solid state and in solution under air, soluble in middle-polar solvents and insoluble in apolar solvents. The presence of the tetrazole ring is confirmed by a strong band in the IR spectra at 1615–1630 cm^{-1} . Singlets with Pt-satellites at δ –56.2, –56.3, and –56.2, ($^1J_{\text{PtP}} = 2497$, 2491, and 2479 Hz) in the $^{31}\text{P}\{^1\text{H}\}$ NMR spectra indicate the *trans* configuration of the phosphines and the existence of only one type of *N*-coordination of the tetrazoles. Crystal structure of **233** confirms the *trans*-square-planar disposition around the Pt atom and shows pseudo-agostic intermolecular interactions between the Pt ion and H atoms of PTA methylene groups of the neighboring molecules [$\text{C} \cdots \text{Pt}$ 3.532(14) and 3.519(13) Å] [84]. Furthermore, it was possible to free the tetrazole ligands from complexes **233–235** by two different ways (Scheme 45) leading to the formation of the PTA-protonated complex *cis*- $[\text{PtCl}_2(\text{PTA-H})_2]\text{Cl}_2$ (**236**) or the dicyano complex *trans*- $[\text{Pt}(\text{CN})_2(\text{PTA})_2]$ (**237**) [84].

The alkynyl derivatives *cis* and *trans*- $[\text{Pt}\{\text{C}\equiv\text{C}(\text{CH}_2)_3\text{NH}_2\}_2(\text{PTA})_2]$ (**238**) were observed as predominant species, in a 3.5:1 ratio, in the Pt(II) catalyzed hydroamination of terminal alkynylamines in aqueous solution [85]. The $^{31}\text{P}\{^1\text{H}\}$ NMR spec-

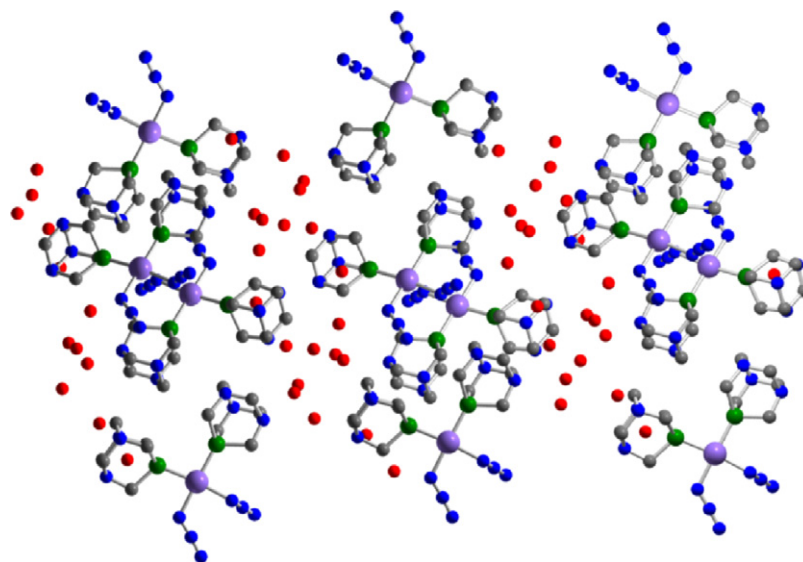


Fig. 24. Crystal network in *cis*-[Pt(N₃)₂(PTA)₂] (**230**). H atoms omitted for clarity. Atom colour code: Pt, lilac; P, green; C, gray; N, blue; O, red. Adapted from ref. [84].

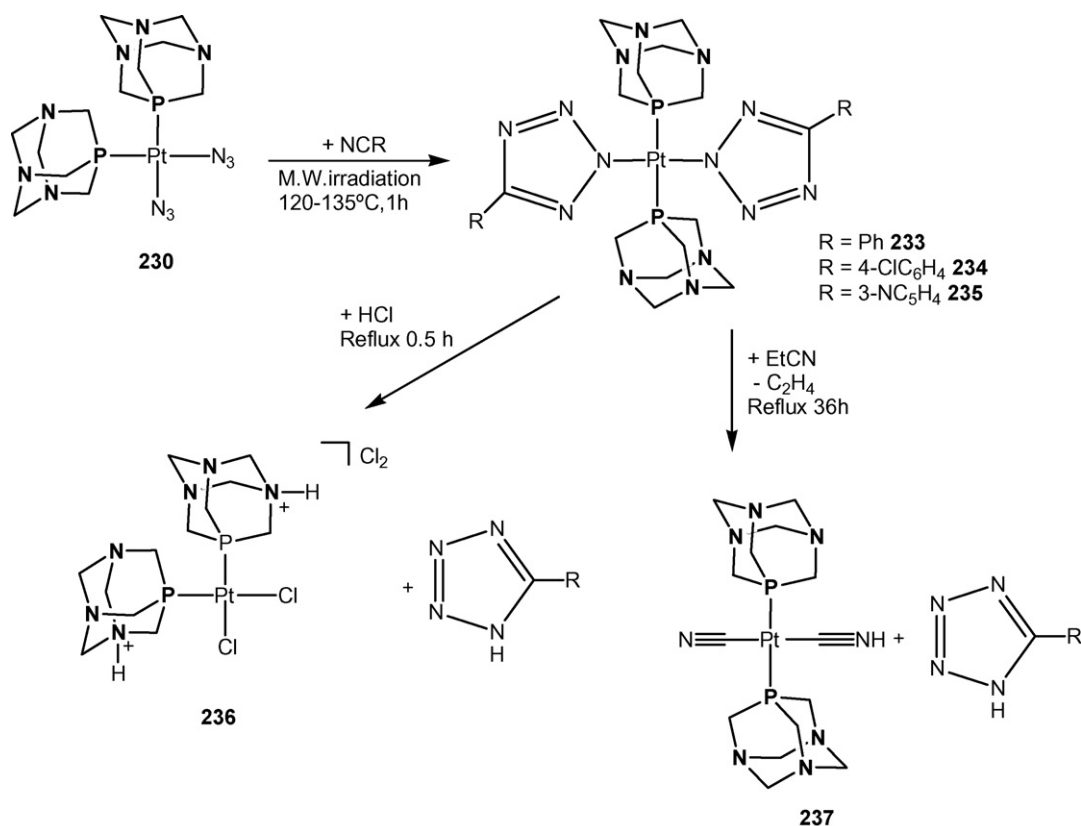
trum in D₂O showed two singlets at −64.5 (78%) and at −58.9 (22%) with the corresponding ¹⁹⁵Pt satellites (¹J_{PtP} = 2167 and 2305 Hz, respectively) [85]. Characterization of both compounds was facilitated by the serendipitous precipitation of microcrystals of *trans*-[Pt{C≡C(CH₂)₃NH₃}₂(PTA)₂]Br₂ formed at the bottom of the NMR tube during a kinetic run involving *cis*-[PtBr₂(PTA)₂] and 4-pentyn-1-amine [85]. The structure was determined by X-ray crystallography and shows a Pt center in a distorted square-planar geometry with two PTA ligands *trans* to each other. The Pt–C_α and C_α–C_β bond distances, 2.032(15) and 1.19(2) Å, respectively,

confirm the σ-alkynyl nature of the other two organic ligands bound to the metal [85].

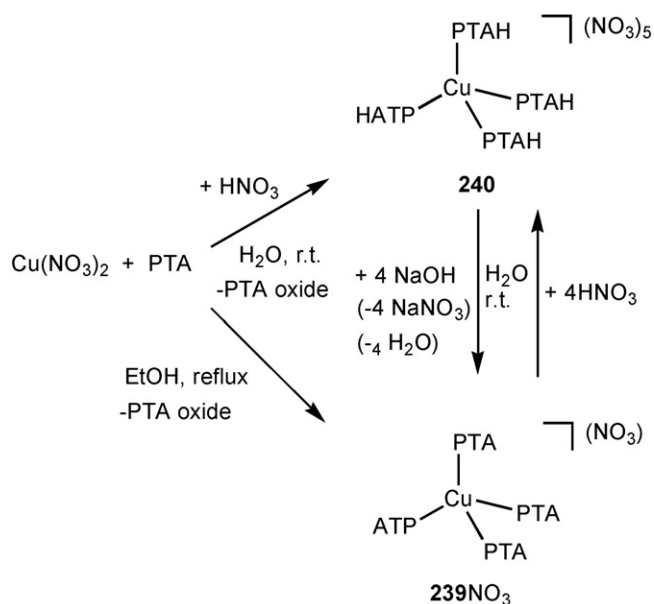
3.6. Copper, silver and gold complexes

The first copper complexes bearing PTA ligands, namely [Cu(PTA)₄](NO₃) (**239NO₃**) and [Cu(PTA-H)₄](NO₃)₅ (**240**), were prepared by Pombeiro et al. (Scheme 46) [86].

The tetrakis-PTA copper(I) cation is also obtained as the chloride derivative [Cu(PTA)₄]Cl·6H₂O, by treating a solution of CuCl₂



Scheme 45.



in ethanol with PTA [87]. The compounds are air-stable solids, soluble and air-stable in water and DMSO. They were characterized by IR, ^1H -, $^{13}\text{C}\{^1\text{H}\}$ -, $^{31}\text{P}\{^1\text{H}\}$ - and ^{63}Cu NMR spectroscopy, FAB-MS(+), and single-crystal X-ray diffraction structural analyses [86]. NMR spectroscopy studies of D_2O solutions of the compounds in the presence of excess of PTA or PTAH ligands show a fast exchange between free and coordinated ligands in compound **240** but not in compound **239NO₃**. Moreover, it can be observed the ^{31}P – ^{63}Cu coupling in **239NO₃** but not in **240** (no ^{63}Cu resonance was detected either). These observations imply that protonation of PTA has a marked effect on the rate of the exchange process and/or on the quadrupolar relaxation of the ^{63}Cu nuclei. Interestingly, changing

the pH of the aqueous solution of **240** to a slightly basic value (pH 8), the singlet in the $^{31}\text{P}\{^1\text{H}\}$ spectrum converts to a 1:1:1:1 quartet and a 1:4:6:4:1 quintet in the ^{63}Cu NMR spectrum appears, in agreement with the deprotonation of **240** to give **239NO₃** [86]. Crystal structures of the three compounds show a tetrahedral arrangement around the Cu atom with bonding parameters similar to those of related tetrahedral-type transition-metal PTA/PTAH complexes. In contrast to **240** [86] and **239Cl** [87] the PTA ligands are not geometrically equivalent in compound $[\text{Cu}(\text{PTA})_4](\text{NO}_3)$ [86].

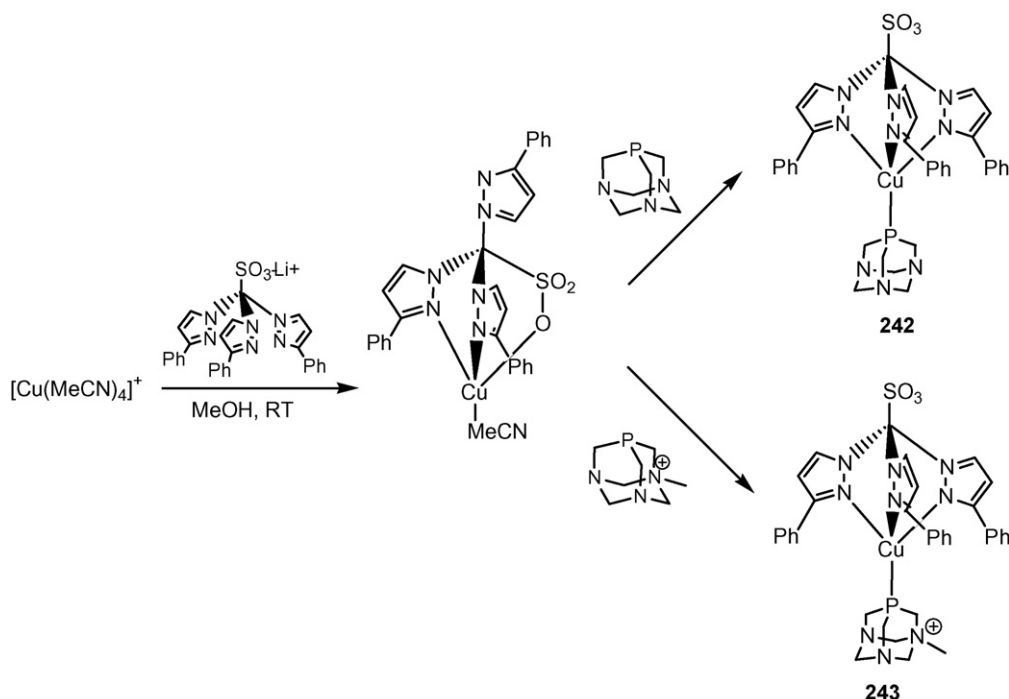
The copper(I) PTA complex $[\text{Cu}(\text{LCS}_2)(\text{PTA})]$ (LCS_2 = bis-(3,5-dimethylpyrazolyl)dithioacetate) (**241**) is obtained by reacting 1 equiv of LCS_2 with equimolar quantities of CuCl and PTA in a MeOH/NCMe (1:2) solution at room temperature [88]. The complex is stable in air and soluble in MeOH , acetone and chlorinated solvents. The presence of the CS_2 moiety is confirmed by absorptions at 1095(s), 1066(s) and 1040(s) cm^{-1} (ν_{sym}) and 880 (m), 851(s) and 812(s) cm^{-1} in the IR spectrum.

The new sterically demanding and coordination flexible tris(3-phenyl-1-pyrazolyl)methanesulfonate ligand (Tpms^{Ph}) is used for the synthesis of the PTA and mPTA Cu(I) complexes $[\text{Cu}(\text{Tpms}^{\text{Ph}})(\text{PTA})]$ (**242**) and $[\text{Cu}(\text{Tpms}^{\text{Ph}})(\text{mPTA})]\text{PF}_6$ (**243**) (Scheme 47) [89].

Complexes **242** and **243** are fairly soluble in water ($S_{25^\circ\text{C}} \sim 6\text{--}7 \text{ g L}^{-1}$), in acetone and CH_2Cl_2 . X-ray structures of both complexes show a tridentate N,N',N'' behaviour of the anionic Tpms^{Ph} ligand with a high degree of tilting of the pyrazolyl rings. Besides, compound **243** presents an intramolecular $\pi \cdots \text{H-C}$ interaction (2.489 Å) between a proton of the PTA ligand and the closest phenyl ring [89] (Fig. 25).

Variable temperature NMR experiments show that the N,N',N'' coordination mode is maintained in solution for compound **242**, but in the case of compound **243**, a $N,N'O$ coordination mode is preferred, with a fluxional behaviour that makes the three pyrazolyl arms equivalent at room temperature [89].

The neutral 2D polymer $[\text{Cu}_2(\mu\text{-I})_3(\text{mPTA})]_n$ (**244**) is obtained by treatment of an aqueous solution of $\text{Cu}(\text{NO}_3)_2$ and HNO_3



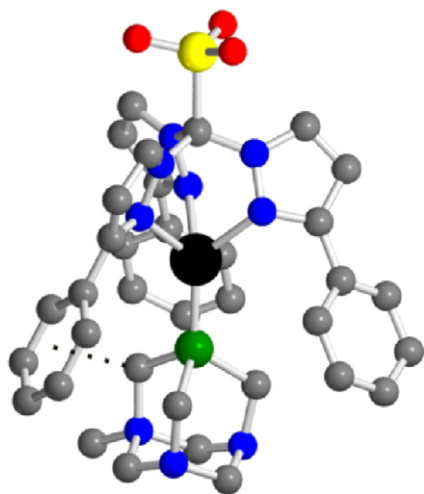


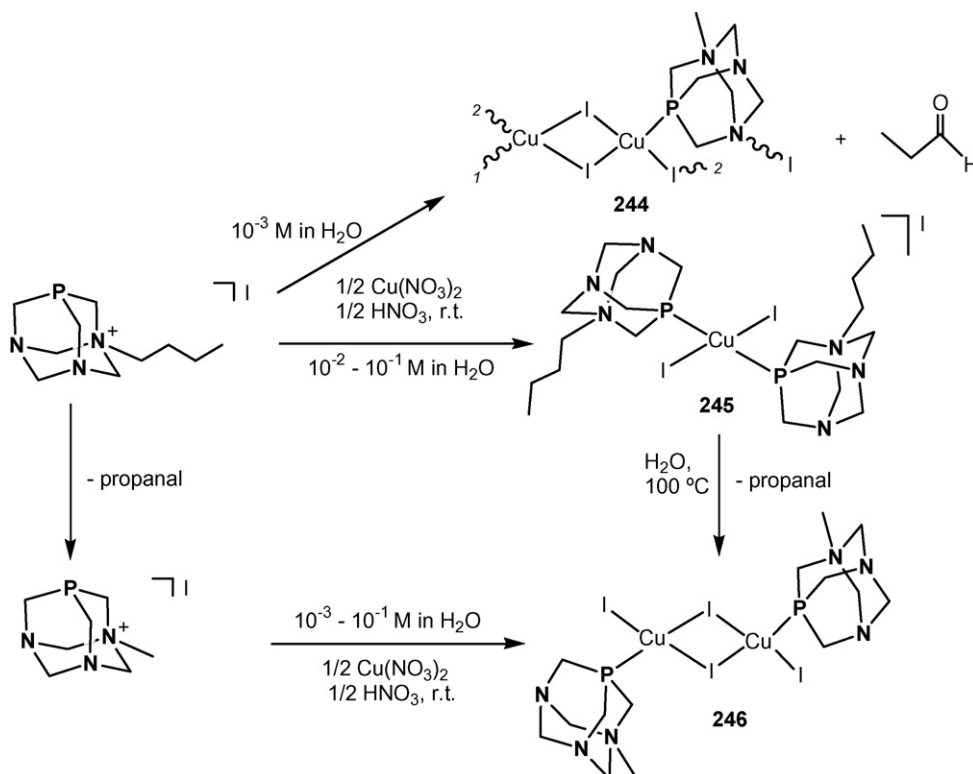
Fig. 25. X-ray crystal structure of $[\text{Cu}(\text{Tpms}^{\text{Ph}})(\text{mPTA})]\text{PF}_6$ (**243**). H atoms omitted for clarity. Intramolecular $\pi \cdots \text{H}-\text{C}$ interaction demonstrated by a dotted line. Adapted from ref. [89].

with $[\text{Bu}-\text{PTA}]\text{I}$ (Scheme 48) [13]. The reaction involves an $\alpha\text{-C}-\text{C}$ bond cleavage of the butyl arm of the PTA (with the formation of propanal) and the reduction of $\text{Cu}(\text{II})$ to $\text{Cu}(\text{I})$. The rare P,N -coordination mode of the PTA cage, which behaves as a bridging bidentate ligand, is confirmed by X-ray studies [13]. Reaction of the $[\text{Bu}-\text{PTA}]\text{I}$ with a more concentrate solutions of $\text{Cu}(\text{II})$ (ca. 10^{-2} to 10^{-1} M) yields the $\text{Cu}(\text{I})$ complex $[\text{Cu}_2(\text{Bu}-\text{PTA})_2]\text{I}$ (**245**). On the other hand, reaction with $[\text{mPTA}]\text{I}$ leads to the formation of $[\text{Cu}_2\text{I}_2(\mu\text{-I})_2(\text{mPTA})_2]$ (**246**) bearing the conventional P -coordination of the $[\text{mPTA}]^+$ ligands as shown by X-ray diffraction analysis. The $\text{Bu}-\text{PTA}$ ligand in complex $[\text{Cu}_2(\text{Bu}-\text{PTA})_2]\text{I}$ undergoes $\text{C}-\text{C}$ bond cleavage in water at 100°C leading to compound **246** [13].

Upon mixing aqueous solutions containing equimolar amounts of AgNO_3 and PTA, the first complex containing PTA in a triply bridging P,N,N' -coordination mode $[\text{Ag}(\text{PTA})(\text{H}_2\text{O})]\text{NO}_3$ is obtained. The crystal structure of the compound shows a silver atom in a distorted tetrahedral coordination geometry with one P -bound PTA, two N -bound PTA and one water molecule (Fig. 26a). Each PTA ligand is bridging three silver atoms configuring a polymeric network containing hexagonal cavities occupied by the nitrate anions (Fig. 26b) [90].

The thiolato gold(I) complexes $[\text{Au}(\text{SR})(\text{PR}'_3)]$ (**248**) (SR =various thiolato derivatives as shown in Scheme 49; $\text{PR}'_3 = \text{PTA}$, DAPTA) were easily prepared in good yields by treating the complexes $[\text{AuCl}(\text{PR}'_3)]$ with the thiol derivatives in the presence of a base [72]. The complex $[\text{AuCl}(\text{DAPTA})]$ was prepared by replacement of tetrahydrothiophene (tht) from $[\text{AuCl}(\text{tht})]$ with the appropriate phosphine. The thiolato complexes were characterized by spectroscopic techniques and by X-ray diffraction in the case of $[\text{Au}(\text{S}_2\text{CNET}_2)(\text{PTA})]$ [72] and $[\text{Au}(\text{SPyrim})(\text{PTA})]$ [79].

Complexes **248** show singlet resonances in their $^{31}\text{P}\{^1\text{H}\}$ NMR spectra shifted to lower fields relative to those of the free phosphines. As observed for other PTA gold derivatives, the NCH_2P resonances appear as doublets in free PTA and as singlets in the thiolato derivatives, whilst the NCH_2N resonances appear as singlets in free PTA and as an AB system in the thiolato complexes [72,79]. The ^1H NMR spectra of the DAPTA thiolato derivatives show a pattern similar to that of the free ligand. The lack of symmetry of the compound makes two of the three NCH_2P and the two NCH_2N methylene groups diastereotopic. Mono- and bidimensional NMR experiments allowed the whole assignment of the resonances of all the methylene protons, and all couplings among them [72,79]. The MS spectra of the gold(I) thiolato complexes show in all cases the parent peak and, in some cases higher mass adducts formed by the addition of $\text{Au}(\text{PTA})$ or $\text{Au}(\text{DAPTA})$ fragments can be observed, which is typical behaviour in mass spectra of thiolate gold(I) complexes.



Scheme 48.

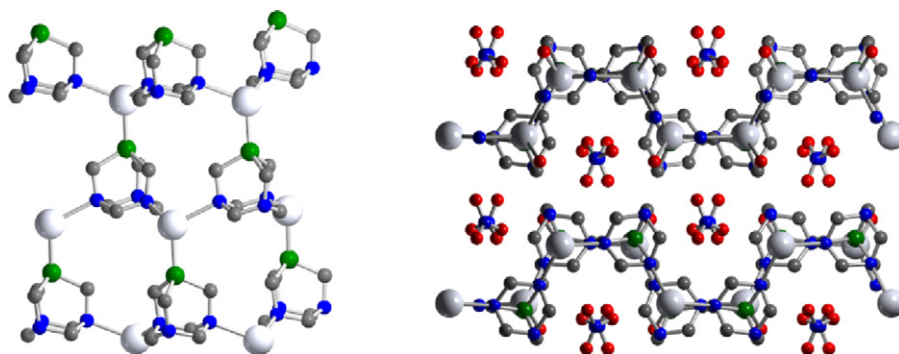
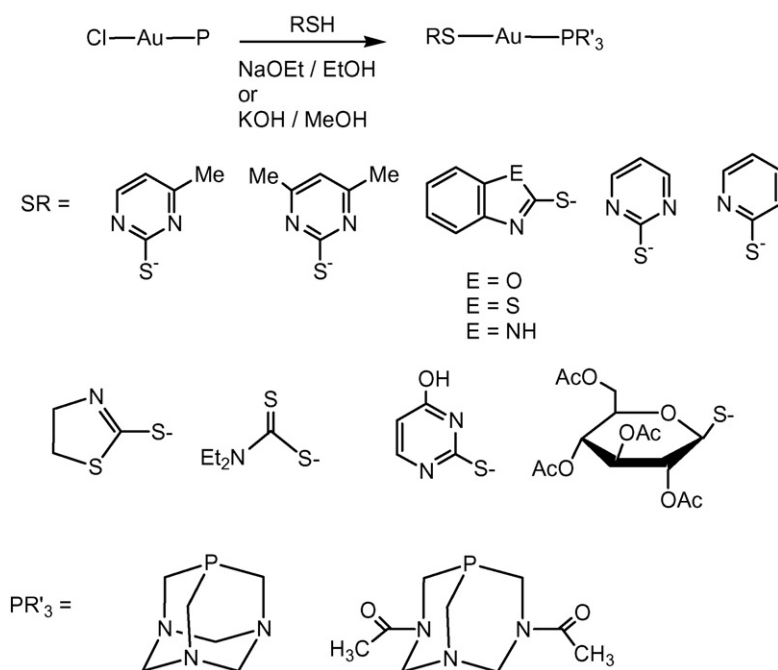


Fig. 26. Coordination network in the crystal lattice of [Ag(PTA)(H₂O)]NO₃ and a view of the hexagonal cavities containing NO₃⁻. Adapted from ref. [90].



Scheme 49.

Water solubility of Au-PTA complexes bearing 2-thiopyrimidine, 2-thiopyridine, methylpyrimidine- and thiazoline-thiolates are high, while the rest of the complexes tend to be quite soluble in MeOH or MeOH/H₂O mixtures. Thermal analysis experiments show that the complexes are stable at room temperature but start to decompose at about 200 °C and ultimately give metallic gold at *ca.* 750–800 °C.

The X-ray crystal structure of [Au(S₂CNEt₂)(PTA)] (Fig. 27) comprises a linear gold atom geometry defined by the S1 and P1 atoms. The relatively close approach of the S2 atom [Au–S2 2.7806(15) Å] is

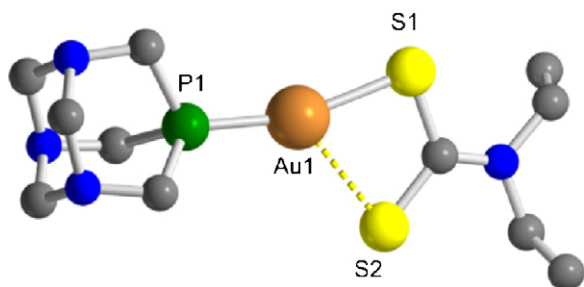
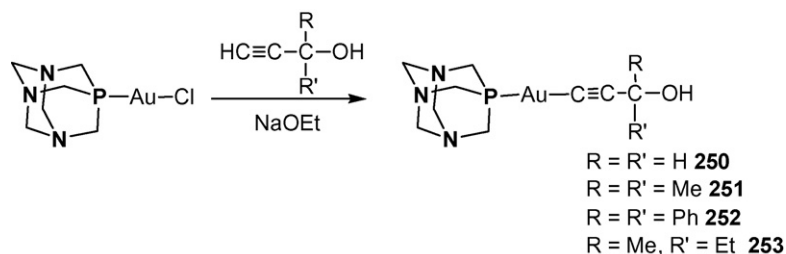


Fig. 27. X-ray crystal structure of [Au(S₂CNEt₂)(PTA)]. Short intermolecular Au(1)···S(2) contact in broken line. Adapted from ref. [72].

responsible for the significant distortion away from the ideal linear geometry, the angle P1–Au–S1 measures 163.54(5)° [72]. The complex [Au(SPyrin)(PTA)] displays the typical linear geometry about the gold center [P1–Au–S1 177.33(6)° with pairs of molecules associated in a near perpendicular arrangement (torsion angle 70.2°) through a gold–gold interaction [Au1–Au1: 3.3536(7) Å] [79].

The complex [Au(3,5-Ph₂pz)(PTA)] (3,5-Ph₂pz = 3,5-diphenylpyrazolate) (249) was synthesized by addition of [AuCl(PTA)] to a MeOH solution of Na[3,5-Ph₂pz] which is prepared in situ by the addition of one equivalent NaOH (aq) to 3,5-diphenylpyrazole and PTA ligands [91]. The white solid obtained was recrystallized from THF and diethylether. The compound was analyzed by X-ray diffraction. The asymmetric unit consists of two gold molecules with a crossed molecular structure. The gold(I) centers are nearly linearly coordinated with N–Au–P angles equal to 174.8(2) and 177.1(2)°. The Au–N bonds are almost identical at 2.049(5) and 2.044(5) Å and the Au–P bond lengths are 2.227(2) and 2.213(2) Å, typical of Au–P distances. The complex exhibits Au···Au interactions in the solid state with distances equal to 3.0962(6) Å. The Au···Au contacts provide the three-coordination that is required for the observation of metal-centered luminescence from gold(I) complexes [91].

Reaction of propargyl alcohols, HC≡CRR'OH (R = R' = H, Me, Ph and R = Me, R' = Et) with PTA, was reported by Laguna et al. [92]



Scheme 50.

as a tool to increase both water solubility and water stability of organometallic gold complexes. Thus, $[\text{AuCl}(\text{PTA})]$ and propargyl alcohols gave in basic media the colourless or pale-yellow alkynyl-gold(I) complexes $[\text{Au}(\text{C}\equiv\text{CCR}'\text{OH})(\text{PTA})]$ ($\text{R} = \text{R}' = \text{H}$ **250**, Me **251**, Ph **252**; $\text{R} = \text{Me}, \text{R}' = \text{Et}$ **253**) in good yields (Scheme 50) [92]. Complexes **251** and **253** are soluble (ca. 8 mg mL^{-1}) and also stable in water. Surprisingly, complex **251** having the smallest R groups, is only very poorly soluble in water (ca. 0.7 mg mL^{-1}) and dmsol and completely insoluble in other common organic solvents. Similarly, the phenyl derivative (**252**) is poorly soluble in dmsol and, as expected, insoluble in water [92].

Complexes **250–253** show singlet resonances at ca. -50 ppm in their $^{31}\text{P}\{^1\text{H}\}$ NMR spectra, consistent for linear gold(I) compounds containing PTA acting as a P-donor ligand. 2D (HETCOR) and $^1\text{H}\{^{31}\text{P}\}$ NMR spectra could unambiguously confirm the assignment of the PTA ligand protons [92]. The IR spectra of complexes **250–253** show a weak band due to the $\text{C}\equiv\text{C}$ stretching at ca. 2100 cm^{-1} , characteristic for alkynyls σ -bonded to a gold(I) center, as well as a very broad band at ca. 3400 cm^{-1} due to the O–H stretching. The structure (Scheme 50), consisting of linear alkynyl gold(I) complexes containing P-coordinated PTA ligands, was confirmed by an X-ray diffraction study of *rac*- $[\text{Au}\{\text{C}\equiv\text{C}(\text{Et})(\text{Me})\text{OH}\}(\text{PTA})]$, **253** [92]. This consists of a PTA ligand and the chiral alkyne linearly coordinated to a gold atom. Three of such units self-assemble in a head-to-tail arrangement, with a torsion angle of ca. 105° , through short intramolecular gold–gold contacts [$3.1178(1)$ and $3.1164(9) \text{ \AA}$] into a trinuclear chain. In addition, a further single molecule of **253** is attached, again via a short gold–gold contact of $3.1388(11) \text{ \AA}$, to the last gold atom in the chain. These tetranuclear units are then connected via slightly longer gold–gold contacts of $3.3294(9) \text{ \AA}$ to form an infinite chain polymer with gold “side chains” as shown in Fig. 28. In addition to the aurophilic interactions present in the polymer, the tetranuclear units are held together by hydrogen-bonding interactions between hydroxyl groups (O–O ca. 2.75 \AA) as well as between hydroxy groups and one of the PTA nitrogen atoms (O–N ca. 2.87 \AA) [92]. The gold–gold distances in the structure [$3.1178(10)$, $3.1164(9)$, $3.1388(11)$, and $3.3294(9) \text{ \AA}$] fall in the range typically observed for aurophilic bonds between two gold(I) centers. The polymeric structure of complex **253** containing gold “side chains” finds no precedence in the literature.

The neutral gold(I) complex $[\text{Au}(\text{C}_6\text{F}_5)(\text{PTA})]$ (**254**) and the first gold(III) complexes containing PTA *trans*- $[\text{Au}(\text{C}_6\text{F}_5)_2(\text{PTA})_2]\text{OTf}$ (**255**) and $[\text{Au}(\text{C}_6\text{F}_5)_3(\text{PTA})]$ (**256**) were prepared by displacement of the weakly coordinated tetrahydrothiophene (tht) ligand from $[\text{Au}(\text{C}_6\text{F}_5)(\text{tht})]$, *trans*- $[\text{Au}(\text{C}_6\text{F}_5)_2(\text{tht})_2]\text{OTf}$, and $[\text{Au}(\text{C}_6\text{F}_5)_3(\text{tht})]$, respectively (Scheme 51) [92]. The $^{31}\text{P}\{^1\text{H}\}$ and ^1H NMR spectra of complexes **254–256** display resonances due to PTA, with chemical shifts and coupling constants similar to those of complexes **250–253**. However, the $^{19}\text{F}\{^1\text{H}\}$ NMR spectra provide some further information in order to confirm the structures of these compounds. The C_6F_5 group gives three resonances for the *ortho*-, *meta*-, and *para*-fluorine atoms [92]. For complexes **254** and **255** only one set of C_6F_5 signals is observed in addition to a singlet resonance due

to the triflate anion of complex **255**. In contrast, the $^{19}\text{F}\{^1\text{H}\}$ NMR spectrum of compound **256** shows two sets of C_6F_5 signals in a 1:2 ratio, corresponding to the C_6F_5 groups *trans* and *cis* to the PTA ligand. The *trans* stereochemistry of complex **255** was deduced from the IR spectrum. A single band at 801 cm^{-1} is characteristic of two mutually *trans* C_6F_5 groups; in the starting material also one single band at 797 cm^{-1} is observed [92]. The structure of complex **256** was confirmed by an X-ray diffraction study. The complex consists of one PTA molecule and three C_5F_6 groups coordinated to the gold atom in a slightly distorted square-planar arrangement with CAuCl and CAuP angles ranging from $87.67(8)^\circ$ to $94.14(6)^\circ$ (molecule A) and $87.67(8)^\circ$ to $92.36(6)^\circ$ (molecule B). Unfortunately, none of the C_6F_5 complexes described here are soluble in water. Complex **256** is soluble in MeOH, whereas the cationic complex **255** containing two PTA ligands, which could be expected to be more water soluble, is soluble in acetone but poorly soluble in CH_2Cl_2 and CHCl_3 .

Treatment of the digold(II) bis(ylide) complex $[\text{Au}_2\text{Cl}_2\{\mu-(\text{CH}_2)_2\text{PPh}_2\}_2]$ with the silver(I) phosphine compounds $[\text{Ag}(\text{OTf})(\text{P})]$ ($\text{P} = \text{PTA}, \text{DAPTA}$), prepared from AgOTf and phosphines, affords the orange dicationic gold(II) complexes $[\text{Au}_2\{\mu-(\text{CH}_2)_2\text{PPh}_2\}_2(\text{P})_2](\text{OTf})_2$ (**257**) in high yields (Scheme 52) [93]. The structures of the complexes were deduced by ^1H and $^{31}\text{P}\{^1\text{H}\}$ NMR spectroscopy, mass spectrometry, and, in the case of the PTA derivative, X-ray diffraction. The ^1H NMR spectra display signals, consistent with a symmetric structure. The $^{31}\text{P}\{^1\text{H}\}$ NMR spectra consist of two triplet resonances ($^3J_{\text{PP}} = 33 \text{ Hz}$) due to coupling between the phosphorus atoms of the ylide and the coordinated P ligands, respectively. In case of the DAPTA complex, the P resonance due to the DAPTA phosphorus atoms appears as two overlapping triplets due to the presence of a mixture

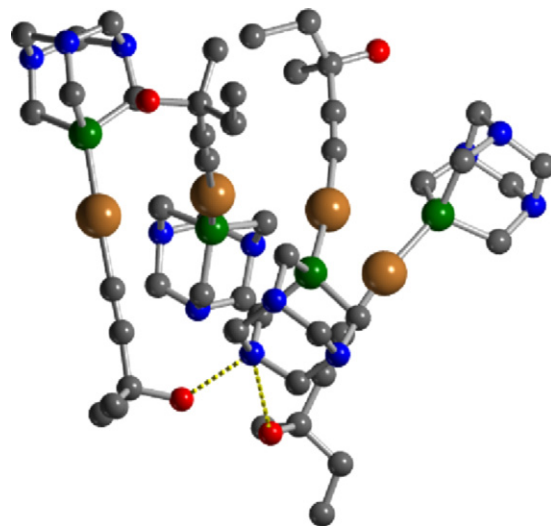
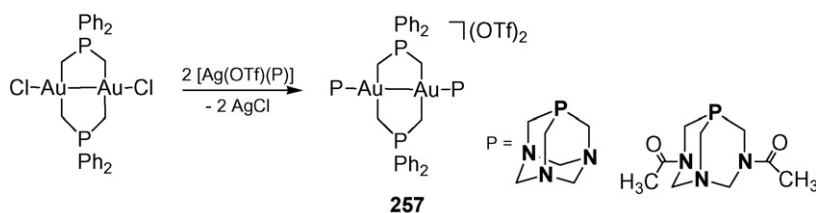
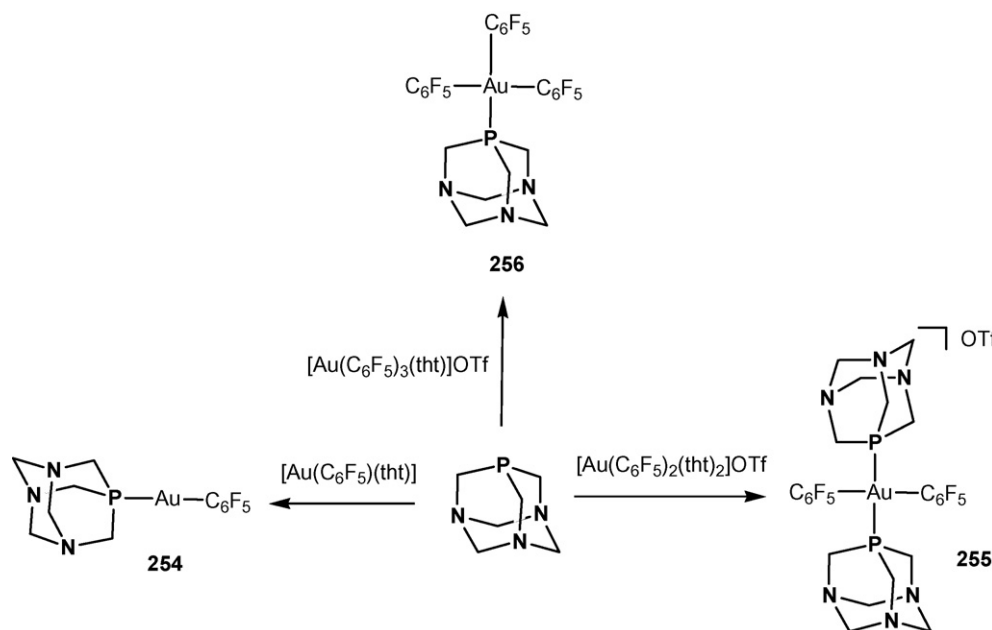


Fig. 28. Crystal lattice of *rac*- $[\text{Au}\{\text{C}\equiv\text{C}(\text{Et})(\text{Me})\text{OH}\}(\text{PTA})]$ (**253**). H atoms omitted for clarity. Adapted from ref. [92].



of *syn* and *anti* conformations of the acyl groups in the DAPTA unit [93].

The solid-state structure of **257**, isolated as a tetra-acetone solvate, shows that the complex consists of two gold atoms with an Au–Au bond length of 2.6275(4) Å, bridged by two bis(ylide) units, forming a twisted eight-membered ring [93]. Furthermore, two PTA ligands coordinate to the gold centers through the P atom linearly along the Au–Au axis. The overall coordination about the gold(II) atoms is square planar. The Au–Au bond is slightly longer than that of the starting dichloro complex [2.600(1) Å] and than most reported Au–Au bond distances for binuclear bis(ylide) complexes. Aqueous solutions of the compounds remain unchanged for at least 7 days with no sign of decomposition. This last result is particularly significant given that other known digold(II) complexes undergo various isomerization processes in nonaqueous media or polar solvents [93].

In a study on the cytotoxicity of gold(III) compounds bearing dithiocarbamate ligands and water-soluble phosphines (Section 5), the PTA complex $[\text{Au}\{\kappa^2\text{-C}_6\text{H}_4(\text{PPh}_2=\text{N}(\text{C}_6\text{H}_5))\text{-2}\}(\text{PTA})_2]\text{PF}_6$ (**258**) was obtained by reaction of $[\text{Au}\{\kappa^2\text{-C}_6\text{H}_4(\text{PPh}_2=\text{N}(\text{C}_6\text{H}_5))\text{-2}\}\text{Cl}_2]$ with 1 equiv of NaPF_6 and subsequent addition of 1 equiv of PTA (Chart 12) [94]. Compound **258** is only soluble in DMSO or in DMSO–water mixtures. The $^{31}\text{P}\{^1\text{H}\}$ NMR spectrum (DMSO) clearly shows the incorporation of PTA [δ –56.6 (s + br, $\text{P}_\text{B} + \text{P}_\text{C}$) and its cationic nature [δ –144.1 (sept, P_D)].

3.7. Zinc complexes

The first example of a zinc complex bearing PTA, i.e. $[\text{ZnCl}_2(\text{PTA})_2]$ (**259**) was recently reported by Smolenski et al. [95].

The complex was obtained by reaction of ZnCl_2 with PTA in 1:2 molar ratio, with PTA binding to the metal atom by an unusual *N*-coordination mode. When the reaction is carried out with $[\text{mPTA}]\text{I}$ in the same conditions, the hybrid organic–inorganic salt $[(\text{mPTA})_2(\text{ZnCl}_2\text{I}_2)]$ (**260a**) is obtained, whereas $[(\text{mPTA})_2(\text{ZnI}_4)]$ (**260b**) is formed in the presence of an excess of KI (Scheme 53) [95].

The compounds are air-stable in the solid state and in aqueous and methanol solutions. The ^1H [δ 4.06 (d, $^1J_{\text{HP}} = 9.6$ Hz), $\text{P}-\text{CH}_2-\text{N}$; 4.69 (s), $\text{N}-\text{CH}_2-\text{N}$] and $^{31}\text{P}\{^1\text{H}\}$ [δ –93.2 (s), PTA] NMR spectra supports the *N*-coordination of PTA in **259**. Structures of the compounds **259** and **260a** were authenticated by X-ray diffraction analysis. In complex **259** (Fig. 29) the asymmetric unit consists of three molecules of the complex. Each of the Zn ions is in an approximately tetrahedral geometry arising from two chloride atoms and two PTA molecules. The Zn–Cl distances range from 2.2131(13)

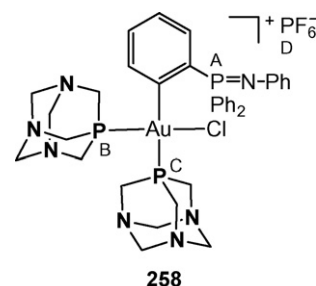
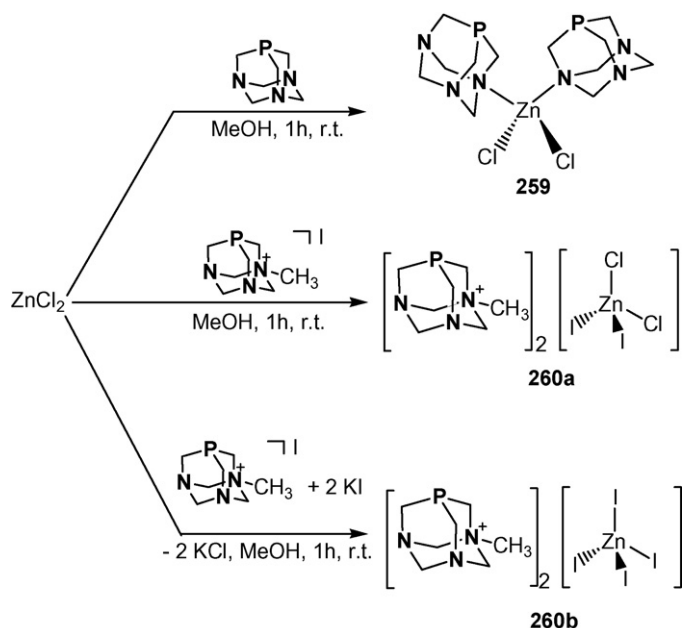


Chart 12.



Scheme 53.

to 2.2461(12) Å and the Zn–N distances range from 2.055(3) to 2.101(3) Å. In the molecular structure of **260a** only one of the mPTA cations was found and refined, being the other one highly disordered [95].

4. Catalytic applications of transition-metal complexes of PTA and its derivatives

It was recently published [4c] that free PTA is a versatile phosphine catalyst for Morita–Baylis–Hillman (MBH) reaction of activated olefins and also of *N*-thiophosphoryl imines (Aza-MBH reaction) [4a]. PTA is highly efficient for the MBH reaction of both aromatic and aliphatic aldehydes with activated olefin acrylates and methyl vinyl ketone (Tables 9 and 10).

Intramolecular **hydroamination** is a 100% atom efficient process towards pharmaceutically important N-heterocycles. Iridium compounds [Ir(cod)(PTA)₃]Cl (**186**), [IrCl(CO)(PTA)₃] (**261**) and [Ir(CO)(PTA)₄]Cl (**262**) were active for the cyclization of 4-pentyn-1-amine to 2-methyl-pyrroline in water at 50 °C [68]. From Table 11 it can be seen that all three Ir compounds are moderately active in hydroamination of 4-pentyn-1-amine, with activities comparable to *cis*-[PtCl₂(PTA)₂]·H₂O, *cis*-[PtBr₂(PTA)₂] (**225**), and *cis*-[PtI₂(PTA)₂] (**226**) albeit less active than Pd(II)-PTA complexes [82,85].

The rate of the catalytic runs is independent of the nature of the halide, and the reactions are faster in water. The acetylde interme-

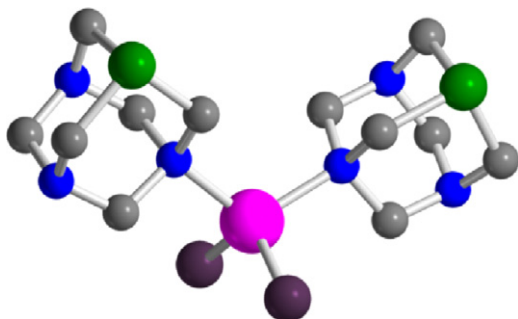


Fig. 29. X-ray crystal structure of $[\text{ZnCl}_2(\text{PTA})_2]$ (**259**). Adapted from ref. [95].

Table 9

The PTA-catalyzed Baylis–Hillman reaction of aromatic aldehydes with ethyl (*n*-butyl)acrylates.

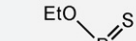
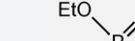
Entry	Ar	R	Time [h]	Yield ^a [%]
1	2-NO ₂ C ₆ H ₄	Et	9	84
2	3-NO ₂ C ₆ H ₄	Et	7	72
3	4-NO ₂ C ₆ H ₄	Et	5	91
4	2,4-Cl ₂ C ₆ H ₃	Et	15	80
5	2-F-4-ClC ₆ H ₃	Et	7	60
6	2-pyridyl	Et	7	59
7	2-NO ₂ C ₆ H ₄	n-Bu	19	93
8	4-NO ₂ C ₆ H ₄	n-Bu	15	79

Products were identified by ^1H and ^{13}C NMR, and in some cases by microanalysis.

^a Isolated yield based on the aldehyde.

Table 10

Different catalysts used in the aza-MBH reaction of imines with MVK^a.

				
Catalyst	Time [h]	Yield [%] ^b	Time [h]	Yield [%] ^b
PTA	96	84	48	82
DABCO	96	78	68	59
PPh ₃	96	82	48	78

^a All reactions were carried out in acetonitrile in the presence of 10 mol% of catalyst with a 1:3 molar ratio of imine to activated MVK.

^b Isolated yield.

diates were identified and a plausible catalytic cycle was proposed (Scheme 54) [85].

Complexes $[\text{CuRuCl}(\text{PTA})_2]$ (**53a**), $[\text{Cu}^*\text{RuCl}(\text{PTA})_2]$ (**53b**), $[\text{Cu}^*\text{IrCl}(\text{PTA})_2]\text{Cl}$ (**183**) [67,96] were tested as catalysts for **CO₂/HCO₃ reduction** to formate, in the absence of base additive and under mild conditions, in the pH range 5.30–10.54 and in the temperature range 30–100 °C (Table 12). Precatalyst **183** was

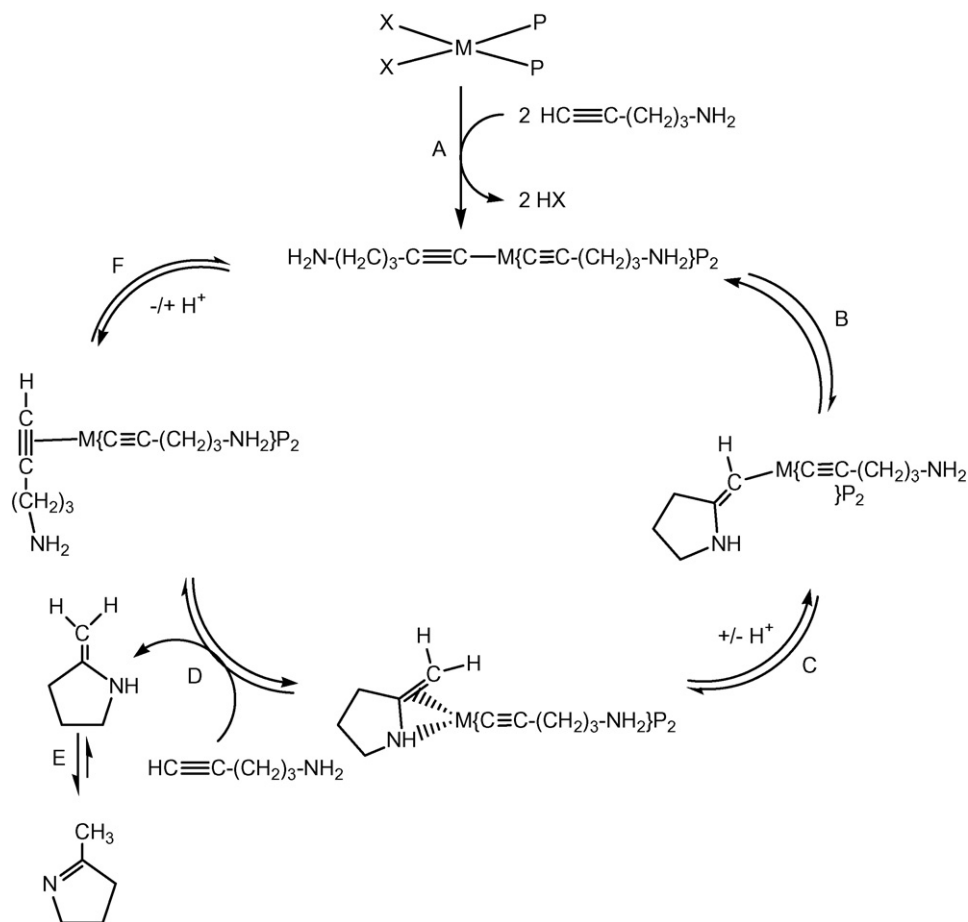
Table 11

Metal-PTA-catalyzed hydroamination of 4-pentyn-1-amine in various solvents at 50 °C.

Complex	Solvent	N_t (h ⁻¹) ^a	% Conv. ^b
<i>cis</i> -[PtCl ₂ (PTA) ₂]	D ₂ O	0.35	27
<i>cis</i> -[PtCl ₂ (PTA) ₂]	CD ₃ OD	0.33	25
<i>cis</i> -[PtCl ₂ (PTA) ₂]	d ₆ -DMSO	0.021	8.7
<i>cis</i> -[PtBr ₂ (PTA) ₂] (225)	D ₂ O	0.36	28
<i>cis</i> -[PtBr ₂ (PTA) ₂] (225)	CD ₃ OD	0.38	27
<i>cis</i> -[PtBr ₂ (PTA) ₂] (225)	d ₆ -DMSO	0.023	6.3
<i>cis</i> -[PtI ₂ (PTA) ₂] (226)	D ₂ O	0.34	26
<i>cis</i> -[PtI ₂ (PTA) ₂] (226)	CD ₃ OD	0.25	20
<i>cis</i> -[PtI ₂ (PTA) ₂] (226)	d ₆ -DMSO	0.023	6.8
<i>cis</i> -[PdCl ₂ (PTA) ₂]	D ₂ O	6.0	97
<i>cis</i> -[PdCl ₂ (PTA) ₂]	CD ₃ OD	4.5	92
<i>cis</i> -[PdCl ₂ (PTA) ₂]	d ₆ -DMSO	1.0	49
<i>cis</i> -[PdBr ₂ (PTA) ₂]	D ₂ O	5.6	96
<i>cis</i> -[PdBr ₂ (PTA) ₂]	CD ₃ OD	3.9	89
<i>cis</i> -[PdBr ₂ (PTA) ₂]	d ₆ -DMSO	0.75	40
[Ir(cod)(PTA) ₃]Cl (186)	D ₂ O	0.33	24
[Ir(CO)(PTA) ₃]Cl (261)	D ₂ O	0.36	28
[Ir(CO)(PTA) ₄]Cl (262)	D ₂ O	0.32	23

^a Calculated as the number of moles of product/moles of catalyst/hour at 50% conversion.

^b Determined by integration of the ¹H NMR spectra after 48 h.



Scheme 54.

Table 12

Catalyst screening for aqueous hydrogenation of bicarbonate at different values of pH and temperature.

Catalyst	<i>T</i> (°C)	pH	Initial TOF (h ⁻¹) ^a
[CpRuCl(PTA) ₂] 53a	50	10.54	0.04
	50	7.87	1.2
	50	5.94	1.56
	65	7.87	4.5
	80	10.54	0.05
	80	9.46	1.4
	80	7.87	5.2
	25	10.2	1.0
[Cp*RuCl(PTA) ₂] 53b	25	9.4	7.4
	25	6.24	12.1
	30	9.46	0.4
	30	8.14	2.3
	30	5.60	5.0
	50	9.46	3.9
	62	10.3	11.4
	80	12.2	16.0
[Cp*IrCl(PTA) ₂]Cl 183	70	8.4	4.0
	80	8.4	10.7
	90	8.4	16.5
	100	8.4	22.6
	80	5.9	6.5
	80	9.0	12.7
	80	9.2	9.1
	80	9.5	6.5
	80	9.8	5.4
	80	10.3	2.3

^a Turnover frequencies (TOF = mol formate/mol catalyst/h) were calculated by non-linear least-square fits of the experimental data from the initial part of the reactions.

the most active, performing best at elevated temperatures and in slightly basic aqueous solution (pH 9). The active species was determined to be the corresponding cationic [Cp*IrH(PTA)₂]⁺ complex (**185**).

The hydrogenation of CO₂/bicarbonate under mild conditions was also studied in the presence of the half-sandwich [RuCl₂(PTA)([9]aneS₃)] (**146**) [97]. Catalytic tests were carried out adding **146** to an aqueous (H₂O/D₂O) solution of NaH¹³CO₃ (0.15 M), which was then pressurised with hydrogen (P_{H2} = 100 bar) and heated to 303 K. Monitoring the reaction by ¹³C NMR spectroscopy, it was observed that this compound produces sodium formate in the absence of additives, but with low activity. No induction period is required probably due to the rapid hydrolysis of the compound in water. An intermediate was observed and the structure [Ru(H)(CO₃H)(PTA)([9]aneS₃)] and a mechanism of the catalytic hydrogenation was proposed [97].

Water-soluble ruthenium(II) complexes [RuCl₂(η⁶-arene)(PTA)], [RuCl₂(η⁶-arene)(PTA-Bz)]Cl, and [RuCl₂(η⁶-arene)(DAPTA)]; (η⁶-arene = C₆Me₆, 1,3,5-C₆H₃Me₃, *p*-cymene, C₆H₆, see numbering scheme in Table 13) were used as catalysts for the **hydrogenation of nitriles** in pure aqueous media and under neutral conditions [98]. All complexes led to benzamide from benzonitrile in almost quantitative yield (≥98%), and appreciable differences in activity were observed as function of the arene ligand used. Thus, the rate order observed C₆Me₆ > 1,3,5-C₆H₃Me₃ > *p*-cymene > C₆H₆ indicates that higher performances are found for the more sterically demanding and electron-rich arenes (Table 13). Among the complexes studied, [RuCl₂(η⁶-C₆Me₆)(PTA-Bz)] was the most active and it was an efficient catalyst for the selective hydration of a large number of nitriles [98].

Table 13Ru-catalyzed hydration of benzonitrile to benzamide in water^a.

$\text{Ph}-\text{C}\equiv\text{N} \xrightarrow[\text{H}_2\text{O} / 100^\circ\text{C}]{5 \text{ mol\% of Ru}} \text{Ph}-\text{C}(=\text{O})\text{NH}_2$					
Entry	Catalyst	S [mg mL ⁻¹] ^b	t [h]	Yield [%] ^c	TOF [h ⁻¹] ^d
1	[RuCl ₂ (C ₆ H ₆)(PTA)] 119	50.0	9	98	2.2
2	[RuCl ₂ (p-cymene)(PTA)] 116a	10.1	8	99	2.5
3	[RuCl ₂ (1,3,5-C ₆ H ₃ Me ₃)(PTA)] 263	33.3	5	99	4.0
4	[RuCl ₂ (C ₆ Me ₆)(PTA)] 123	9.1	4	99	5.0
5	[RuCl ₂ (C ₆ H ₆)(PTA-Bz)]Cl 264a	16.0	10	99	2.0
6	[RuCl ₂ (p-cymene)(PTA-Bz)]Cl 264b	12.5	4	99	5.0
7	[RuCl ₂ (1,3,5-C ₆ H ₃ Me ₃)(PTA-Bz)]Cl 264c	13.5	4	99	5.0
8	[RuCl ₂ (C ₆ Me ₆)(PTA-Bz)]Cl 264d	25.0	2	99	9.9
9	[RuCl ₂ (C ₆ H ₆)(DAPTA)] 265a	6.3	19	99	1.0
10	[RuCl ₂ (p-cymene)(DAPTA)] 265b	6.3	9	98	2.2
11	[RuCl ₂ (1,3,5-C ₆ H ₃ Me ₃)(DAPTA)] 265	9.0	8	98	2.5
12	[RuCl ₂ (C ₆ Me ₆)(DAPTA)] 265d	8.3	9	98	2.2

^a Reactions performed under N₂ at 100 °C using 1 mmol benzonitrile (0.33 M in water). [Substrate]/[Ru] ratio = 20:1.^b Solubility of the catalyst in water at 20 °C.^c Yield of benzamide determined by GC.^d Turnover frequencies (mol product/mol Ru/time) were calculated at the time indicated in each case.**Table 14**Sonogashira coupling of aryl bromides with terminal alkynes in the presence of **195**.

$\text{R}-\text{C}_6\text{H}_4-\text{Br} + \text{R}'-\text{C}\equiv\text{C}-\text{H} \longrightarrow \text{R}-\text{C}_6\text{H}_4-\text{C}\equiv\text{C}-\text{R}'$					
Entry	Product	Yield (%) ^a	Entry	Product	Yield (%) ^a
1	R = MeOC, R' = Ph	100	11	R = Me, R' = 1-cyclohexene	96
2	R = MeOC, R' = Cy	100	12	R = Me, R' = tBu	100
3	R = MeOC, R' = 1-cyclohexene	100	13	R = Mes, R' = Ph	76
4	R = MeOC, R' = tBu	100	14	R = Mes, R' = Cy	45
5	R = H, R' = Ph	70	15	R = Mes, R' = 1-cyclohexene	75
6	R = H, R' = Cy	100	16	R = Mes, R' = tBu	80
7	R = H, R' = 1-cyclohexene	98	17	R = Ms, R' = Ph	60
8	R = H, R' = tBu	100	18	R = MeO, R' = Cy	88
9	R = Me, R' = Ph	70	19	R = MeO, R' = 1-cyclohexene	80
10	R = Me, R' = Cy	92	20	R = MeO, R' = tBu	100

^a Determined by GC. Conditions: 1.0 equiv of aryl bromide, 1.5 equiv of alkyne, 1.5 equiv of Cs₂CO₃, 4.0 mL of CH₃CN, 2.5 mol% of [Pd], 80 °C, 24 h. Cy = cyclohexyl; Mes = mesityl.

Complex [Pd(dmba)Cl(PTA)] (**195**) and Pd(OAc)₂/PTA (1:3 molar ratio) were screened for catalytic activity in the **Sonogashira cross-coupling** reaction of either aryl bromides (Table 14) or aryl chlorides (Table 15) with terminal alkynes under copper- and

amine-free conditions [73]. Comparable results were observed for the two catalytic systems applied. In the case of the reaction of the activated aryl chlorides with terminal alkynes the yields of products with both catalytic systems were excellent using MeCN as solvent

Table 15Sonogashira coupling of aryl chlorides with terminal alkynes in the presence of **195**.

$\text{R}-\text{C}_6\text{H}_4-\text{Cl} + \text{R}'-\text{C}\equiv\text{C}-\text{H} \longrightarrow \text{R}-\text{C}_6\text{H}_4-\text{C}\equiv\text{C}-\text{R}'$					
Entry	Product	Yield (%) ^a	Entry	Product	Yield (%) ^a
1	R = MeOC, R' = Ph	80	11	R = NC, R' = 1-cyclohexene	100
2	R = MeOC, R' = Cy	100	12	R = NC, R' = tBu	100
3	R = MeOC, R' = 1-cyclohexene	100	13	R = H, R' = Ph	50
4	R = MeOC, R' = tBu	100	14	R = H, R' = Cy	60
5	R = HOOC, R' = Ph	100	15	R = H, R' = 1-cyclohexene	66
6	R = HOOC, R' = Cy	100	16	R = H, R' = tBu	70
7	R = HOOC, R' = 1-cyclohexene	100	17	R = 4-py, R' = Ph	100
8	R = HOOC, R' = tBu	100	18	R = 4-py, R' = Cy	100
9	R = NC, R' = Ph	100	19	R = 4-py, R' = 1-cyclohexene	100
10	R = NC, R' = Cy	100	20	R = 4-py, R' = tBu	100

^a Determined by GC. Conditions: 1.0 equiv of aryl chloride, 1.5 equiv of alkyne, 1.5 equiv of Cs₂CO₃, 1.5 equiv of TBAB, 4.0 mL of CH₃CN, 3 mol% of [Pd], 80 °C, 24 h. 4-py = 4-pyridyl.

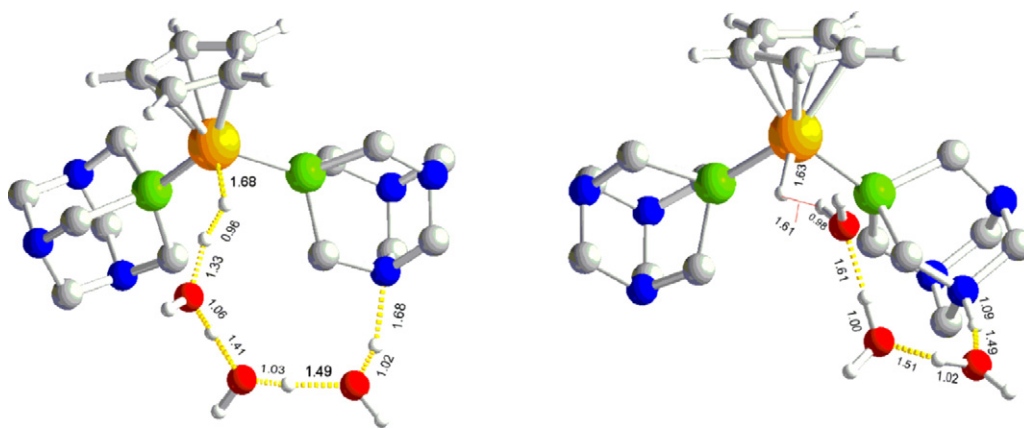


Fig. 30. Optimized structures of the transition state for the heterolytic splitting ($\text{TS}_2 \cdot (\text{H}_2\text{O})_3$) (left) and water-stabilized monohydride $[\text{CpRuH}(\text{PTA-H})(\text{PTA})]^+ \cdot (\text{H}_2\text{O})_3$ (right). Selected bond lengths reported (Å). The figure was reproduced from ref. [99], with permission of the copyright holders.

and Cs_2CO_3 as a base in the presence of 1.5 equivalents of tetrabutylammonium chloride. Good conversions were also obtained in the case of chlorobenzene. Also in the case of heterocyclic chlorides such as 4-chloropyridine, excellent results (i.e. 100% yields) were obtained [73]. Low Pd catalyst concentrations could be used and no Pd contamination of the products was observed, as required for applications in pharmaceutical synthesis.

Ruthenium(II) (substituted) cyclopentadienyl (Cp) and pentamethylcyclopentadienyl (Cp^*) complexes **53a**, **53b**, **59–62**, **73** and **74** were active catalysts for the **chemoselective hydrogenation** of benzylidene acetone (BZA) to 4-phenyl-butan-2-one in $\text{H}_2\text{O}/n$ -octane at mild temperatures (80–120 °C) under hydrogen pressure (200–450 psi) giving full conversion after 16 h [39].

On the same topic, Frost et al. reported that $[\text{CpRuH}(\text{PTA})_2]$ (**85**) catalytically reduces benzylidene acetone in a biphasic $\text{H}_2\text{O}/\text{Et}_2\text{O}$ solvent system at room temperature and low pressures of H_2 (10–150 psi), albeit with modest TOFs. An important role is played by pH, which has a strong influence on the activity ($\text{pH} > 7$, $\text{pH} < 3.6$ values give a poor catalytic performance, highest activity at pH 4.7). Interestingly, the reduction is selective for the C=C bond for all the pH values tested, except at pH 2.1, in which the selectivity changes with the type of buffer used ($\text{HBF}_4/\text{NaH}_2\text{PO}_4$, 99% of 4-phenylbutan-2-one; $\text{HCl}/\text{NaH}_2\text{PO}_4$, 77.5% of 4-phenylbut-3-en-2-ol). Addition of different salts (KCl, NaNO_3 , NaBF_4 , or NaPF_6) shows a significant influence of the anion, being BF_4^- the one that

produces the highest conversion, possibly stabilizing a coordinatively unsaturated intermediate generated during the reaction. The results of this study seem to indicate that the active species in catalysis is $[\text{CpRu}(\text{PTA})\text{H}(\text{PTAH})]^+$ resulting from protonation of PTA and the reaction occurs via an ionic hydrogenation mechanism [36].

A DFT study on the role of water in the activation of dihydrogen by $[\text{CpRu}(\text{PTA})_2\text{Cl}]$ indicates that both water and PTA take an active part in the process, with three water molecules making a hydrogen-bonded chain that connects the chloride and a N atom from one PTA ligand promoting heterolytic activation of the $\text{Ru}(\eta^2\text{-H}_2)$ via solvent mediated intramolecular proton transfer (Fig. 30), and confirms, in line with experimental results, the formation of intermediate monohydride species [99].

Ruthenium complexes bearing Cp, Dp, and Ind as ancillary ligands were tested as catalysts for the selective **transfer hydrogenation** of CNA, BZA and chalcone, in aqueous media and in the presence of formic acid ($\text{pH} \leq 3$). The indenyl complex **77** was less active than either the Cp, **66** or Dp **76** analogues. The chemoselectivity of reduction of the substrate depends on the arene ligand of the catalysts, the substrate, and the pH of the solution (Table 16) [41].

Comparable results using $[\text{CpRu}(\text{PTA})_2\text{Cl}]$ (**53a**) were obtained by Bolaño et al. who also tested $[\text{Cp}^*\text{Ru}(\text{PTA})_2\text{Cl}]$ (**53b**) as catalyst for CNA reduction. A remarkable difference in conversion, from moderate (36%, 6 h) using **53a** to excellent (97%, 6 h) in the presence of **53b**

Table 16

Selective transfer hydrogenation of benzylidene acetone using HCOOH or HCOONa as the reducing agents^g.

Entry	Catalyst	% Conv.	TOF (h^{-1})	% Selectivity		
1	$[\text{CpRu}(\text{PTA})(\text{PPh}_3)\text{Cl}]$ 66	79.4	0.7	55.9	0.0	34.7
2	$[\text{CpRu}(\text{PTA})_2\text{Cl}]$ 53a	66.7	0.6	100.0	0.0	0.0
3 ^{a,b}	$[\text{CpRu}(\text{PTA})_2\text{Cl}]$ 53a	78.9	0.6	>99.0	<1.0	0.0
4 ^{c,d}	$[\text{CpRu}(\text{PTA})_2\text{Cl}]$ 53a	36.1	6.0	93.9	6.1	0.0
5 ^c	$[\text{DpRu}(\text{PTA})(\text{PPh}_3)\text{Cl}]$ 76	51.1	1.7	100	0.0	0.0
6	$[\text{DpRu}(\text{PTA})_2\text{Cl}]$ 65	81.4	0.8	58.7	41.3	0.0
7 ^a	$[\text{DpRu}(\text{PTA})_2\text{Cl}]$ 65	83.7	0.8	100.0	0.0	0.0
8 ^e	$[\text{IndRu}(\text{PTA})(\text{PPh}_3)\text{Cl}]$ 77	48.9	0.41	100.0	0.0	0.0
9 ^f	$[\text{CpRu}(\text{PTA})(\text{PPh}_3)\text{H}]$	38.5	0.64	100.0	0.0	0.0

^a 0.9 mmol (61.2 mg) of HCO_2Na in lieu of HCO_2H , pH \approx 9.

^b 25 h.

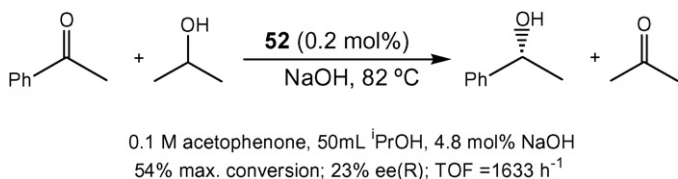
^c 6 h.

^d 0.75 mmol of substrate, 7.5×10^{-3} mmol of catalyst, 7.5 mmol of HCO_2Na , 3 mL of MeOH, 3 mL of H_2O , 90 °C, 6 h.

^e 150 μL of HCOOH , 2 mL of H_2O , 1 mL of MeOH.

^f 100 μL of HCOOH , 12 h.

^g General conditions: 5 mol% of catalyst; 4.3 mg of benzylidene acetones; 40 μL of 88% HCO_2H ; 2 mL of H_2O ; 24 h at 80 °C; pH \approx 3.



Scheme 55.

(conditions: BZA, 0.75 mmol; catalyst, 7.5×10^{-3} mmol; HCO₂Na, 7.5 mmol; MeOH, 3 mL; H₂O, 3 mL; 90 °C) was observed [39].

Complex *fac*-[RuCl₂(PTA)₂{κ²(*P,N*)-FcPN}] (**52**) is an active catalyst for the asymmetric transfer hydrogenation (ATH) of acetophenone [34]. Moderate conversions and *ee*'s were obtained in the presence of **52** (0.2 mol%) using the ⁱPrOH/NaOH reducing system (Scheme 55).

Complexes κ¹-*P*-[RhCl(cod){PTN(R)}] (R = Me, **179a**; R = Ph, **179b**) and κ²-*P,N*-[Rh(cod){PTN(R)}](BAR^F₄) (R = Me, **180a**; R = Ph, **180b**, Scheme 35) were tested as catalysts for **olefin hydroformylation** and benzylidene acetone and acetophenone **transfer hydrogenations** [66]. 1-Hexene hydroformylation were run in THF under very mild conditions and the results are summarized in Table 17 below.

As expected, the linear aldehyde was the favoured product, with *l/b* ratio ranging from 1.35 (**179b** in CHCl₃, 4 h) to 3.13 (**179a** in THF, 1 h). The best conversion was achieved with **179b** (99%), although a larger amount of isomerized alkenes were found by GC analysis of the reaction mixture after the run. Interestingly, in THF the systems afford very little amounts of hydrogenation products. Styrene hydroformylation tests were also carried out both under strictly homogeneous (chloroform) and biphasic (*n*-octane/water) conditions. High conversions and chemoselectivity to the branched aldehydes (>94%) were achieved (Table 18) and only traces of hydrogenated product (ethylbenzene, <0.5%) were determined. Control runs with [Rh(cod)Cl₂]₂ showed that in CHCl₃ at 55 °C a slightly higher *l/b* ratio is obtained at complete conversion

(0.11, corresponding to 88.9% branched and 9.9% linear aldehyde), whereas in water/octane at 60 °C a higher amount of ethylbenzene is produced (5.9% against 0.1 in CHCl₃) accompanied by a small increase in regioselectivity (*l/b* 0.08).

Complexes **179** and **180** were tested in the transfer hydrogenation of benzylideneacetone (BZA) and acetophenone. Very high chemoselectivity to C=C bond hydrogenation was obtained with all complexes in the transfer reduction of BZA using NaHCO₂ as hydrogen source in water (Table 19). The highest conversions (>95%) were observed in the presence of **180b**. Hydrogen transfer reduction of acetophenone was achieved using the KOH/ⁱPrOH protocol (Table 19). Interestingly, good conversions (57–69%) were achieved using the monocoordinated Rh(I) neutral complexes **179** while moderate conversions were obtained with the cationic κ²-*P,N* chelated complexes **180**. At higher substrate/catalyst ratio (1000), hydrogen transfer to acetophenone still occurred albeit with lower conversion (20%, TON 198).

PTA and the *N*-benzylated derivative (*N*-Bz-PTA)Cl were tested for their interaction with the *randomly methylated β-cyclodextrin* (RAME-β-CD, Scheme 56) [100]. Results showed that both ligands could be considered as non-interacting phosphines with respect to RAME-β-CD.

This effect has been efficiently applied in rhodium-catalyzed **1-decene hydroformylation**. The study included comparative tests in the presence of other water-soluble phosphines such as TPPTS (tri-*m*-sulfonated triphenylphosphine). The chemoselectivities in aldehydes obtained with PTA and (*N*-Bz-PTA)Cl were very high (>98%) (Table 20), without a decrease in regioselectivity as the linear to branched aldehydes ratio remained constant, contrary to what was observed with TPPTS. The absence of interaction between the CD mass-transfer promoter and the PTA ligands has beneficial effects on the chemo- and regioselectivity in the hydroformylation reaction of 1-decene since no alteration of the catalytic performances was detected.

Apart from the applications as molecular catalysts in either biphasic or water phase reactions, transition-metal PTA com-

Table 17
1-Hexene hydroformylation under homogeneous conditions^a in the presence of complexes **179**, **180**.

Catalyst	Conv. % (h)	Linear %	Branched %	<i>l/b</i>	Isom %	Hydrog %
179a	20.2(1)	12.2	3.9	3.13	4.0	0.1
179a	61.5(4)	31.9	13.4	2.38	16.1	0.1
179a^b	83.0(4)	43.5	20.9	2.08	18.4	0.2
179a^c	92.5(4)	50.7	26.2	1.94	15.5	0.1
179b	63.4(1)	33.6	12.3	2.73	17.4	0.1
179b	99.3(4)	48.3	26.1	1.85	20.9	4.0
179b^c	82.5(4)	33.5	24.9	1.35	19.9	4.2 ^d
180a	27.4(1)	14.8	5.5	2.69	7.0	0.1
180a	70.0(4)	35.8	15.8	2.27	17.6	0.8
180b	52.6(1)	29.8	11.3	2.64	11.3	0.2

^a 1-Hexene: 2.5 mmol; cat 0.01 mmol; H₂:CO (2:1), 600 psi; THF: 30 mL; 60 °C; 4 h.

^b CO/H₂ (1:1) 600 psi.

^c CHCl₃ 30 mL, 55 °C, CO/H₂ (1:1) 600 psi.

^d Including alcohols.

Table 18
Styrene hydroformylation under homogeneous^a and biphasic conditions^b using complexes **179**, **180** and **181** as precatalysts.

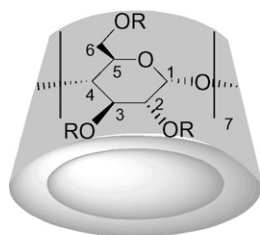
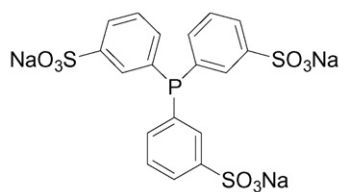
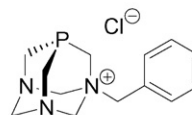
Complex	Conv. (%)	Branched (%)	Linear (%)	<i>l/b</i>	EtPh (%)
179a^a	99.3	95.4	3.7	0.039	0.2
179a^b	57.7	52.9	2.3	0.043	1.9
179b^a	88.4	84.5	3.7	0.044	0.2
179b^b	71.0	66.9	3.2	0.047	0.9
180a^a	80.8	74.7	5.5	0.074	0.5
180b^b	99.9	95.3	4.7	0.049	0.0
181^b	40.6	39.5	0.1	0.003	1.0

^a Styrene: 2.5 mmol; cat: 0.01 mmol; H₂:CO (1:1), 600 psi; CH₃Cl: 40 mL; 55 °C; 6 h.

^b As above, except H₂O/*n*-octane (2/1), 60 °C.

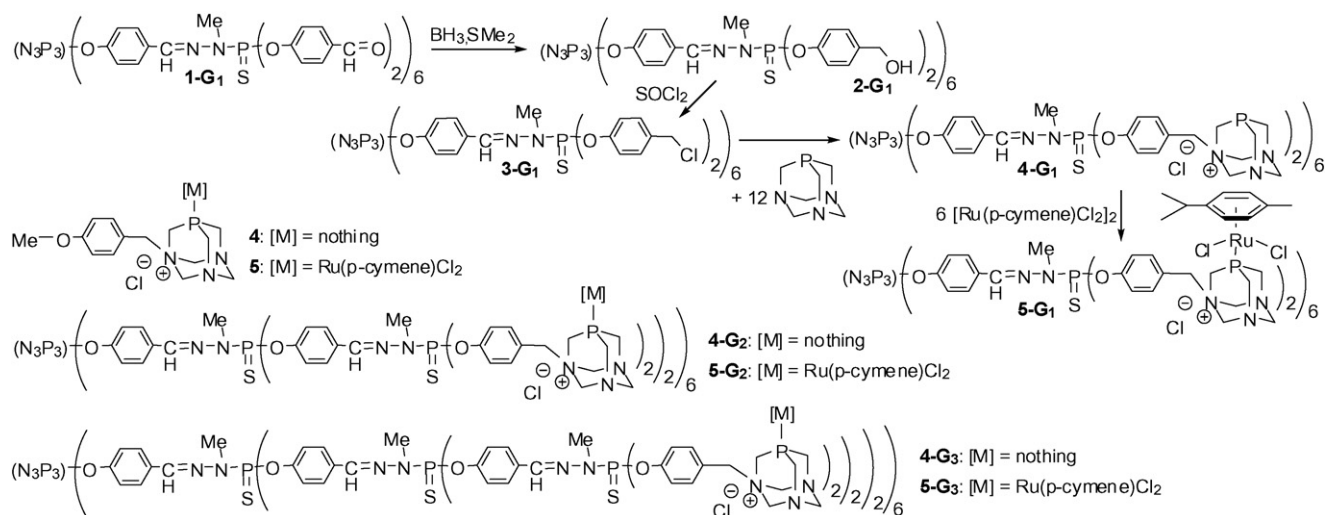
Table 19Transfer hydrogenation of BZA^a and acetophenone^b in the presence of **179** and **180**.

Catalyst	Substrate	Conv. (%)	Selectivity			Average TON
			% A ^c	% B ^c	% C ^c	
10a	BZA	59.9	98.6	1.4	–	60
10a	PhC(O)Me	69.3	–	–	100	347
10b	BZA	96.4	99.8	0.2	–	97
10b	PhC(O)Me	57.7	–	–	100	288
11a	BZA	59.3	98.8	1.2	–	60
11a	PhC(O)Me	22.3	–	–	100	112
11b	BZA	100	>99.9	0.0	–	100
11b	PhC(O)Me	17.4	–	–	100	87

^a BZA:catalyst:NaHCO₂ (100:1:1000); MeOH (3 mL); H₂O (3 mL); 80 °C, 5 h.^b Conditions: catalyst:acetophenone:KOH (1:500:5); PrⁱOH (10 mL); 80 °C, 6 h.^c GC values based on pure samples. A = 4-phenyl-2-butanone; B = 4-phenyl-3-buten-2-ol; C = 1-phenylethanol.**Native β-CD:** R = H**RAME-β-CD:** R = H or CH₃ (substitution degree = 1.7 per glucopyranose unit)**TPPTS****PTA****(N-Bz-PTA)Cl****Scheme 56.** Reproduced from ref. [100], with permission of the copyright holders.**Table 20**Biphasic rhodium-catalyzed hydroformylation of 1-decene in the presence of randomly methylated β-cyclodextrins and water-soluble phosphines^a.

<div>CH₃-(CH₂)₇-CH=CH₂</div>		<div>CO/H₂ Rh</div> <div>water soluble phosphine</div>	<div>CH₃-(CH₂)₇-CH-CH-CHO (l)</div> <div>CH₃-(CH₂)₇-CH(CHO)CH₃ (b)</div> <div>alkene isomers (by-products)</div>			
Entry	Phosphine	Cyclodextrin	T (°C)	Conv. (%) ^b	Selectivity (%) ^c	l/b ratio ^d
1	TPPTS	–	80	3	59	2.8
2	TPPTS	–	100	28	42	2.9
3	TPPTS	–	120	50	30	3.0
4	TPPTS	RAME-β-CD	80	95 (65 ^e)	96	1.8
5	TPPTS	RAME-β-CD	100	100 (74 ^e)	88	1.9
6	TPPTS	RAME-β-CD	120	100 (85 ^e)	73	2.2
7	PTA	–	80	<1	n.d.	n.d.
8	PTA	–	100	2	90	1.9
9	PTA	–	120	81	96	1.9
10	PTA	RAME-β-CD	80	<1	n.d.	n.d.
11	PTA	RAME-β-CD	100	11	98	1.9
12	PTA	RAME-β-CD	120	94	99	1.7
13	(N-Bz-PTA)Cl	–	80	19	98	1.9
14	(N-Bz-PTA)Cl	–	100	77	99	1.8
15	(N-Bz-PTA)Cl	RAME-β-CD	80	24	98	1.9
16	(N-Bz-PTA)Cl	RAME-β-CD	100	86	96	1.8

^a Rh(acac)(CO)₂ (4.07 × 10^{−2} mmol), water-soluble ligand (0.21 mmol), cyclodextrin (0.48 mmol), H₂O (11.5 mL), 1-decene (20.35 mmol), 1500 rpm, CO/H₂ (1/1): 50 bar, time: 6 h.^b Calculated with respect to the starting olefin.^c (Mol. of aldehydes)/(mol of converted olefins) × 100. The side products were mainly isomeric olefins.^d Ratio of linear to branched aldehyde product.^e After 3 h.



Scheme 57.

plexes were recently used as **dendrimer-supported catalysts** by Servin et al. [101]. Three-generations dendrimers terminated by PTA or [Ru(p-cymene)Cl₂(PTA)] groups were obtained as shown in Scheme 57.

The solubility in pure water at room temperature of compounds **5-Gn** is high for monomer **5**, moderate for **5-G₁** but very poor for **5-G₂** and **5-G₃**. Compounds **5-Gn** have a hydrophilic surface and a hydrophobic interior. The complexes were used in **phenylacetylene hydration** in water/isopropanol mixtures. After 48 h at 90 °C, the first generation gave higher conversion than the monomer, but a decreasing efficiency was observed with generations 2 and 3. Conversely, the selectivity for the ketone increases from the monomer to the third generation from 91 to 98%, showing a slightly positive dendritic effect (Fig. 31a).

The dendrimer-supported catalysts were also tested in **allylic alcohol isomerization**. Thus, isomerization of 1-octen-3-ol into octan-3-one was carried out using 1 mol% of Ru catalysts and 2% of Cs₂CO₃ as co-catalyst, in mixtures water/heptane at 75 °C for 8 h under vigorous stirring. At the end of the reaction phase separation allowed for recycling of the catalyst (Fig. 31b).

Redox isomerization of allyl alcohol in aqueous solution under mild conditions was also carried out by Joó and co-workers in the presence of the water-soluble imidazolyl complexes **144** and **145**. Under a hydrogen pressure of 10 bar, with a catalyst concentration of 4.73 mM, substrate concentration 667 mM, after 1 h at 80 °C in buffered water solution (pH 6.9, phosphate buffer), 85.6% con-

version was obtained using **144** and 95.6% in the presence of **145**. The complexes can also catalyze the hydrogenation of cinnamaldehyde (CNA), benzylidene acetone (BZA) and acetophenone under the same conditions, albeit with lower conversions (CNA: 27.3%, **144**; 42.0%, **145**. BZA: 20.8%, **144**; 42.3%, **145**. PhC(O)Me: 28.4%, **144**; 46.1%, **145**). For α,β-unsaturated compounds, the catalysts proved to be selective for C=C bond hydrogenation [55].

5. Medicinal chemistry of PTA complexes and structural derivatives

The fortuitous discovery by Rosenberg [102] of the antitumoral properties of *cis*-diamine dichloroplatinum(II), later known as cisplatin, has paved the way to the development of the research field in metallodrugs, which has steadily grown in the last 30 years to the size of an independent branch in medicinal chemistry. The fact that cisplatin is effective only on primary tumours and not on metastases and its high general toxicity, leading to heavy side-effects, have however required more detailed and diversified approaches to the design and testing of new antitumoral metal-based drugs. Another transition metal which was found useful to broaden the armory of metallodrugs is ruthenium, also due to its rich synthetic chemistry, the wide range of oxidation states (Ru^{II}, Ru^{III} and Ru^{IV}) compatible with physiological conditions, and lower toxicity compared to platinum [103]. Among the most successful antimetastatic ruthenium-based

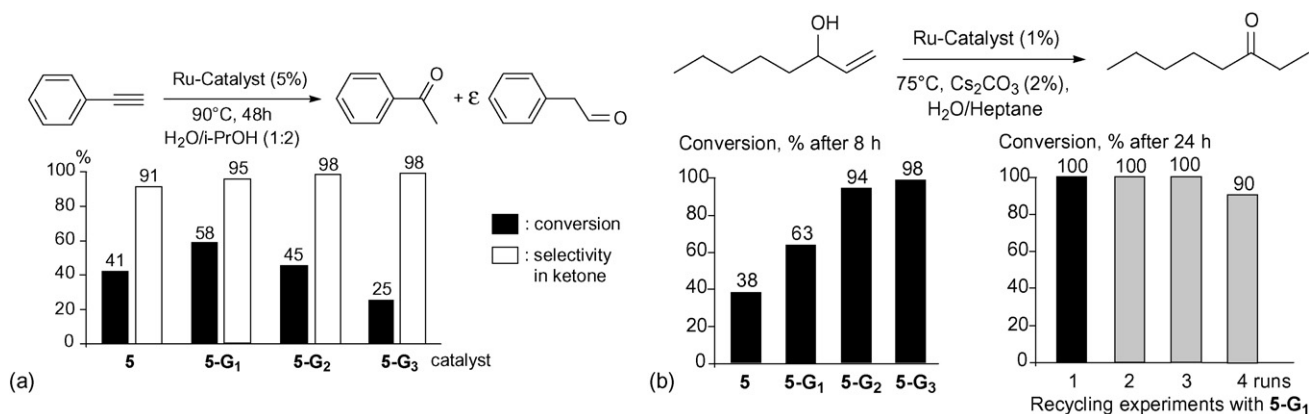
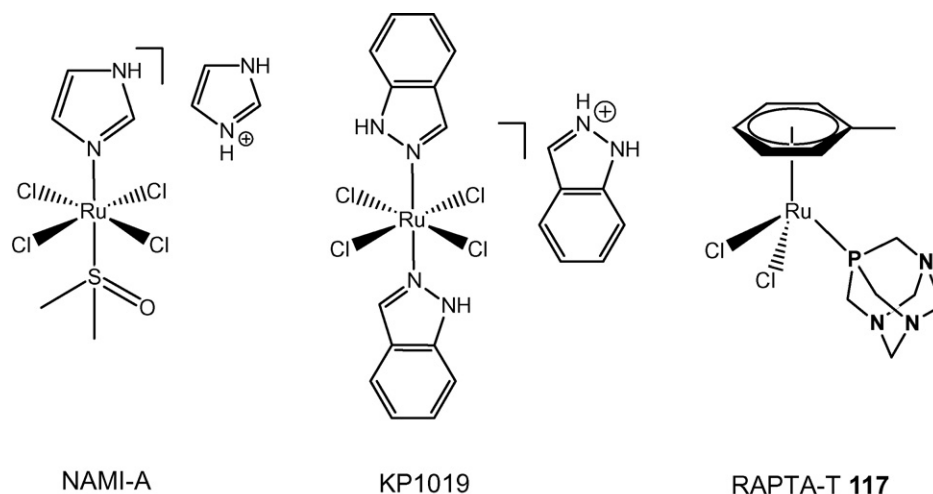


Fig. 31. (a) Hydration of phenylacetylene using monomer **5** and dendrimers **5-Gn** ($n = 1-3$) as catalysts. (b) Isomerization of 1-octen-3-ol using the monomer **5** and dendrimers **5-Gn** ($n = 1-3$) as catalysts. On the right: recycling experiments with **5-G₁**. The figure was reproduced from ref. [101], by permission of the Royal Society of Chemistry.



Scheme 58.

drugs available today, $\text{ImH}[\text{trans-Im}(\text{DMSO})\text{RuCl}_4]$ (NAMI-A), [104] $\text{trans-}[\text{tetrachlorobis}(1\text{H-indazole})\text{ruthenate(III)}]$ (KP1019) [105] (Scheme 58) and a series of $[\text{RuCl}_2(\eta^6\text{-arene})(\text{PTA})]$ complexes (RAPTA-type, Chart 8) [106] inhibit significantly secondary tumour growth in different cell lines, as widely reviewed by the authors who discovered and studied these compounds during the last few years [107–110].

In their seminal paper, [46] Dyson and co-workers compared the *in vitro* and *in vivo* activity and cytotoxicity of a series of RAPTA-type complexes bearing PTA and $[\text{PTAm}] \text{Cl}$. *in vitro* biological experiments demonstrate that these compounds are active towards the TS/A mouse adenocarcinoma cancer cell line whereas cytotoxicity on the HBL-100 human mammary (nontumour) cell line was not observed at concentrations up to 0.3 mM, which indicates selectivity of these ruthenium(II)-arene complexes to cancer cells. In the case of the mPTA complexes, these proved to be cytotoxic towards both cell lines. RAPTA-C (**116a**) and the benzene analogue RAPTA-B (**119**) were selected for *in vivo* experiments to evaluate their anticancer and antimetastatic activity. The complexes reduce the growth of lung metastases in CBA mice bearing the MCa mammary carcinoma in the absence of a corresponding action at the site of primary tumour growth. Complementary pharmacokinetic studies of RAPTA-C indicate that ruthenium is rapidly eliminated from the organs and the bloodstream.

More interesting aspects of the structure-activity relationship were discovered along the years. In particular, it was shown that **117** and its analogues bearing different arenes, such as $\eta^6\text{-(p-cymene)}$ (RAPTA-C, **116a**) or $\eta^6\text{-(benzene)}$ (RAPTA-B, **119**) exhibit markedly pH-dependent DNA binding properties *in vitro*, in particular it was found that **116a**, DNA was damaged at pH 6.8 whereas at pH characteristic of healthy cells (typically pH 7.2), little or no damage was detected [46]. In some way this is in line with the general understanding that traditional metal-based drugs target DNA to inhibit tumour cell replication, and led to the proposal of a mechanism based on activation by protonation to favour direct DNA damage. As cancer cells display lower pH values (<6) than healthy ones (*ca.* 7), it was thought that the action of RAPTA complexes could be related to the ability of PTA to protonate at low pH values and hence show selective DNA damage for cancer cells.

The pK_a values of the complexes bearing PTA was therefore established using $^{31}\text{P}\{^1\text{H}\}$ NMR spectroscopy in D_2O for a series of complexes (Table 21). Upon coordination, the pK_a of PTA decreases, to a value depending on the nature of the arene ligand [46]. The experimental data have been substantiated by a DFT/continuum electrostatics study. The calculations confirmed that PTA binding

to a Ru center significantly reduces the basicity of the ligand. The observations are rationalized by the hydroxo/aqua ligand equilibrium in $[\text{Ru}(\eta^6\text{-benzene})\text{Cl}(\text{OH}_2)(\text{PTA})]^+$. Fine-tuning of the pK_a can be obtained by modifying the substituents attached to the arene ring, i.e. electron-withdrawing groups lower the pK_a and electron-rich groups increase the pK_a [50].

Rh(III) pentamethylcyclopentadienyl chloride and Os(II) p-cymene dichloride complexes with either PTA or $[\text{mPTA}]\text{Cl}$ ligands have also shown anticancer activity [59]. $[\text{Os}(\eta^6\text{-p-cymene})\text{Cl}_2(\text{PTA})]$ (**154**) and $[\text{M}(\eta^6\text{-p-cymene})\text{Cl}_2(\text{mPTA})]\text{Cl}$ ($\text{M}=\text{Ru}$ **116b**, Os **156**), were also characterized by single-crystal x-ray diffraction (see Section 3.3). The PTA complexes are selective anticancer agents, whereas the mPTA complexes are indiscriminate and damage both cancer and healthy cells. In spite of this, mPTA complexes were useful and were chosen as models for the protonated PTA adduct which was thought to be implicated in drug activity. The study was complemented by binding studies to DNA model compounds, nucleosides and purine bases. The products were characterized by NMR spectroscopy and electrospray ionization mass spectrometry (ESI-MS), the latter confirming that in general, the N7 position on guanine (the most basic site) was the preferred donor atom for coordination to the metal complexes.

Electrospray ionization mass spectrometry (ESI-MS) was used as a valuable tool to correlate biological activity and effects on DNA, in particular the reactivity of the complexes with a 14-mer oligonucleotide (5'-ATACATGGTACATA-3') was studied in details. Binding energies between the metal centers and the ligands were calculated by DFT methods. Calculations showed that PTA ligands are relatively strongly bound to the metal. Exchange of metal center (Ru vs. Os), methylation or protonation of PTA, or change of the arene (p-cymene vs. benzene) results in significant differences in the metal-arene binding energies leaving the metal-PTA bond strength unchanged. The exchange of the arene ligand by nucleotides is expected to give significantly lower binding energies [50]. However, upon estimation of pK_a of RAPTA complexes obtained via

Table 21
 pK_a values for the PTA ligand and related Ru complexes at 298 K in 0.1 M NaCl.

Compound	pK_a	Ref
PTA	5.63 ± 0.05^a	[46]
$[\text{RuCl}_2(\eta^6\text{-p-cymene})(\text{PTA})]$ 116a	3.13 ± 0.02	[46]
$[\text{RuCl}_2(\eta^6\text{-toluene})(\text{PTA})]$ 117	3.31 ± 0.03	[46]
$[\text{RuCl}_2(\eta^6\text{-benzene})(\text{PTA})]$ 119	3.23 ± 0.06	[46]
$[\text{RuCl}_2(\eta^6\text{-C}_6\text{Me}_6)(\text{PTA})]$ (123)	2.99 ± 0.02	[46]
$[\text{Ru}(\text{C}_2\text{O}_4)(\eta^6\text{-C}_{10}\text{H}_{14})(\text{PTA})]$ (133)	2.35 ± 0.02	[50]
$[\text{Ru}(\text{C}_6\text{H}_6\text{O}_4)(\eta^6\text{-C}_{10}\text{H}_{14})(\text{PTA})]$ (134)	2.64 ± 0.03	[50]

NMR titration, it was established that unless arene loss is taken into account (by exchange with the 14-mer oligonucleotide), protonation is unlikely to occur under physiological conditions.

At a later stage, an *in vitro* evaluation of Rh(III), Ru(II) and Os(II) complexes bearing Cp or Cp* instead of neutral arenes, together with **154** and **116a** was undertaken using HT29 colon carcinoma, A549 lung carcinoma, and T47D breast carcinoma cells. In the HT29 cell line, the two nearest congeners to **116a**, i.e. [Cp*Rh(PTA)Cl₂] (**166**) and [Os(η⁶-p-cymene)Cl₂(PTA)] (**154**), demonstrated very similar cytotoxicity profiles. Complex **166** proved significantly more cytotoxic in A549 cells and [Cp*Rh(PTA)₂Cl]Cl (**167**) 3-fold more cytotoxic in T47D cells, both relative to **116a**. Thus, organometallic anticancer drugs based on the neighboring elements to ruthenium have shown a potential to further investigation [64].

Theoretical calculations often provide invaluable details about reaction mechanisms, including drug interactions with proteins and DNA. A complete study based on *in vacuo* DFT calculations, classical MD, and mixed QM/MM Car-Parrinello MD explicit solvent simulations was used to rationalize the binding mode of RAPTA complexes to double-stranded DNA (dsDNA). Results indicated the presence of a pH-dependent mechanism for the activity of the RAPTA-type complexes. The adducts are formed with the DNA sequence d(CCTCTG*G*TCTCC)/d(GGAGACCAGAGG), where G* are guanosine bases that bind to the Ru through their N(7) atom. The resulting binding sites were characterized in QM/MM molecular dynamics simulations showing that DNA can easily adapt to accommodate the Ru compounds [111].

The two classes of compounds [Ru(η⁶-arene)X(en)] (RA-en) and [Ru(η⁶-arene)(X)₂(PTA)] (RAPTA) [en = ethylenediamine, X = leaving group] have been later on the subject of a comparative theoretical investigation on the binding processes double-stranded DNA to characterize the resulting structural perturbations by means of *ab initio* and classical molecular dynamics simulations. The high flexibility of DNA allows for fast accommodation of the ruthenium complexes into the major groove. The two complexes induce at this stage different DNA structural distortions. It was concluded that the strain induced in the DNA from RA-en is released by a local break of a Watson–Crick base-pair whereas RAPTA complexes bend the DNA helix towards its major groove, as in the case of *cisplatin* [112].

As RAPTA-type compounds possess a modular structure comprising a ruthenium-bound arene, one PTA molecule and two halides, it was possible to design compounds potentially able to increase the drug activity. In this regard, insertion of functional groups on the arenes able to enhance hydrogen bonding with DNA was tested (**124–131**, Chart 8, bottom). Cell viability studies using the TS/A mouse adenocarcinoma cancer cell line and the non-tumorigenic HBL-100 human mammary cell line, combined with uptake determinations were compared to the nonfunctionalized analogues, previously shown to be active tumours. Surprisingly, this resulted in a decrease in toxicity towards cancer cells and increased toxicity in healthy ones [47]. A possible explanation could be that easier arene loss is obtained for charged fragments in their interaction with oligonucleotides, and increased hydrophilicity could be detrimental to drug uptake.

From these studies it was evident that both hydrophobicity and resistance to hydrolysis were important parameters to be evaluated upon the rationale PTA-based drug design. Replacement of chloride with oxalate chelating ligands was carried out [51]. The new complexes (oxalo RAPTA **133**, carbo RAPTA **134**, Scheme 26), were highly soluble and kinetically more stable than their RAPTA precursor towards hydrolysis. Moreover, they exhibit significantly lower pK_a values than the RAPTA analogues (Table 21) under physiological conditions. Importantly, **133** and **134** showed a similar order of activity in inhibiting cancer cell-growth pro-

liferation (*in vitro* assays) and exhibited oligonucleotide 14-mer 5'-ATACATGGTACATA binding characteristics similar to those of the RAPTA precursor. The interaction of **133** and **134** with the oligonucleotide proceed via loss of carboxylate and to a minor extent, loss of arene ligands (as demonstrated by matrix-assisted laser desorption ionization mass spectrometry).

ESI-MS techniques are nowadays among the most powerful tools to study the interactions between metal based drugs and protein sites, as demonstrated for example by the complete study of the interaction of **116a**, **133** and **134** with horse heart cytochrome c (cyt c). About 30% of cyt c is present in its reduced form after 24 h at 25 °C incubation conditions in the presence of **133** but not **134**. Extensive protein metalation was demonstrated for **166a**, moderate with **133** and low with **134**, reflecting the ability of various RAPTA-type species to release leaving groups and react with the protein side chains [113].

The interaction of RAPTA complexes with proteins could be indeed among the preferred activation mechanisms. The ability of RAPTA complexes **116a**, **116b**, **117**, **120**, **123**, **125**, **131**, **133**, **134** and derivatives (Chart 8) to inhibit cytosolic or mitochondrial thioredoxin reductase (an ubiquitous flavoenzyme that maintains the cellular redox state) and cathepsin B (a prognostic enzyme marker for several types of cancer, taking part in metastasis, angiogenesis and tumour progression) was established. As the steric demand of the arene ligand is increased, a decrease in thioredoxin reductase inhibition was observed, as if the protein could not accommodate bulky arene substituents. More important is the effect on cathepsin B inhibition, the anchoring site likely being cysteine active sites [114]. Further studies on the apoptosis in EAC (Ehrlich ascites carcinoma) cells in mice caused by RAPTA complexes was demonstrated to occur via mitochondrial and p53-JNK (JNK = c-Jun NH(2)-terminal kinase, a critical mediator in drug-induced cell growth inhibition) [115].

The importance of lipophilicity was shown by studying a series of compounds of general formula [Ru(η⁶-p-cymene)(R₂acac)(PTA)][X] (R₂acac = Me₂acac, tBu₂acac, Ph₂acac, Me₂acac-Cl; X = BPh₄, BF₄ **135–138**, Scheme 27). The tetrafluoroborate salts were water soluble, quite resistant to hydrolysis, and were evaluated for cytotoxicity against A549 lung carcinoma and A2780 human ovarian cancer cells, among the most insensitive tumours against the common chemotherapeutic agents. The compounds are highly cytotoxic although stable to hydrolysis, which in turn could mean that their action may be different from DNA or protein targeting, perhaps more related to a receptor-based mechanism [53].

On the basis of the results discussed above, a series of mixed PTA/PPh₃ ruthenium complexes were prepared and tested, in the attempt to correlate the fine-tuning of the hydrophobicity of RAPTA complexes with the uptake capacities, biomolecular interactions and efficacy of the corresponding metallodrugs [54]. The results show that the presence of the PPh₃ ligand in **142** increases the cytotoxicity towards the TS/A adenocarcinoma cancer cells, giving increased uptake, and decrease in selectivity As cytotoxic to non-tumorigenic HBL-100 cells. This was in turn correlated to increased DNA interactions with proteins, as demonstrated by reactivity with model proteins ubiquitin and cytochrome-c.

Variations of the electrophoretic mobility of plasmid DNA supported on agarose gels is considered a good test to evaluate direct DNA-metal interaction. Supercoiled (SC) DNA undergoes retardation in the mobility due to alteration of DNA structure caused by the interaction with the metal and corresponding unfolding of the plasmid. Mixed PTA/PPh₃ ruthenium complexes [CpRuCl(PPh₃)(PTA)] (**66**), [CpRu(PPh₃)(PTA)] (**67**), [CpRuCl(PPh₃)(mPTA)]OTf (**68**), [CpRu(PPh₃)(mPTA)]X [X = Cl (**69-Cl**), OTf, (**69-OTf**)], [CpRu(mPTA)₂](OTf)₂ (**71**), were tested by Romerosa et al. [11]. In water containing phosphate buffer at pH

7.0, 37 °C in the presence of SC plasmid DNA for 14 h. From this study it emerged that either methylation of PTA or substitution of one PTA with PPh₃ increase the interaction with SC DNA, although no rationale was provided. Interestingly, no activity was shown by **71**, perhaps indicating that halide dissociation (favoured for Cl vs. I) is a pre-requisite to interaction with SC DNA.

Tris-phosphine complexes [CpRu(mTPPMS)(PTA)₂] (**80**), Na[CpRu(mTPPMS)₂(PTA)] (**81**) and [CpRu(mPTA)(mTPPMS)₂] (**82**) were also evaluated for DNA interaction through the mobility shift test [42]. As free mTPPMS showed interaction with DNA, it was suggested that complexes bearing this ligand may work following a non-dissociative mechanism, including both ligand substitution at the metal and interaction between the Ru-coordinated mTPPMS and DNA without ligand dissociation.

Another issue which was taken into account for the design of PTA-based metal complexes for use as anti-tumoral agents was the importance of the nature and presence of the coordinated arene ligand. New half-sandwich Ru complexes bearing the sulfur macrocycle [9]aneS3 ([9]aneS3 = 1,4,7-trithiacyclononane), both containing PTA, i.e. [RuCl₂(PTA)([9]aneS3)] (**146**), [RuCl(PTA)₂([9]aneS3)] [OTf] (**147**), and bearing nitrogen based ligands such as enac or bipy [enac = 1,2-bis(isopropyleneimino)ethane; bipy = 2,2'-bipyridine], i.e. [RuCl(en)([9]aneS3)] [OTf], [RuCl(enac)([9]aneS3)] [OTf], [RuCl(bipy)([9]aneS3)] [OTf] and [Ru(dmso)(bipy)([9]aneS3)] [OTf]₂ [enac = 1,2-bis(isopropyleneimino)ethane] were synthesized [56]. Complexes **146** and **147** can be considered as analogues of the known cytotoxic organometallic Ru(η⁶-arene) and Ru(η⁵-cyclopentadienyl) complexes, replacing the arene with the sulfur macrocycle 1,4,7-trithiacyclononane, leaving unchanged the remaining coordination sites around the metal. Preliminary *in vitro* tests performed on the complexes against the mouse adenocarcinoma cancer cell line (TS/A) and the human mammary normal cell line (HBL-100) showed a cytotoxicity comparable to that of the corresponding organometallic analogues. The authors concluded that the aromatic fragment of the piano-stool Ru complexes is not an essential feature for the *in vitro* anticancer activity, and other face-capping ligands with a low steric demand such as [9]aneS3 could be used.

The effect of the replacement of arenes by hydridotris(pyrazolyl)borate ligand (Tp) on the interaction of Ru–PTA complexes with DNA was also tested together with antimicrobial activity. [TpRuCl(PPh₃)(PTA)] (**92**, X = Cl, **a**; I, **b**), [TpRuX(PTA)₂] (**93**) and the mPTA derivatives [TpRuCl(PPh₃)(mPTA)]⁺ (**96**) and [TpRuCl(mPTA)₂]²⁺ (**97**) were all examined in SC DNA shift mobility test [43]. No interaction was shown by **92b** and **93** and the largest interactions were shown for the least water-soluble complexes.

The importance of the nature of substituents on the cyclopentadienyl ring was however demonstrated as a remarkable effect on the cytotoxicity of the corresponding RAPTA-type complexes. The water-soluble complexes [(Cp'OR)RuCl(PTA)₂] (Cp'OR = η⁵-1-alkoxy-2,4-di-tert-butyl-3-neopentylcyclopentadienyl; R = Me, **148**; Et, **149**, Scheme 29) [57] were considerably more cytotoxic, of about 2 orders of magnitude, than the cyclopentadienyl analogue **116a**. IC₅₀ ranged from 4 to 10 compared to 1000 μM of **116a**, depending on the cell line tested (typically ovarian cancer cell lines A2780 and cisplatin-resistant analogue A2780cisR).

Always pertaining to the field of arene modifications, the important issue of drug delivery was successfully addressed by Dyson and co-workers [48,116]. Human serum albumin (HSA) and the commercially available recombinant HSA (rHSA) accumulate in tumours and therefore can be used as efficient carriers for anti-carcinogenic agents. In order to introduce RAPTA-type moieties within rHSA, a conjugation method cross-linking the organometallic fragment to biomolecules via an acid-labile hydrazone bond was devised. Thus, the arene ligand was prepared from 1-methylamine-

1,4-cyclohexadiene, by reaction with α-bromoacetyl bromide, followed by a second step using 4-hydroxyl-benzaldehyde, complexation to RuCl₃·xH₂O and final reaction with PTA to yield compound **132** (Chart 8). A positive response was observed in the A2780 cell line exposed to rHSA conjugated with RAPTA, i.e. the IC₅₀ value was 20-fold lower than in **132** alone (11 mM vs. 288 mM, the latter comparable to the activity of RAPTA-C **116a**). The acidic environment of lysosomes cleaves the hydrazone bond and affords targeted release of the drug into the tumour cell.

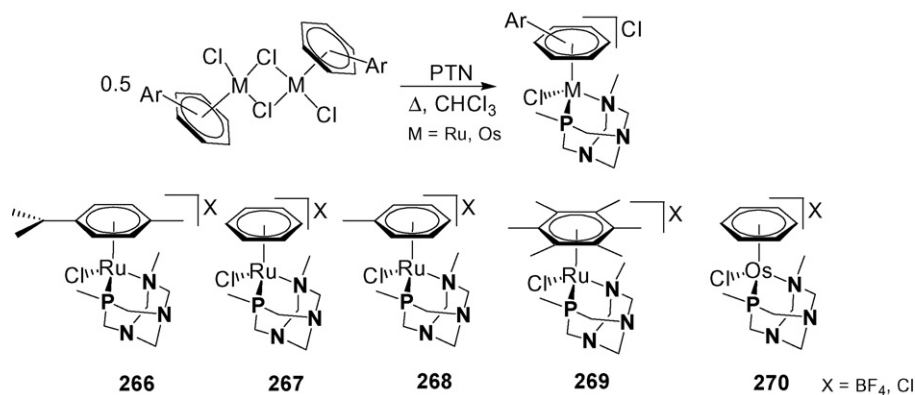
More influences of structural variations on the anticancer activity of RAPTA-type complexes have been tested using *in vitro* techniques. For example, a library of 19 cycloruthenated derivatives was obtained, the structures being modified using mono- or bidentate ligands, such as bipyridine, 1,10-phenanthroline (phen), 1,2-bis(diphenylphosphino)ethane (dppe), dimethylphenylphosphine, PPh₃ and PTA [33]. IC₅₀ values against mammalian cells (A-172, HCT-116, and RDM-4) were determined and some of those derived from orthoruthenated phenylpyridine such as [Ru(C₆H₄-2-C₅H₄N)(PMe₂Ph)(NCMe)₃]PF₆, *trans*-[Ru(C₆H₄-2-C₅H₄N)(PPh₃)₂(NCMe)₂]PF₆, *cis*-[Ru(C₆H₄-2-C₅H₄N)(dppe)(NCMe)₂]PF₆, *cis*-[Ru(C₆H₄-2-C₅H₄N)(phen)(MeCN)₂]PF₆, display activity of the same order of magnitude as cisplatin. Disappointingly, low activity was shown by complex [Ru(C₆H₄-2-C₅H₄N)(PTA)(NCMe)₃]PF₆ (**50**, Chart 5).

The thiosemicarbazone complex *trans*-[RuCl(L)(PTA-H)₂]Cl₂ (**49**) (L = 2-acetylpyridine N⁴,N⁴-dimethylthiosemicarbazone) [32] shows strong antiproliferative effects in low micromolar concentrations in the ovarian carcinoma cell line 41 M (IC₅₀ = 0.87 μM) and more moderate activity in the breast cancer cell line SK-BR-3 (IC₅₀ = 39 μM). A remarkable pH effect was observed in the cell growth inhibition. The activity was 6.5- and 5.4-times higher at pH 6.0 than at pH 7.4 in the lung cancer cell line A549 and the colon carcinoma cell line HT-29 (GI₅₀ = 24 and 8.0 μM at pH 6.0 for A549 and HT-29, respectively).

RAPTA-type Ru(II) and Os(II) complexes bearing κ²-P,N chelating open-cage ligand PTN (**266–270**, PTN = 3,7-dimethyl-7-phospha-1,3,5-triazabicyclo[3.3.1]nonane) were also tested for biomedical applications [117]. A series of compounds of the general formula [M(η⁶-arene)(PTN)Cl]X; (M = Ru and Os, arene = *p*-cymene, benzene, toluene and hexamethylbenzene, X = Cl[−] and BF₄[−]) have been prepared and fully characterized (Scheme 59). The complexes are relatively resistant to hydrolysis and are stable even at high chloride concentrations and at low pH, making the possibility of a ring-opening activation mechanism under physiological conditions unlikely. The cytotoxicity was evaluated in A2780 ovarian cancer cells and comparable to known RAPTA complexes. The reactivity of the complexes towards double-stranded oligonucleotides and the model protein ubiquitin was investigated using Fourier transform ion cyclotron resonance mass spectrometry (FT-ICR-MS) and gel electrophoresis, showing a preference for the formation of covalent adducts with the protein. The reactivity of Ru–PTN complexes towards DNA was lower than the PTA-based analogues, possibly due to a much slower rate of hydrolysis.

Transition metals else than Ru, Rh and Os bearing PTA or derivatives have also been tested for their biological properties. Pt(II) complexes bearing PTA and thiocarbamate esters *trans*-[Pt{SC(OMe)=NC₆H₄R}₂(PTA)₂] (R = H, **220**; Cl, **221**; OMe, **222**; NO₂, **223**; Me **224**) were tested *in vitro* in four human cancer cell lines (CH1, HT29, A549, SK-OV-3) using MTT assay [81]. IC₅₀ values using **220** were promising low if compared to cisplatin, ranging from 0.4 μM (CH1, vs. 0.16 for cisplatin) to 1.0 μM (SK-OV-3, vs. 1.9), to 2.9 μM (HT29, vs. 5.5) in spite of the *trans*-coordination.

The *trans*-platinum thiolate complexes bearing PTA or DAPTA ligands *trans*-[Pt(SR)₂(P)₂] [P = PTA, SR = 2-thiopyrimidine (**215**), 2-thiopyridine (**216**); P = DAPTA, SR = 2-thiopyrimidine (**217**), 2-thiopyridine (**218**)] and gold(I) complexes [Au(SR)(PR'₃)] (**248**)



Scheme 59.

(SR=various thiolato derivatives, Scheme 48; PR₃ = PTA, DAPTA) were tested for *in vitro* cytotoxicities against a panel of seven human cancer cell lines. Au(I) complexes [Au(SR)(P)] [P=PTA, SR=SPy, SPyrim; P=DAPTA, SR=SPy, SPyrim] showed low cytotoxicity, while the Pt(II) complexes demonstrated high cytotoxicity for ovarian, colon, renal, and melanoma cancer cell lines from a comparison with ID₅₀ values for some established cytotoxic drugs [79].

Also for some Pt-PTA complexes, the activity towards cancer cell growth inhibition is sensibly lower than the corresponding PPh₃ derivatives, as in the case of [Pt(μ-S,N-8-TT)(PTA)₂]₂ (**212**) and *cis*-[PtCl(8-MTT)(PTA)₂] (**213**) [8-TT=bis(deprotonated) 8-thiotheophylline; 8-MTT=8-(methylthio)theophylline], indicating that also in the case of Pt complex a mere increase of hydrophilicity is not a pre-requisite for high activity [78]. The homobimetallic complexes **209–211** (Chart 10) bearing thiopurinic ligands, instead showed enhanced activity against cisplatin-resistant T2 and SK-OV-3 cell lines, possibly due to an appropriate balance between hydro- and lipophilicity, independently from the length of the groups bridging the metal moieties [76].

The Au–PTA complex [Au{κ²-C,N-C₆H₄(PPh₂=N(C₆H₅))₂}(PTA)₂Cl]PF₆ (**258**) has been tested as potential anticancer agent together with analogues containing dithiocarbamate ligands in place of PTA, and their cytotoxicity properties were evaluated *in vitro* against HeLa human cervical carcinoma and Jurkat-T acute lymphoblastic leukemia cells. Preferential induction of apoptosis in HeLa cells after treatment with all compounds was observed. The interactions with calf thymus DNA have been evaluated by thermal denaturation methods, showing absence or little interaction with DNA [94].

Finally, the radiochemically active complex [⁶⁴Cu(PTA)₄]⁺ (**271**) was synthesized and used to establish the *in vitro* behaviour against EMT-6 tumour cells. The complex showed a rapid cell association (8.5% at 2 h) significantly higher than congeners not bearing PTA [118].

Acknowledgements

MP and LG thank EC for supporting this research through projects AQUACHEM (MRTN-CT-2003-503864) and HYDROCHEM (HPRN-CT-2002-00176). The support of Ente Cassa di Risparmio di Firenze (project FIRENZE HYDROLAB), COST Action D29 and CM0802 (“PhoSciNet”), MIUR (PRIN2007) and CNR-RAS bilateral agreement is thankfully acknowledged. LG thanks the Italian Ministry for Foreign Affairs for sponsoring a project within the Italy-USA Joint Programme of Exchange of Researchers 2008–2010. Dr A. Rossin (ICCOM-CNR) is kindly acknowledged for the invaluable help with the figures showing X-ray crystal structures.

References

- [1] A.D. Phillips, L. Gonsalvi, A. Romerosa, F. Vizza, M. Peruzzini, *Coord. Chem. Rev.* 248 (2004) 955.
- [2] J. Mathew, T. Thomas, C.H. Suresh, *Inorg. Chem.* 46 (2007) 10800.
- [3] A. Muller, S. Otto, A. Roodt, *Dalton Trans.* (2008) 650.
- [4] (a) X. Xu, C. Wang, Z. Zhou, X. Tang, Z. He, C. Tang, *Eur. J. Org. Chem.* (2007) 4487; (b) Z. He, X. Tang, Y. Chen, Z. He, *Adv. Synth. Catal.* 348 (2006) 413; (c) X. Tang, B. Zhang, Z. He, R. Gao, Z. He, *Adv. Synth. Catal.* 349 (2007) 2007.
- [5] A. Lu, X. Xu, P. Gao, Z. Zhou, H. Song, C. Tang, *Tetrahedron: Asymmetry* 19 (2008) 1886.
- [6] B. Zhang, Z. He, S. Xu, G. Wu, Z. He, *Tetrahedron* 64 (2008) 9471.
- [7] S. Otto, A. Ionescu, A. Roodt, *J. Organomet. Chem.* 690 (2005) 4337.
- [8] P. Smoleński, A.M. Kirillov, M.F.C. Guedes da Silva, A.J.L. Pombeiro, *Acta Cryst. E64* (2008) o556.
- [9] A.M. Kirillov, Piotr Smoleński, M.F.C. Guedes da Silva, A.J.L. Pombeiro, *Acta Cryst. E64* (2008) o496–o497.
- [10] (a) P. Smolenski, F.P. Pruchnik, Z. Ciunik, T. Lis, *Inorg. Chem.* 42 (2003) 3318; (b) J. Kovács, F. Joó, A.C. Bényei, G. Laurenczy, *Dalton Trans.* (2004) 2336.
- [11] (a) A. Romerosa, T. Campos-Malpartida, C. Lidrisi, M. Saoud, M. Serrano-Ruiz, M. Peruzzini, J.A. Garrido-Cárdenas, F. García-Maroto, *Inorg. Chem.* 45 (2006) 1289; (b) B. González, P. Lorenzo-Luis, P. Gili, A. Romerosa, M. Serrano-Ruiz, *J. Organomet. Chem.* 694 (2009) 2029.
- [12] Adrián Mena-Cruz, Pablo Lorenzo-Luis, Antonio Romerosa, Mustapha Saoud, Manuel Serrano-Ruiz, *Inorg. Chem.* 46 (2007) 6120.
- [13] A.M. Kirillov, P. Smoleński, M. Haukka, M.F.C. Guedes da Silva, A.J.L. Pombeiro, *Organometallics* 28 (2009) 1683.
- [14] (a) D.J. Darensbourg, C.G. Ortiz, J.W. Kamplain, *Organometallics* 23 (2004) 1747; (b) D.A. Krogstad, G.S. Ellis, A.K. Gunderson, A.J. Hamrich, J.W. Rudolf, J.A. Halfen, *Polyhedron* 26 (2007) 4093.
- [15] S. Bolaño, A. Albinati, J. Bravo, L. Gonsalvi, M. Peruzzini, *Inorg. Chem. Commun.* 9 (2006) 360–363.
- [16] B.J. Frost, C.A. Mebi, P.W. Gingrich, *Eur. J. Inorg. Chem.* (2006) 1182.
- [17] G.W. Wong, J.L. Harkreader, C.A. Mebi, B.J. Frost, *Inorg. Chem.* 45 (2006) 6748.
- [18] (a) M. Erlandsson, L. Gonsalvi, A. Ienco, M. Peruzzini, *Inorg. Chem.* 47 (2008) 8–10; (b) G.W. Wong, W.-C. Lee, B.J. Frost, *Inorg. Chem.* 47 (2008) 612–620.
- [19] R. Huang, B.J. Frost, *Inorg. Chem.* 46 (2007) 10962.
- [20] D.A. Krogstad, K.E. Gohmann, T.L. Sunderland, A.L. Geis, P. Bergamini, L. Marvelli, Vi. G. Young Jr., *Inorg. Chim. Acta* 362 (2009) 3049.
- [21] B.J. Frost, S.B. Miller, K.O. Rove, D.M. Pearson, J.D. Korinek, J.L. Harkreader, C.A. Mebi, J. Shearer, *Inorg. Chim. Acta* 359 (2006) 283–288.
- [22] B.J. Frost, C.M. Bautista, R. Huang, J. Shearer, *Inorg. Chem.* 45 (2006) 3481.
- [23] A. Marchi, E. Marchesi, L. Marvelli, P. Bergamini, V. Bertolasi, V. Ferretti, *Eur. J. Inorg. Chem.* (2008) 2670.
- [24] P. Smoleński, A.J.L. Pombeiro, *Dalton Trans.* (2008) 87–91.
- [25] S. Bolaño, L. Gonsalvi, P. Barbaro, A. Albinati, S. Rizzato, E. Gutsul, N. Belkova, L. Epstein, E. Shubina, M. Peruzzini, *J. Organomet. Chem.* 691 (2006) 629–637.
- [26] X. Tu, G.S. Nichol, R. Wang, Z. Zheng, *Dalton Trans.* (2008) 6030.
- [27] S.A.T. Dillinger, H.W. Schmalle, T. Fox, H. Berke, *Dalton Trans.* (2007) 3562.
- [28] (a) Z. Wang, J. Liu, C. He, S. Jiang, B. Åkermar, L. Sun, *Inorg. Chim. Acta* 360 (2007) 2411; (b) J. Hou, X. Peng, Z. Zhou, S. Sun, X. Zhao, S. Gao, *J. Organomet. Chem.* 691 (2006) 4633; (c) R. Mejia-Rodriguez, D. Chong, J.H. Reibenspies, M.P. Soriaga, M.Y. Darensbourg, *J. Am. Chem. Soc.* 126 (2004) 12004; (d) Y. Na, M. Wang, K. Jin, R. Zhang, L. Sun, *J. Organomet. Chem.* 691 (2006) 5045.
- [29] C.A. Mebi, B.J. Frost, *Inorg. Chem.* 46 (2007) 7115.
- [30] R. Girotti, A. Romerosa, S. Mañas, M. Serrano-Ruiz, R.N. Perutz, *Inorg. Chem.* 48 (2009) 3692.

- [31] D.N. Akbayeva, S. Moneti, M. Peruzzini, L. Gonsalvi, A. Ienco, F. Vizza, C. R. Chimie 8 (2005) 1491.
- [32] S. Grguric-Sipka, C.R. Kowol, S.-M. Valiahdi, R. Eichinger, M.A. Jakupc, A. Roller, S. Shova, V.B. Arion, B.K. Keppler, Eur. J. Inorg. Chem. (2007) 2870.
- [33] L. Leyva, C. Sirlin, L. Rubio, C. Franco, R. Le Lagadec, J. Spencer, P. Bischoff, C. Gaidon, J.-P. Loeffler, M. Pfeffer, Eur. J. Inorg. Chem. (2007) 3055.
- [34] C.A. Madrigal, A. García-Fernández, J. Gimeno, E. Lastra, J. Organomet. Chem. 693 (2008) 2535.
- [35] B. Gonzalez, P. Lorenzo-Luis, A. Romerosa, M. Serrano-Ruiz, P. Gili, J. Mol. Struct. (Theochem.) 894 (2009) 59–63.
- [36] B.J. Frost, C.A. Mebi, Organometallics 23 (2004) 5317.
- [37] C.A. Mebi, B.J. Frost, Organometallics 24 (2005) 2339.
- [38] Ch. Lidri, A. Romerosa, M. Saoud, M. Serrano-Ruiz, L. Gonsalvi, M. Peruzzini, Angew. Chem. Int. Ed. 44 (2005) 2568.
- [39] S. Bolaño, L. Gonsalvi, F. Zanolini, F. Vizza, V. Bertolasi, A. Romerosa, M. Peruzzini, J. Mol. Catal. A: Chem. 224 (2004) 61–70.
- [40] M.S. Ruiz, A. Romerosa, B. Sierra-Martin, A. Fernandez-Barbero, Angew. Chem. Int. Ed. 47 (2008) 8665.
- [41] C.A. Mebi, R.P. Nair, B.J. Frost, Organometallics 26 (2007) 429–438.
- [42] A. Romerosa, M. Saoud, T. Campos-Malpartida, C. Lidri, M. Serrano-Ruiz, M. Peruzzini, J.A. Garrido, F. García-Maroto, Eur. J. Inorg. Chem. (2007) 2803.
- [43] A. García-Fernández, J. Díez, A. Manteca, J. Sánchez, M.P. Gamasa, E. Lastra, Polyhedron 27 (2008) 1214.
- [44] S. Bolaño, J. Bravo, J. Castro, M^c.M. Rodríguez-Rocha, M^c.F.C. Guedes da Silva, A.J.L. Pombeiro, L. Gonsalvi, M. Peruzzini, Eur. J. Inorg. Chem. (2007) 5523.
- [45] A. García-Fernández, J. Díez, M.P. Gamasa, E. Lastra, Inorg. Chem. 48 (2009) 2471.
- [46] C. Scolaro, A. Bergamo, L. Brescacin, R. Delfino, M. Cocchietto, G. Laurency, T.J. Geldbach, G. Sava, P.J. Dyson, J. Med. Chem. 48 (2005) 4161.
- [47] C. Scolaro, T.J. Geldbach, S. Rochat, A. Dorcier, C. Gossens, A. Bergamo, M. Cocchietto, I. Tavernelli, G. Sava, U. Rothlisberger, P.J. Dyson, Organometallics 25 (2006) 756–765.
- [48] W.H. Ang, E. Daldini, L. Juillerat-Jeanneret, P.J. Dyson, Inorg. Chem. 46 (2007) 9048.
- [49] A. Dorcier, P.J. Dyson, C. Gossens, U. Rothlisberger, R. Scopelliti, I. Tavernelli, Organometallics 24 (2005) 2114.
- [50] C. Gossens, A. Dorcier, P.J. Dyson, U. Rothlisberger, Organometallics 26 (2007) 3969.
- [51] W.H. Ang, E. Daldini, C. Scolaro, R. Scopelliti, L. Juillerat-Jeanneret, P.J. Dyson, Inorg. Chem. 45 (2006) 9006.
- [52] S. Bolaño, G. Ciancaleoni, J. Bravo, L. Gonsalvi, A. Macchioni, M. Peruzzini, Organometallics 27 (2008) 1649.
- [53] C.A. Vock, A.K. Renfrew, R. Scopelliti, L. Juillerat-Jeanneret, P.J. Dyson, Eur. J. Inorg. Chem. (2008) 1661.
- [54] C. Scolaro, A.B. Chaplin, C.G. Hartinger, A. Bergamo, M. Cocchietto, B.K. Keppler, G. Sava, P.J. Dyson, Dalton Trans. (2007) 5065.
- [55] P. Csabai, F. Joó, Organometallics 23 (2004) 5640.
- [56] B. Serli, E. Zangrando, T. Gianferrara, C. Scolaro, P.J. Dyson, A. Bergamo, E. Alessio, Eur. J. Inorg. Chem. (2005) 3423.
- [57] B. Dutta, C. Scolaro, R. Scopelliti, P.J. Dyson, K. Severin, Organometallics 27 (2008) 1355.
- [58] A. Mena-Cruz, P. Lorenzo-Luis, A. Romerosa, M. Serrano-Ruiz, Inorg. Chem. 47 (2008) 2246.
- [59] A. Dorcier, C.G. Hartinger, R. Scopelliti, R.H. Fish, B.K. Keppler, P.J. Dyson, J. Inorg. Biochem. 102 (2008) 1066.
- [60] Ł. Jaremko, A.M. Kirillov, P. Smoleński, T. Lis, A.J.L. Pombeiro, Inorg. Chem. 47 (2008) 2922.
- [61] B.J. Frost, J.L. Harkreader, C.M. Bautista, Inorg. Chem. Commun. 11 (2008) 580–583.
- [62] Ł. Jaremko, A.M. Kirillov, P. Smoleński, T. Lis, M.F.C. Guedes da Silva, A.J.L. Pombeiro, Inorg. Chim. Acta 362 (2009) 1645.
- [63] P. Smoleński, C. Dinio, M.F.C. Guedes da Silva, A.J.L. Pombeiro, J. Organomet. Chem. 693 (2008) 2338.
- [64] A. Dorcier, W.H. Ang, S. Bolaño, L. Gonsalvi, L. Juillerat-Jeanneret, G. Laurency, M. Peruzzini, A.D. Phillips, F. Zanolini, P.J. Dyson, Organometallics 25 (2006) 4090.
- [65] S. Bolaño, A. Albinati, J. Bravo, M. Caporali, L. Gonsalvi, L. Male, M^c.M. Rodríguez-Rocha, A. Rossin, M. Peruzzini, J. Organomet. Chem. 693 (2008) 2397.
- [66] A.D. Phillips, S. Bolaño, S.S. Bosquain, J.-C. Daran, R. Malacea, M. Peruzzini, R. Poli, L. Gonsalvi, Organometallics 25 (2006) 2189.
- [67] M. Erlandsson, V.R. Landaeta, L. Gonsalvi, M. Peruzzini, A.D. Phillips, P.J. Dyson, G. Laurency, Eur. J. Inorg. Chem. (2008) 620–627.
- [68] D.A. Krogstad, A.J. DeBoer, W.J. Ortmeyer, J.W. Rudolf, J.A. Halfen, Inorg. Chem. Commun. 8 (2005) 1141.
- [69] D.H. Leung, R.G. Bergman, K.N. Raymond, J. Am. Chem. Soc. 128 (2006) 9781.
- [70] B. Korthals, I. Göttker-Schnetmann, S. Mecking, Organometallics 26 (2007) 1311.
- [71] V.V. Grushin, W.J. Marshall, Organometallics 27 (2008) 4825.
- [72] E. Vergara, S. Miranda, F. Mohr, E. Cerrada, E.R.T. Tiekink, P. Romero, A. Mendía, M. Laguna, Eur. J. Inorg. Chem. (2007) 2926.
- [73] J. Ruiz, N. Cutillas, F. López, G. López, D. Bautista, Organometallics 25 (2006) 5768.
- [74] A.M.M. Meij, S. Otto, A. Roodt, Inorg. Chim. Acta 358 (2005) 1005.
- [75] M. Caporali, C. Bianchini, S. Bolaño, S.S. Bosquain, L. Gonsalvi, W. Oberhauser, A. Rossin, M. Peruzzini, Inorg. Chim. Acta 361 (2008) 3017.
- [76] P. Bergamini, V. Bertolasi, L. Marvelli, A. Canella, R. Gavioli, N. Mantovani, S. Mañas, A. Romerosa, Inorg. Chem. 46 (2007) 4267.
- [77] P. Bergamini, E. Marchesi, V. Bertolasi, M. Fogagnolo, L. Scarpantonio, S. Manfredini, S. Vertuani, A. Canella, Eur. J. Inorg. Chem. (2008) 529–537.
- [78] A. Romerosa, P. Bergamini, V. Bertolasi, A. Canella, M. Cattabriga, R. Gavioli, S. Mañas, N. Mantovani, L. Pellacani, Inorg. Chem. 43 (2004) 905–913.
- [79] S. Miranda, E. Vergara, F. Mohr, D. de Vos, E. Cerrada, A. Mendía, M. Laguna, Inorg. Chem. 47 (2008) 5641.
- [80] S.-W.A. Fong, T.S.A. Hor, S.M. Devoy, B.A. Waugh, B.K. Nicholson, W. Henderson, Inorg. Chim. Acta 357 (2004) 2081.
- [81] D. Dolfen, K. Schottler, S.-M. Valiahdi, M.A. Jakupc, B.K. Keppler, E.R.T. Tiekink, F. Mohr, J. Inorg. Biochem. 102 (2008) 2067.
- [82] D.A. Krogstad, S.B. Owens, J.A. Halfen, V.G. Young Jr., Inorg. Chem. Commun. 8 (2005) 65–69.
- [83] Z.A. Sam, A. Roodt, S. Otto, J. Coord. Chem. 59 (2006) 1025.
- [84] P. Smoleński, S. Mukhopadhyay, M.F.C. Guedes da Silva, M.A.J. Charmier, A.J.L. Pombeiro, Dalton Trans. (2008) 6546.
- [85] D.A. Krogstad, J. Cho, A.J. DeBoer, J.A. Klitzke, W.R. Sanow, H.A. Williams, J.A. Halfen, Inorg. Chim. Acta 359 (2006) 136–148.
- [86] A.M. Kirillov, P. Smoleński, M.F.C. Guedes da Silva, A.J.L. Pombeiro, Eur. J. Inorg. Chem. (2007) 2686.
- [87] A.M. Kirillov, P. Smoleński, M.F.C. Guedes da Silva, M.N. Kopylovich, A.J.L. Pombeiro, Acta Cryst. E64 (2008) m603–m604.
- [88] M. Pellei, S. Alidori, M. Camalli, G. Campi, G.G. Lobbia, M. Mancini, G. Papini, R. Spagna, C. Santini, Inorg. Chim. Acta 361 (2008) 1456.
- [89] R. Wanke, P. Smoleński, M.F.C. Guedes da Silva, L.M.D.R.S. Martins, A.J.L. Pombeiro, Inorg. Chem. 47 (2008) 10158.
- [90] F. Mohr, L.R. Falvello, M. Laguna, Eur. J. Inorg. Chem. (2006) 3152.
- [91] A.A. Mohamed, T. Grant, R.J. Staples, J.P. Fackler Jr., Inorg. Chim. Acta 357 (2004) 1761.
- [92] F. Mohr, E. Cerrada, M. Laguna, Organometallics 25 (2006) 644–648.
- [93] F. Mohr, S. Sanz, E.R.T. Tiekink, M. Laguna, Organometallics 25 (2006) 3084.
- [94] N. Shaik, A. Martínez, I. Augustin, H. Giovino, A. Varela-Ramírez, M. Sanaú, R.J. Aguilera, M. Contel, Inorg. Chem. 48 (2009) 1577.
- [95] P. Smoleński, L. Benisy, M.F.C. Guedes da Silva, A.J.L. Pombeiro, Eur. J. Inorg. Chem. (2009) 1181.
- [96] S.S. Bosquain, A. Dorcier, P.J. Dyson, M. Erlandsson, L. Gonsalvi, G. Laurency, M. Peruzzini, Appl. Organomet. Chem. 21 (2007) 947–951.
- [97] G. Laurency, S. Jedner, E. Alessio, P.J. Dyson, Inorg. Chem. Commun. 10 (2007) 558–562.
- [98] V. Cadierno, J. Francos, J. Gimeno, Chem. Eur. J. 14 (2008) 6601.
- [99] A. Rossin, L. Gonsalvi, A.D. Phillips, O. Maresca, A. Lledós, M. Peruzzini, Organometallics 26 (2007) 3289.
- [100] F.-X. Legrand, F. Hapiot, S. Tilloy, A. Guerriero, M. Peruzzini, L. Gonsalvi, E. Monflier, Appl. Catal. A: Gen. 362 (2009) 62–66.
- [101] P. Servin, R. Laurent, L. Gonsalvi, M. Tristany, M. Peruzzini, J.-P. Majoral, A.-M. Caminade, Dalton Trans. (2009) 4432.
- [102] V.H. Mansour, B. Rosenberg, L. Vancamp, J.E. Trosko, Nature 222 (1969) 385–386.
- [103] C.S. Allardice, P.J. Dyson, Platinum Met. Rev. 45 (2001) 62–69.
- [104] G. Sava, S. Zorzet, C. Turrin, F. Vita, M.R. Soranzo, G. Zabucchi, M. Cocchietto, A. Bergamo, S. Di Giovone, G. Pezzoni, L. Sartor, S. Garbisa, Clin. Cancer Res. 9 (2003) 1898.
- [105] S. Kapitza, M. Pongratz, M.A. Jakupc, P. Heffeter, W. Berger, L. Lackinger, B.K. Keppler, B. Marian, J. Cancer Res. Clin. Oncol. 131 (2005) 101–110.
- [106] C.S. Allardice, A. Dorcier, C. Scolaro, P.J. Dyson, Appl. Organomet. Chem. 19 (2005) 1–10.
- [107] P.J. Dyson, G. Sava, Dalton Trans. (2006) 1929.
- [108] W.H. Ang, P.J. Dyson, Eur. J. Inorg. Chem. (2006) 4003.
- [109] M.A. Jakupc, M. Galanski, V.B. Arion, C.G. Hartinger, B.K. Keppler, Dalton Trans. (2008) 183–194.
- [110] C.G. Hartinger, P.J. Dyson, Chem. Soc. Rev. 38 (2009) 391–401.
- [111] C. Gossens, I. Tavernelli, U. Rothlisberger, Chimia 59 (2005) 81–84.
- [112] C. Gossens, I. Tavernelli, U. Rothlisberger, J. Am. Chem. Soc. 130 (2008) 10921.
- [113] A. Casini, G. Mastrobuni, W.H. Ang, C. Gabbiani, G. Pieraccini, G. Moneti, P.J. Dyson, L. Messori, ChemMedChem 2 (2007) 631–635.
- [114] A. Casini, C. Gabbiani, F. Sorrentino, M.P. Rigobello, A. Bindoli, T.J. Geldbach, A. Marrone, N. Re, C.G. Hartinger, P.J. Dyson, L. Messori, J. Med. Chem. 51 (2008) 6773.
- [115] S. Chatterjee, S. Kundu, A. Bhattacharyya, C.G. Hartinger, P.J. Dyson, J. Biol. Inorg. Chem. 13 (2008) 1149.
- [116] P.J. Dyson, W.H. Ang, PCT WO2007/128158A1.
- [117] A.K. Renfrew, A.D. Phillips, A. Egger, C.G. Hartinger, S.S. Bosquain, A.A. Nazarov, B.K. Keppler, L. Gonsalvi, M. Peruzzini, P.J. Dyson, Organometallics 28 (2009) 1165.
- [118] S. Alidori, G. Gioia Lobbia, G. Papini, M. Pellei, M. Porchia, F. Refosco, F. Tisato, J.S. Lewis, C. Santini, J. Biol. Inorg. Chem. 13 (2008) 307–315.